2001

Behaviour and strength of concrete beams reinforced and/or prestressed with FRP bars.

Sameh Michel Rafla. Salib
University of Windsor

INFORMATION TO USERS

BEHAVIOUR AND STRENGTH OF CONCRETE BEAMS

REINFORCED AND/OR PRESTRESSED

WITH FRP BARS

BY

SAMEH MICHEL RAFLA SALIB

A Dissertation Submitted to
Faculty of Graduate Studies and Research through
Civil and Environmental Engineering Program
in partial fulfilment of the requirements for the degree of
Doctor of Philosophy at the
University of Windsor

Windsor, Ontario, Canada
2001

The author has granted a non-exclusive licence allowing the National Library of Canada to reproduce, loan, distribute or sell copies of this thesis in microform, paper or electronic formats.

The author retains ownership of the copyright in this thesis. Neither the thesis nor substantial extracts from it may be printed or otherwise reproduced without the author's permission.

L'auteur a accordé une licence non exclusive permettant à la Bibliothèque nationale du Canada de reproduire, prêter, distribuer ou vendre des copies de cette thèse sous la forme de microfiche/film, de reproduction sur papier ou sur format électronique.

L'auteur conserve la propriété du droit d'auteur qui protège cette thèse. Ni la thèse ni des extraits substantiels de celle-ci ne doivent être imprimés ou autrement reproduits sans son autorisation.

0-612-62332-7

Canada

928812

I hereby declare that I am the sole author of this document

I authorise the University of Windsor to lend this document to other institutions or individuals for the purpose of scholarly research.

<div align="right">Sameh Michel Rafla Salib</div>

I further authorise the University of Windsor to reproduce the document by photocopying or by other means, in total or part, at the request of other institutions or individuals for the purpose of scholarly research.

<div align="right">Sameh Michel Rafla Salib</div>

The UNIVERSITY OF WINDSOR requires the signatures of all persons using or

photocopying this document.

Please sign below, and give address and date.

ABSTRACT

Concrete beams reinforced and/or prestressed with steel bars are used in a wide range of structures. However, the deterioration of such structures due to reinforcement corrosion is a major problem. The repair and maintenance of steel reinforced concrete structures, especially highway bridges, is quite costly in locations subject to severe weather conditions of rain and/or snow as in Canada and the USA.

In order to overcome this problem, Advanced Composite Materials (ACM), which are produced in the form of Fibre Reinforced Polymers (FRP), are becoming a desirable replacement to the traditional steel reinforcement. While both materials have identical functions, basic differences exist in the mechanical properties between steel and FRP that should be taken into account in the structural design and analysis of concrete beams reinforced and/or prestressed with FRP bars. For example, a ductile failure takes place for steel bars subjected to tensile and/or shear stresses, while brittle failure takes place for FRP bars. Further more, FRP bars provide high tensile strength, while their modulus of elasticity and shear strength are lower than those of steel bars.

These variations in properties lead to significant differences in the behaviour between concrete beams reinforced and/or prestressed with FRP bars and those reinforced and/or prestressed with steel bars. The properties of the reinforcing material, in both longitudinal and transverse directions, interact with the characteristics of the formed cracks, i.e. crack geometry and crack width, to determine the beam strength, as well as

the mode of failure. Therefore, a reliable study of the behaviour and strength of concrete beams reinforced with FRP bars should include some parameters that used to be neglected in case of steel reinforcement such as crack geometry, crack width, and the mechanical properties of bars in their transverse direction.

An experimental program has been conducted at the University of Windsor to study the above mentioned parameters and their effects on the behaviour and strength of both prestressed and non-prestressed concrete beams reinforced with Carbon Fibre Reinforced Polymer (CFRP) bars. The results of the study have been expressed through an analytical model that describes the interactive behaviour between crack progress, and the stresses induced in concrete as well as in both flexural and shear reinforcement. The degree of accuracy in modelling the crack path geometry has been also found to control the reliability of the calculated beam strength.

A comparison has been made between the results of the proposed analytical modelling and those obtained from the experimental program mentioned above, as well as from other published test data. A good agreement has been observed between the analytical and experimental results. Another comparison has been made between the experimental beam strength, the strength obtained by the present analytical model, and the strength calculated by the formulas recommended by different design guidelines issued recently for FRP reinforced and/or prestressed concrete structures. The comparison emphasised the necessity of considering the above-mentioned parameters in order to achieve an accurate prediction of beam strength.

TO YOU...

WHO KNOWS

ACKNOWLEGEMENTS

TABLE OF CONTENTS

LIST OF TABLES

LIST OF FIGURES

CHAPTER 1

INTRODUCTION

1.1 General

Advanced Composite Materials (ACM) are produced in the form of Fibre Reinforced Polymer (FRP). The main groups of FRP are Carbon Fibre Reinforced Polymer (CFRP), Glass Fibre Reinforced Polymer (GFRP), and Aramid Fibre Reinforced Polymer (AFRP), where in all cases, the fibres are embedded in a matrix (e.g. epoxy for CFRP). The behaviour of an FRP product is governed, in general, by the type of fibres, the ratio of fibre volume to the total volume of the product, and the orientation of fibres (CSCE/ACMBS, 1994).

FRP were first used for industrial applications, providing a combination of low density, high strength, and high durability. These properties were suitable for special components of aeronautics, aeroplanes, racing cars, high-speed trains, and sporting goods (CSCE/ACMBS, 1994). FRP products have also drawn the attention of structural engineers for use as a replacement for traditional steel reinforcement in concrete structures, taking advantage of their high corrosion resistance. The problem of steel corrosion is a real danger for many structures, especially at locations of harsh weather conditions (e.g. heavy rain and snow). This problem is magnified with freeze-thaw cycles and when applying de-icing salts over steel-reinforced concrete such as decks of bridges. These factors justify the increase in interest in using FRP in structural engineering (Belarbi et al. 1999).

1

Several studies have been conducted to evaluate the properties of the reinforcing bars made of FRP and to study the effect of these properties on the behaviour and strength of structural concrete elements reinforced with FRP bars. The mechanical properties of few commonly used FRP bars are given in Table 1-1. The stress-strain relationship of each is presented in Fig. 1-1 together with that of standard steel reinforcing bars. It can be seen that there are basic differences between steel and FRP regarding the modulus of elasticity, and the type of failure. All the FRP bars show linear elastic behaviour up to their tensile strength with brittle failure. CFRP bars have the highest values of both tensile strength and modulus of elasticity.

As a step to establishing design recommendations for concrete structures reinforced with FRP bars, modifications have been suggested to the current methods for analysis and design of concrete structures reinforced and/or prestressed with steel bars based on experimental results obtained for concrete components reinforced and/or prestressed with FRP bars. Herein, it is noted that the design codes of concrete structures reinforced and/or prestressed with steel bars have been established on certain bases of the mechanical properties of steel, the interaction characteristics between steel and concrete, and the observed behaviour of concrete elements reinforced and/or prestressed with steel bars.

These bases differ when replacing steel with FRP. For example, the steel is an isotropic material, while the properties of FRP bars in the longitudinal direction differ from those in the transverse direction. Since the fibres are oriented in the longitudinal

2

direction of the FRP reinforcing bars, the properties in the transverse direction are governed mainly by the matrix that bonds the fibres, leading to an anisotropic product with maximum strength and rigidity in the longitudinal direction and minimum strength and rigidity in the transverse direction.

The experimental program carried out at the University of Windsor (Chapter 3), for prestressed and non-prestressed concrete beams reinforced with CFRP bars, demonstrated the significant influence of parameters such as crack geometry and crack width on the shear deformation of FRP bars crossing the crack, and consequently on the beam strength, and its mode of failure (Salib et al. 1999a). These parameters are usually neglected when dealing with steel-reinforced concrete beams as well as in the current design guidelines for FRP-reinforced concrete beams (ACI 1995; Surendra et al. 1995; CSA 1994; Leet 1991; CHBDC 2000; ACI 1999; and BIR 1997).

1.2 Objectives

The main objective of the research work presented here is to develop an analysis/design procedure for concrete beams reinforced and/or prestressed with FRP bars, taking into account the mechanical characteristics of FRP bars and their effect on all the possible modes of failure. Consideration is also given to specific parameters which are neglected in the current design guidelines for FRP reinforced and/or prestressed concrete beams. These parameters are as follows:

-the geometry of the crack path profile while progressing through concrete,

3

- the induced crack width at the reinforcement level,

-the mechanical properties and behaviour of FRP bars in their transverse direction, and

-the rigid body movement of the beam portions on both sides of the crack.

1.3 Research Procedure

As a first step towards a comprehensive modelling of beam behaviour, an analytical model was established to define the geometry of any crack path that may form within the beam span. Another step was to revise the formulas commonly used for crack width prediction of steel-reinforced concrete beams, to be applicable for FRP-reinforced concrete beams. The results of both the analytical model of crack geometry and the modified formula for crack width were in good agreement with the corresponding experimental results.

Thereafter, the study continued taking into account the effects of other parameters such as the shear span to depth ratio, shear reinforcement ratio, concrete strength, and prestressing force. The proposed analytical model of crack geometry as well as the modified formula for crack width were expressed through a comprehensive analytical model which presents the interaction between crack progress, crack width and the stresses induced in concrete and reinforcement in both longitudinal and transverse directions. The model was also able to trace the failure mechanism and to evaluate the overall beam strength.

4

The reliability of the developed model was examined by comparing the results with the corresponding ones obtained from the experimental work presented herein, as well as from other experimental programs for concrete beams reinforced and/or prestressed with FRP bars (Park and Namaan 1999c; Shehata et al. 1999: Erki and Bakht 1996). A good agreement was observed between the analytical and the experimental results.

The strength value calculated by the formulas recommended by the current design guidelines for FRP-reinforced concrete structures (CHBDC 2000; ACI 1999; BIR 1997) was compared with the actual beam strength as well as with the beam strength obtained by the proposed analytical model. The comparison showed significant reliability and accuracy of the model results over the corresponding results of the currently available strength formulas.

1.3 Scope

A brief background of the research work related to the subject of the present study is given in Chapter 2.

Chapter 3 covers the details of the experimental program, including the specimen configurations, the material properties, the test set-up, and the observed beam behaviour.

The analytical model of crack path geometry, as well as the modified formula for crack width are explained in Chapters 4 and 5 respectively, including the comparison

between the analytical and the experimental results.

Chapter 6 presents the analytical modelling for the behaviour and strength of concrete beams reinforced and/or prestressed with FRP bars. This chapter also presents the verification process of the developed modelling.

Chapter 7 discusses the extension of the modelling to present the behaviour and strength of concrete beams reinforced in flexure with steel and/or FRP bars and reinforced in shear with FRP stirrups and/or FRP grids.

Chapter 8 identifies the influence of the accuracy of the analytical model of crack path geometry on the predicted beam strength.

The last chapter, Chapter 9, summarises the conclusions of the present research work.

Table 1-1: Typical ACM Properties, (Mufti et al. 1991)

	Modulus of Elasticity MPa (ksi)	Tensile Strength MPa (ksi)
Glass−epoxy	35.000 (5.080)	1050 (153)
Carbon−epoxy	180.000 (26.125)	1500 (218)
Aramid−epoxy	76.000 (11.030)	1400 (203)
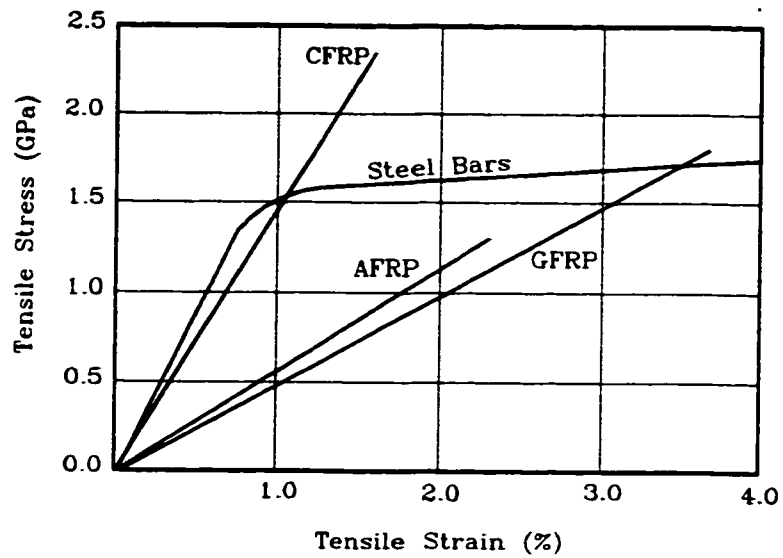
Fig. 1-1: Typical ACM Stress-Strain Curves, (Mufti et al. 1991).

7

CHAPTER 2

BACKGROUND AND LITERATURE REVIEW

2.1 General

Few research programs were conducted in the field of dowel action of reinforcement and/or shear-flexure interaction in reinforced concrete beams and very few of these programs dealt with FRP reinforcement. However, the published information that is related to the present research work is briefly discussed in this chapter.

2.2 Shear-Flexure Interaction

For a concrete beam reinforced in the longitudinal and transverse directions, both shear and flexural stresses are reflected in the principal stresses in concrete. The concrete remains uncracked as long as the principal tensile stress does not exceed the concrete modulus of rupture. After shear-flexure cracks develop within shear span, the beam resists the applied load at crack location through the following:

- compressive and shear stresses in concrete above crack,

- aggregate interlocking/friction at the interface of the crack surfaces,

- shear stresses in longitudinal reinforcement, i.e. dowel action, and

- tensile stresses in both longitudinal and shear reinforcement.

8

Hence, assuming enough anchorage and development of both longitudinal and shear reinforcement, the failure at a crack location has been attributed to one of the following

- compressive/shear failure of concrete.

- tensile failure of longitudinal reinforcement (flexural bars and/or prestressing tendons), and

- tensile failure of shear reinforcement.

Since the reinforcement mode of failure depends on the properties of the reinforcing material, the FRP bars suddenly rupture when failing in tension, i.e. brittle failure, while the failure of steel bars takes its path through yielding which leads to excessive deformations of the loaded beam, i.e. ductile failure (MacGregor 1988).

2.3 Forty-five Degrees Truss Model

The transfer of loads across a cracked section in reinforced concrete beam was expressed in term of a truss model. In this model (Fig. 2-1; where $\theta = 45°$), the diagonal compressed concrete portions act as the diagonal members of the truss, and the shear reinforcement, e.g. vertical stirrups, are the vertical members.

The top chord of the truss is formed by the upper concrete compression zone, while the longitudinal reinforcement acts as the bottom chord. A modification to this

model was introduced, in which the diagonal members were replaced by a continuous field of diagonal compression (Collins and Mitchell 1991; MacGregor 1988).

However, the model in its final form is based on the following assumptions

- The uncracked behaviour of beam is neglected.

- The tensile resistance of concrete in-between cracks is ignored.

- The diagonal cracks have constant slope of 45 degrees.

- The diagonal stresses are constant over the beam web area.

2.4 Variable Angle Truss Model

A reasonable modification was made to the 45-degree truss model as the inclination angle of the diagonal cracks was introduced as one of the model variables. Consequently, the three basic equilibrium equations of the model at a section subject to pure shear will have four unknowns (compressive force of upper chord, tensile force of lower chord, tensile force of diagonal member, and slope of diagonal member). Different solutions have been proposed by assuming a proper value of one of the unknowns based on a possible failure mechanisms (Collins and Mitchel 1991; MacGregor 1988).

For example, assuming a compressive failure of the concrete above crack, the value of the concrete principal compressive stress can be assumed to be the concrete compressive strength multiplied by a certain reduction factor and hence the three equilibrium equations can be solved to determine the remaining three unknowns.

However, the other assumptions of the original 45 degrees model remain unchanged (Fig. 2-1; where θ is variable).

2.5 ACI and CSA Simplified Method

For a concrete beam, the concrete resists the loads until cracks develop, then the reinforcement starts carrying the part of the load in excess of the cracked concrete strength. Currently, a semi-empirical term is applied in many reinforced concrete design codes including the ACI and CSA codes (ACI 1995 and CSA 1994) to account for this fact. This term is referred to as the "concrete contribution" and consequently the total shear resistance of the beam has two components; namely, the concrete contribution and the contribution of the shear reinforcement. It should be mentioned that for all cases, the shear reinforcement contribution term is calculated based on the 45-degree model. The codes also provide various expressions for the concrete contribution, to account for any normal force and/or prestressing force applied on the beam (e.g. for pre-stressed beams, the code limits the concrete contribution to the minimum value of the shear loads corresponding to the initiation of web-shear cracks and flexure-shear cracks).

2.6 Compression Field Theory

This theory is applicable, for any standard reinforced and/or prestressed concrete beam, at a section subject to pure shear. The theory considers five unknowns to be determined at such sections. These unknowns are as follows: the crack angle of

inclination, the principal stresses in concrete, the tensile stresses in longitudinal and shear reinforcement. Consequently, five equations are established to solve the five unknowns. The theory depends on the three basic equilibrium equations of the variable truss model and two more equations that can be obtained based on the strain compatibility conditions (Collins 1978; Collins and Mitchell 1980).

Some assumptions have been introduced to simplify the analytical modelling of the theory as follows

- the modelling equations deal with the average stresses and average strains for both concrete and reinforcement over the longitudinal and transverse beam sections,

- the beam behaviour before cracking as well as the tensile stresses induced in concrete in-between cracks have been neglected, and

- the cracks are uniformly distributed.

2.7 Modified Compression Field Theory (MCFT)

The modified theory is based on the same assumptions of dealing with sections under pure shear, with the average stresses and strains, and with uniform crack distribution. As an improvement over the Compression Field Theory, the MCFT considers both the cracked and the uncracked behaviour as well as the tension stiffening in concrete after cracking (Vecchio and Collins 1986).

As the pre-cracked concrete is usually softer than the regular case of a concrete cylinder loaded in compression due to the induced tensile stresses in the transverse direction, a stress-strain relationship of the diagonally cracked concrete has been proposed based on the tests done by Vecchio and Collins (1986) for reinforced concrete beams tested under pure shear (Figs. 2-2 and 2-3).

Recently, based on a study for shear-critical concrete beams (1999), Vecchio reported that these assumptions should be re-examined, especially for beams with little or no shear reinforcement. In such beams, the cracking pattern is dominated by few major cracks which may exceed several millimetres in width while the neighbouring cracks may remain of negligible width. It has also been observed that a considerable slip took place between the sides of major cracks. Consequently, the local stresses, as well as the flow of forces across the crack have an important influence on the beam behaviour and strength (Vecchio 1999).

It should be noted that the general method of the CSA-1984 standard was based on the Compression Field Theory, while in the CSA-1994 standard, this method is based on the Modified Compression Field Theory.

2.8 Shear-flexure Interaction from the Fracture Mechanics Perspective

When a transverse loading is applied to a simply supported reinforced concrete beam, shear force and bending moment develop in the beam. A biaxial state of stress is

created as a result of the moment-shear combination. Within a mid-span zone, cracks initiate at the bottom of beam web and they continue to propagate vertically since the shear stress is almost zero, while near support, some cracks turn into diagonal cracks as influenced by the shear stresses which induce diagonal tension in concrete. The shear resistance at the diagonal crack location is provided by the concrete zone above crack, the aggregate interlock along cracked surfaces, the dowel action of the longitudinal reinforcement, and the shear reinforcement resistance, if any (Surendra et al. 1995).

The researchers in this field established different fracture mechanics models to describe the diagonal shear failure in steel-reinforced concrete beams including some proposed modelling for the geometry of diagonal cracks. The major models are discussed briefly in the following paragraphs.

2.8.1 *Bazant and Kim Model*

Bazant and Kim (1984) studied the code formulas for diagonal shear failure of concrete beams reinforced in flexure and without shear reinforcement. They obtained some empirical constants statistically to establish their analytical model. The shear span and the flexural reinforcement ratio were considered major parameters of this model. This model was extended to cover the existence of shear reinforcement. However, the dowel action of the longitudinal reinforcement was not included.

2.8.2 *Jenq and Shah Model*

Jenq and Shah (1989) assumed the diagonal failure mechanism of a longitudinally reinforced concrete beam as shown in Fig. 2-4. Also, they assumed that a single diagonal linear crack is responsible for the diagonal failure of the beam, the inclination angle of the crack is around 45 degrees, and both the dowel action of the longitudinal reinforcement and the multiple tensile cracks in concrete were neglected. The model is applicable only for beams without shear reinforcement.

2.8.3 *Gustafsson and Hillerborg Model*

A Finite Element model was developed by Gustafsson and Hillerborg (1988) for a longitudinally reinforced concrete beam without shear reinforcement. Fracture mechanics concepts were imposed in the model to introduce the crack propagation with the increase of the applied loads. They assumed that concrete and longitudinal reinforcement are linear elastic materials, and a single diagonal crack leads to failure. Therefore, several potential crack paths should be checked. The possibility of a compressive failure of concrete above crack and/or a bond failure between flexure reinforcement and concrete at support can be indicated. The model neglects the aggregate interlock between crack surfaces as well as the dowel action of the longitudinal reinforcement.

2.9 Design Recommendations of Japan Society of Civil Engineers

The Japan Society of Civil Engineers, JSCE, issued design recommendations for concrete structures reinforced with ACM (1997). The recommendations related to the beams resisting shear forces can be summarised as follows:

- The total shear resistance is the sum of the concrete contribution and the shear reinforcement contribution. This concept is the same as followed for concrete beams reinforced with steel bars by most of the design codes (ACI 1995; CSA 1994). The shear resistance of concrete beams reinforced longitudinally with FRP bars, but with no shear reinforcement, can be evaluated according to the same equations used in case of steel reinforcement, taking into account the ratio of the modulus of elasticity of FRP to that of steel.

- For concrete beams reinforced longitudinally with FRP bars, and provided with shear reinforcement, the tensile strain induced in the shear reinforcement is influenced by the rigidity of longitudinal reinforcement, shear reinforcement, concrete compressive strength, and axial force, if any.

- The rigidity of longitudinal and shear reinforcement affects not only the tensile strain induced in the shear reinforcement but also the beam failure mode. As this rigidity increases, the failure mode of the concrete above crack shifts from diagonal tensile failure to compressive failure. In other words, the

16

shear force carried by concrete decreases as the reinforcement rigidity increases.

- Providing the beam with axial compressive force, as in case of prestressed beam, has a similar effect to that of increasing the rigidity of reinforcement.

- As the modulus of elasticity of FRP, regardless the FRP type, is less than that of steel, the width of diagonal cracking of the concrete beams reinforced with FRP is more than that of beams reinforced with steel. The tensile strains in concrete in-between these wide cracks increase leading to an actual compressive strength of concrete in-between cracks that is much less than that obtained by the tested standard cylinders as reported by Vecchio and Collins (1986), refer to Section 2-7. This reduction of compressive strength affects the shear load carrying capacity as well.

One of the recent comprehensive Japanese research works has been carried out by the research committee on FRP-reinforced concrete structures organised by the Building Institute for Research, BIR, of the Japanese Ministry of Construction. The committee issued a report, "Design Guidelines of FRP-Reinforced Concrete Building Structures" in 1997. The report recommends the following formula, which is based on Arakawa's Equation (AIJ 1988):

For steel-reinforced concrete beams:

$$V_n = b_w \, j \left[\frac{0.115 \, k_u \, k_p \left(f_c' + 180 \right)}{\dfrac{M}{V \, d} + 0.12} + 2.7 \sqrt{\rho_{sh} \, f_y} \right] \quad \text{(kgf-cm units)} \quad (2\text{-}1)$$

where b_w = width of beam web; d = beam depth; f_c' = concrete compressive strength; f_y = yield stress of steel reinforcement; j = distance between the centres of tension and compression ($\approx 7d/8$); k_p = coefficient depends on ρ_f [=0.82 $(100\rho_f)^{0.23}$]; k_u = coefficient depends on d [=0.72 for $d \geq 40$cm]; M = Bending moment at the beam section under consideration; V = Shear force at the beam section under consideration; ρ_f = flexure reinforcement ratio; and ρ_{sh} = shear reinforcement ratio.

For FRP-reinforced concrete beams:

$$V_n = \left[0.8 \, V_{n1} \right] \text{ or } \left[0.9 \, V_{n2} \right] \quad \textit{whichever is less} \quad (2\text{-}2)$$

$$V_{n1} = b_w \, j \left[\frac{0.115 \, k_u \, k_p' \left(f_c' + 180 \right)}{\dfrac{M}{V \, d} + 0.12} + 2.7 \sqrt{\rho_{sh} \, f_{sh}'} \right] \quad \text{(kgf-cm units)} \quad (2\text{-}3)$$

$$V_{n2} = b_w \, j \left[\frac{0.115 \, k_u \, k_p' \left(f_c' + 180 \right)}{\dfrac{M}{V \, d} + 0.12} + 2.7 \sqrt{\rho_{sh}' \, f_{sh}'} \right] \quad \text{(kgf-cm units)} \quad (2\text{-}4)$$

where E_f = modulus of elasticity of flexure reinforcement; E_s = modulus of elasticity of steel; E_{sh} = modulus of elasticity of shear reinforcement; f_{sh}' = tensile

strength of shear reinforcement; k_p' = equivalent coefficient depends on ρ_f [=0.82 (100ρ_f E_f / E_s)$^{0.23}$]; V_{n1} = shear strength corresponds to stirrups rupture; V_{n2} = shear strength corresponds to concrete compressive failure; ρ_{sh}' = equivalent shear reinforcement ratio [=ρ_{sh} (E_{sh} / E_s)].

It should be mentioned that in Equations 2-1 to 2-4, the dimensions are in (cm), the forces are in (kgf) which is equivalent to (9.8 N), and the stresses are in (kgf/cm^2) which is equivalent to (0.098 MPa).

2.10 Design Recommendations of American Concrete Institute

The American Concrete Institute (ACI-Committee 440H, 1999) issued design recommendations for concrete structures reinforced with FRP. The formulas recommended to calculate the flexural and shear strength of concrete beams reinforced longitudinally and/or transversally with FRP bars are listed in the following paragraphs.

Similar to steel-reinforced concrete beams, the balanced flexure reinforcement ratio, $\rho_{f,b}$, required to introduce compressive concrete failure, i.e. concrete compressive strain reaches its ultimate value, ε_{cu}, when the tensile stress in this reinforcement, f_f, reaches its tensile strength, f_f', can be expressed as follows (US-units):

$$\rho_{f,b} = 0.85\beta_1 \frac{f_c'}{f_f'} \frac{E_f \, \varepsilon_{cu}}{E_f \, \varepsilon_{cu} + f_f'} \tag{2-5}$$

As the compressive failure in concrete is more ductile than the tensile failure of

FRP bars, the committee recommended that the actual flexural reinforcement ratio, ρ_f, to be as follows:

$$\rho_f \geq 1.33 \rho_{f,b}$$ (2-6)

Therefore, the section is classified as over-reinforced section where its flexure strength, M_n, can be calculated as follows:

$$M_n = \rho_f \, f_f \left(1 - 0.59 \frac{\rho_f \, f_f}{f_c'} \right) b \, d^2$$ (2-7)

The corresponding tensile stress in the flexural reinforcement, f_f, at failure can be obtained from the following equation:

$$f_f = \sqrt{\left(0.85 \beta_1 \frac{f_c' \, E_f \, \varepsilon_{cu}}{\rho_f} + \frac{\left(E_f \, \varepsilon_{cu} \right)^2}{4} \right)} - \frac{E_f \, \varepsilon_{cu}}{2}$$ (2-8)

Also, similar to steel-reinforced concrete beams, the shear strength, V_n, consists of two components; the concrete contribution, V_{cr}, and the shear reinforcement contribution, V_{sh}, as follows:

$$V_n = V_{cr} + V_{sh}$$ (2-9)

$$V_{cr} = \left(K' \, \sqrt{f_c'} \, b_w \, d \right)$$ (2-10)

$$V_{sh} = \frac{A_{sh} \, \varepsilon_{sh} \, E_{sh} \, d}{S} \leq 8 \sqrt{f_c'} \, b_w \, d$$ (2-11)

$$\varepsilon_{sh} = [0.002] \, or \left(0.05 \frac{r}{d_b} + 0.3 \right) \frac{f_{sh}}{E_{sh}} \quad whichever \ is \ less$$ (2-12)

where: A_{sh} = cross-sectional area of shear reinforcement within the distance S; d_b = diameter of stirrup bar; K' = modified shear strength constant ($=K^* E_f / E_s$); K = shear strength constant for steel-reinforced concrete beams ($=2$); r = bend raduis of the stirrup

bar; S_{sh} = Spacing between two successive stirrups; and ε_{sh} = tensile strain of shear reinforcement.

Goodspeed and Yost (1994) imposed the effect of both flexural reinforcement ratio, ρ_f, and modular ratio (E_{sh}/E_s) on the concrete contribution as follows:

$$K' = 0.8 + 200\, \rho_f\, \frac{E_f}{E_s}\, \frac{E_{sh}}{E_s}\, \leq 1.4 \tag{2-13}$$

Also Goodspeed and Yost (199) found that the most accurate results obtained from the above equation were when ρ_f ranged between 0.60% and 0.32%.

2.11 Canadian Bridge Design Code Provisions for Fibre-Reinforced Structures

For concrete beams reinforced with FRP bars and reinforced in shear with steel or FRP stirrups, the general design method for shear approved by the Canadian code for the design of concrete structures (CSA 1994) is still applicable with few modifications as follows (CHBDC 2000) (SI-units):

$$V_n = V_{cr} + V_{sh} \qquad ; \qquad V_n \leq 0.25\, \phi_c\, f_c'\, b_w\, d \tag{2-14}$$

$$V_{cr} = 1.3\, \phi_c\, \beta\, \sqrt{f_c'}\, b_w\, d \tag{2-15}$$

$$V_{sh} = \frac{A_{sh}\, \varepsilon_{sh}\, E_{sh}\, d}{S}\, \cot\theta \tag{2-16}$$

Where ε_{sh} equals the steel yield strain, ε_y, for steel stirrups while for FRP stirrups, the value of ε_{sh} to be calculated as follows:

$$\varepsilon_{sh} = \left[0.0001 \sqrt{f_c' \frac{\rho_f E_f}{\rho_{sh} E_{sh}}} \right] or \left[\frac{f_{sh}'}{E_{sh}} \left(0.05 \frac{r}{d_b} + 0.3 \right) \right] or\, [0.002] \quad whichever\ is\ less \tag{2-17}$$

2.12 Shear Transfer in Concrete Reinforced with FRP Bars

The research work done by Tomaszewicz and Markeset (1991) included an experimental programme carried out on push-off tests. The specimens were divided into two groups: the first one consisted of specimens with pre-cracked sections while the second group consisted of specimens with idealised smooth low-friction shear planes. All the specimens were provided with FRP reinforcing bars crossing the crack in the direction perpendicular to the shear plane (Fig. 2-5).

It was observed that most of the pre-cracked specimens reached their ultimate shear capacity corresponding to a sliding of about 2 mm (0.078 in) measured in the direction parallel to the shear plane, i.e. relative vertical displacement between the two sides of the cracked section. The study did not formulate a general recommendation for the design of concrete beams reinforced with FRP due to the limited results of the tested specimens.

However, it was proposed to modify the conventional methods developed for steel reinforcement to impose the different failure mode observed in case of FRP reinforcement, such as the sudden breaking of fibres observed at the dowel failure of the specimens reinforced with FRP bars. This brittle failure mode is different from the ductile failure of steel that allows for considerable deformations within the yielding phase before the complete failure of the reinforced concrete element.

2.13 Dowel Behaviour of FRP Tendons

Park and Namaan (1999a; 1999b) investigated the behaviour of Carbon Fibre Reinforced Polymer (CFRP) tendons subjected to both shear and tensile stresses. This work included testing concrete specimens reinforced with CFRP tendons with different levels of prestressing, see Fig. 2-6. The effect of parameters such as the initial prestressing force, concrete strength, using stirrups, and adding fibres to the concrete mix were studied with respect to the induced shear displacement of the tendons. Based on this research work, the following conclusions were reached:

- CFRP tendons subjected to combined prestressing force and shear displacement show the ultimate dowel force of the tendon to decrease elliptically as the tensile force increases. Also the ultimate dowel shear displacement decreases linearly with the increase of the tensile force.

- The effect of adding fibres to concrete or providing the specimens with stirrups is similar to that of increasing the concrete strength and leads to an increase in the shear displacement and shear strength.

It was also found that this failure can be expressed by a combination of the Tsai-Hill failure criterion and the Beam on Elastic Foundation (BEF) (Park and Namaan 1999b). This combination was adjusted to take into consideration the concrete subgrade stiffness, i.e. concrete stiffness corresponding to the induced shear displacement. Some modifications introduced to this combination have been also proposed to take into

account the cable effect of the tendons, i.e. the resisting reaction of the tensioned tendon due to the change of its curvature. Accordingly, the FRP tendon failed when the value of the failure factor, F, reaches 1.0. This factor is expressed as follows:

$$F = \sqrt{\left(\frac{f}{f'}\right)^2 + \left(\frac{v}{v'}\right)^2} \qquad (2\text{-}18)$$

where: f and v are the tensile and shear stresses induced in the FRP tendon; and f' and v' are the ultimate tensile and shear stresses of the FRP tendon.

2.14 Diagonal Crack Width in FRP-Reinforced Concrete Beams:

Hassan (1991) developed a formula to express the relationship between the diagonal crack width and the tensile strain induced in the stirrups crossing the crack. The formula was verified for concrete beams reinforced longitudinally with FRP bars and in shear with steel stirrups. This formula is as follows (N-mm units):

$$W_{sh} = \frac{1.8 \, S_d \, d_b}{10^6 \, K_{fc} \, \rho_{sh}^{1.3}} \qquad (2\text{-}19)$$

$$K_{fc} = \left(\frac{f_c'}{19.6}\right)^{2/3} \qquad (2\text{-}20); \qquad S_d = 8 \times 10^3 \varepsilon_{sh} + 2 \times 10^6 \varepsilon_{sh}^2 \qquad (2\text{-}21)$$

where: K_{fc} = constant based on the concrete compressive strength; S_d = slip of the stirrup crossing the crack.

Based on the experimental program carried out by Mizukawa et al. (1997), which studied the behaviour of concrete beams reinforced longitudinally with FRP bars and transverally with steel/FRP stirrups, it was found out that Equation 2-19 introduced

accurate results only when using steel stirrups, for which this equation was originally developed, while it should be modified when using FRP stirrups to account for the difference between FRP and steel regarding the mechanical properties as well as the bond characteristics (Mizukawa et al. 1997).

2.15 Maximum Crack width

In 1968, Gergely and Lutz developed a formula to predict the maximum crack width in concrete beams reinforced with steel bars as follows:

$$W_{max} = 0.076 \times 10^{-3} \beta \, f \, \sqrt[3]{d_c \, A_1} \qquad ; \text{(kip-inch units)} \qquad (2\text{-}22)$$

Where: A_1 = tension area per bar; d_c = concrete cover of outer most bar measured from the center of that bar; f = tensile stress in longitudinal bars; W_{max} = maximum crack width measured at the extreme beam bottom level; and β = ratio of distances to the neutral axis from the extreme beam bottom level and from the c.g. of longitudinal bars.

A report published in 1972 (ACI Committee 224) covered most of the research work done to study the cracking behaviour and the formulas developed to predict crack width of both nonprestressed and prestressed concrete beams. In this report, Equation 2-22 was presented to calculate the crack width for concrete beams prestressed with steel tendons taking into account that the term (f) should be replaced by the difference between the stress induced in tendons at the specified loading level, f_2, and the stress induced in

tendons corresponding to either initial cracking moment or the decompression condition, f_l, i.e. the stress in concrete at extreme bottom beam level is zero.

The report recommended that this formula should be modified to account for the surface properties of the tendons, i.e. bond characteristics between the tendons and concrete. It was also mentioned that in the case of multi-layered steel tendons where the extreme bottom tendons experience yielding, the effective concrete cover, d_c, depends on the distance to the nearest elastic tendons.

In 1974, Lutz modified Equation 2-22 to consider the effect of bundled steel bars. The basic idea was to express the difference between the actual perimeter of the bundle and that of its individual bars. One of the proposed approaches was to calculate the equivalent number of steel bars that have the same diameter of the bundle bars and the actual perimeter of the bundle. This number is used to obtain the value of (A_l).

Recently, Faza and Gangarao (1993) proposed to apply Equation 2-22 to predict the maximum crack width of concrete beams reinforced with FRP bars, taking into account the effect of the relative low value of the modulus of elasticity of FRP bars with respect to that of steel in increasing the crack width at the same stress level as follows:

$$W_{max} = 0.076 \times 10^{-3} \beta f \frac{E_s}{E_f} \sqrt[3]{d_c A_l} \qquad ; \text{(kip-inch units)} \qquad (2\text{-}23)$$

Where: E_f = modulus of elasticity of FRP bars; and E_s = modulus of elasticity of steel.

Also, Faza and Gangarao (1993) proposed to use another formula that takes into account the effect of the FRP bars bond characteristics on crack spacing and consequently on the maximum crack width. For this formula, the crack spacing, S_c, has been expressed as follows:

$$S_c = \frac{2\,f_{ct}'\,A_1}{u_{u.f}\,\pi\,d_b}$$

(2-24)

where: $f_{c.t}'$ = concrete tensile strength; and $u_{u.f}$ = FRP bars bond strength.

The maximum crack width can be defined as the elongation of the longitudinal bars segment in between the formed cracks, i.e. the bars segment of a length equals S_c and subject to an average strain equals (f/E_f), the maximum crack width can be calculated as:

$$W_{max} = \frac{2\,f_{ct}'\,f\,A_1}{u_{u.f}\,\pi\,d_b\,E_f}$$

(2-25)

Both formulas, presented in Equations 2-23 and 2-25, were verified for concrete beams reinforced with Glass Fiber Reinforced Polymers (GFRP) bars that had a ratio of (E_s/E_f) equals approximately 4.0 (Faza and Gangarao, 1993).

In 1999, another formula to calculate the maximum crack width for FRP reinforced concrete beams was proposed by Toutanji and Saafi. This formula is as follows:

$$W_{max} = \frac{2f}{E_f} \left\{ d_o + A_o * \tanh \left(\cosh^{-1} \sqrt{\frac{f}{\left(f - \frac{f_{ct}}{\rho_{ft}}\right)}} \right) \right\} \quad ; \text{(SI-units)} \qquad (2\text{-}26)$$

Where:

$$A_o = 70 + f * e^{\left(0.479 - 0.214*(f_c')^{2/3}\right)} \qquad (2\text{-}27)$$

d_o = factor based on the concrete compressive strength, f_c', and the tensile stress in the bars, f ; ρ_{ft} = FRP bars ratio based on the effective tension area of concrete surrounding the bars and having the same centroid.

$$jd/\cos\theta$$

$$M=0.0$$

$$f_2$$

$$v=V/(b_w \cdot jd)$$
$$f_2 = v/\text{sine}$$
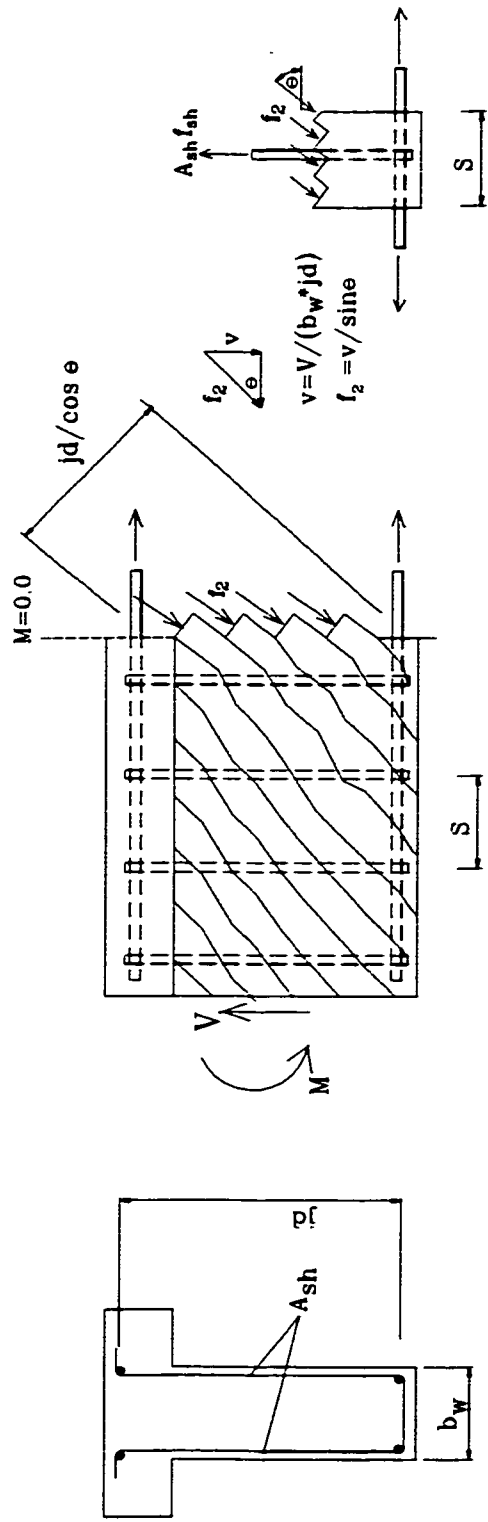
(a) Cross Section

(b) Longitudinal Elevation

(c) Force in Stirrups

Fig. 2-1: Equilibrium Conditions for Truss Models.

$$f_c = f_c' \left[\frac{2\varepsilon_c}{\varepsilon_o'} - \left(\frac{\varepsilon_c}{\varepsilon_c'} \right)^2 \right]$$
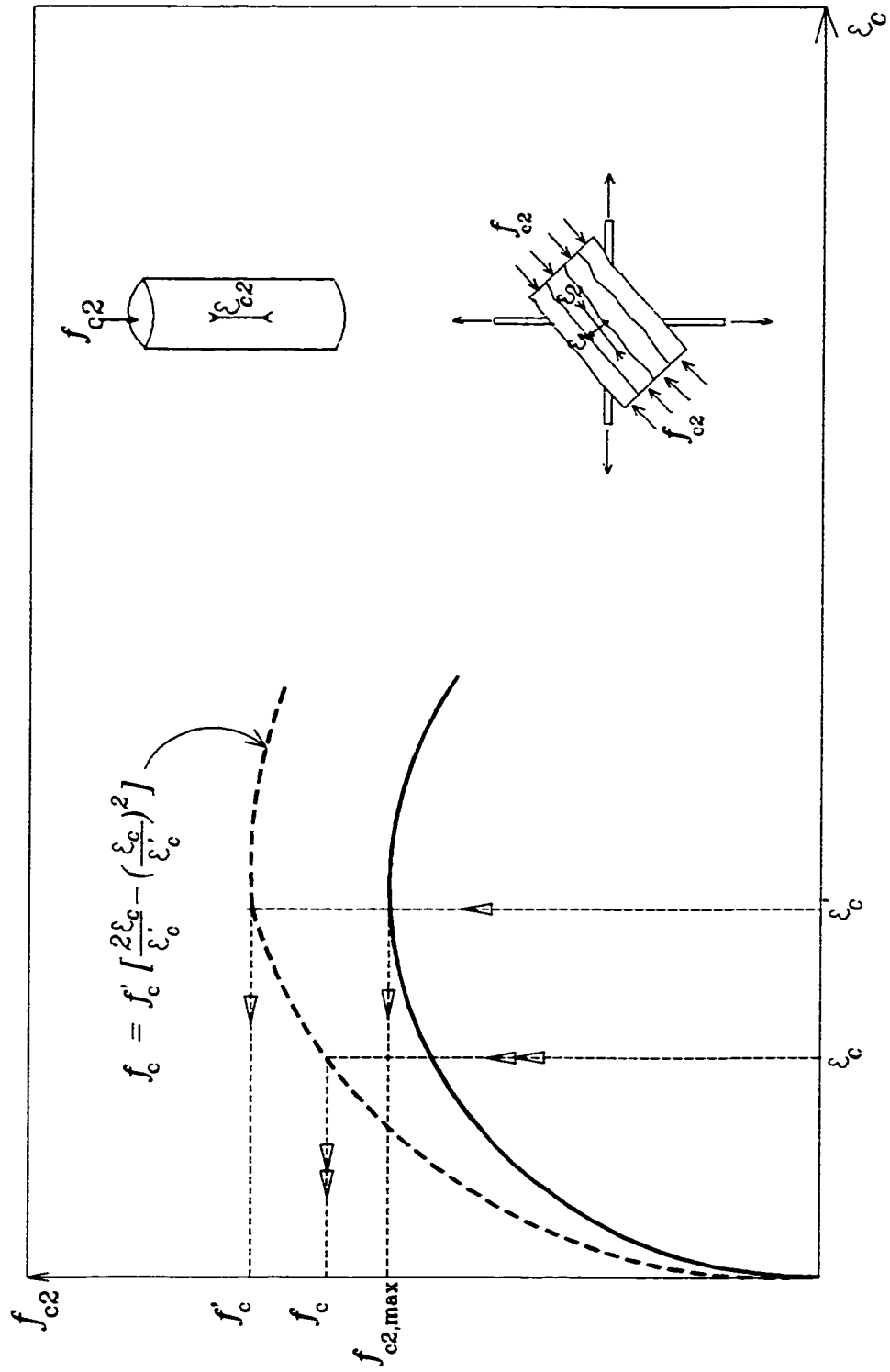
Fig. 2-2: Stress-Strain Curve for Cracked Concrete in Compression.

(a) Cross Section

(b) Principal Stresses in Concrete

(c) Force in Stirrups

$v = V / (b_w * jd)$

$f_2 = v / \sin \theta$
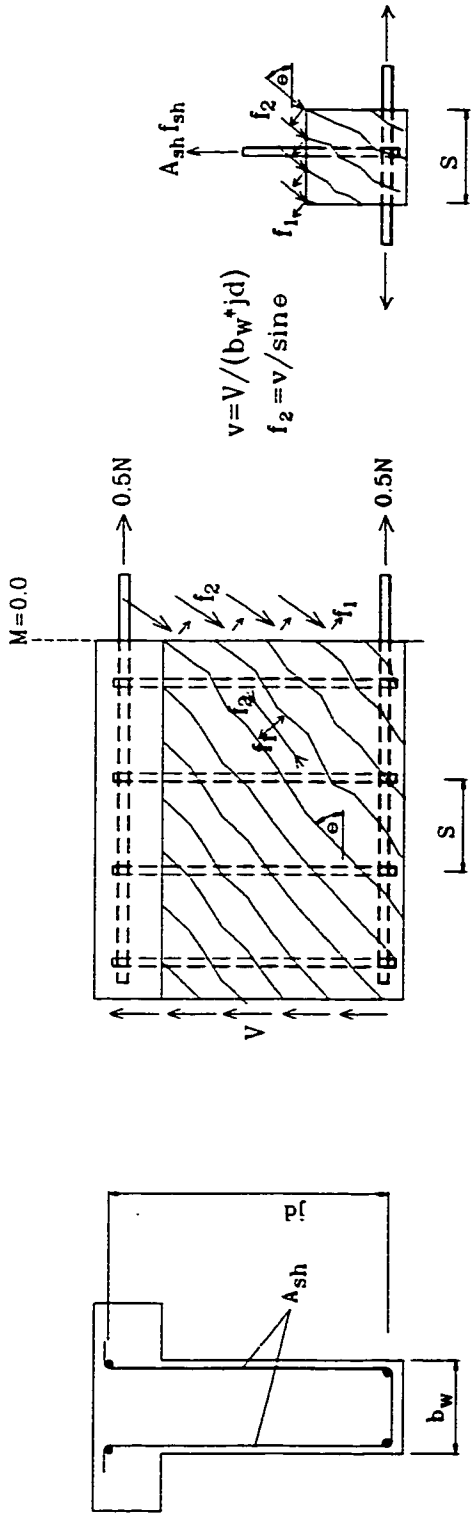
Fig. 2-3: Equilibrium Conditions for the Modified Compression Field Theory.
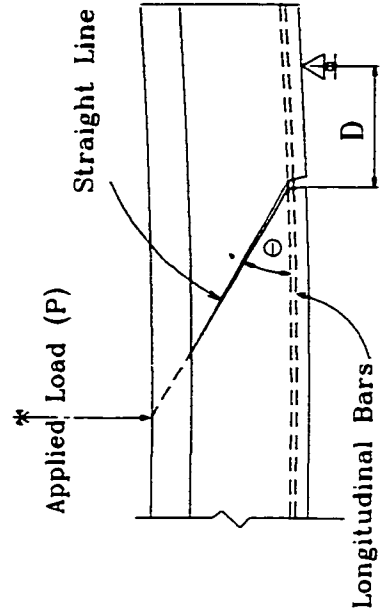
Fig. 2-4: Modelling of Diagonal Crack, (Surendra et al. 1995).

31
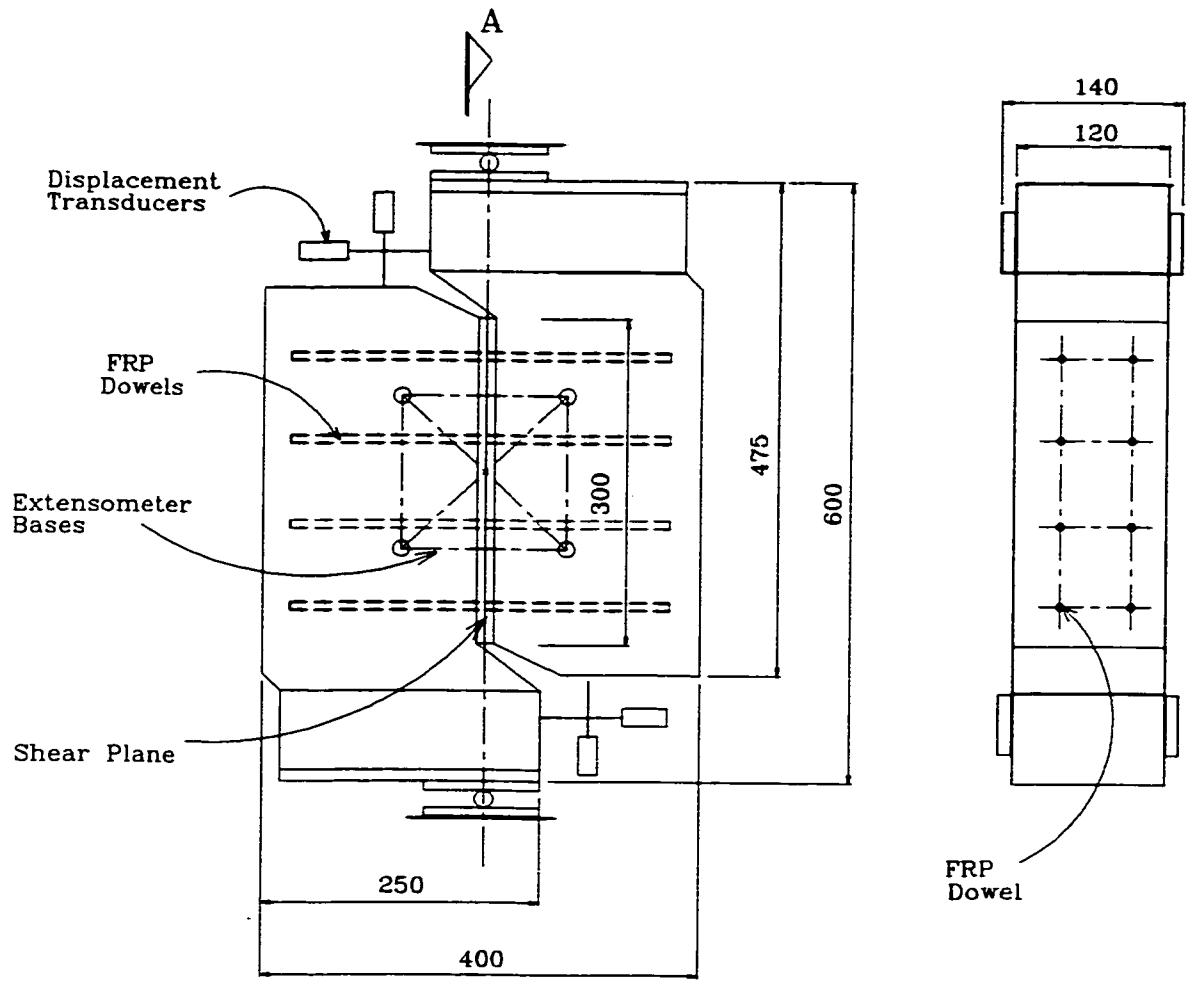
(a) Longitudinal Elevation   (b) Cross Sec. A—A.

Fig. 2-5: Specimen Configuration and Instrumentation, (Tomaszewicz and Markeset. 1997).
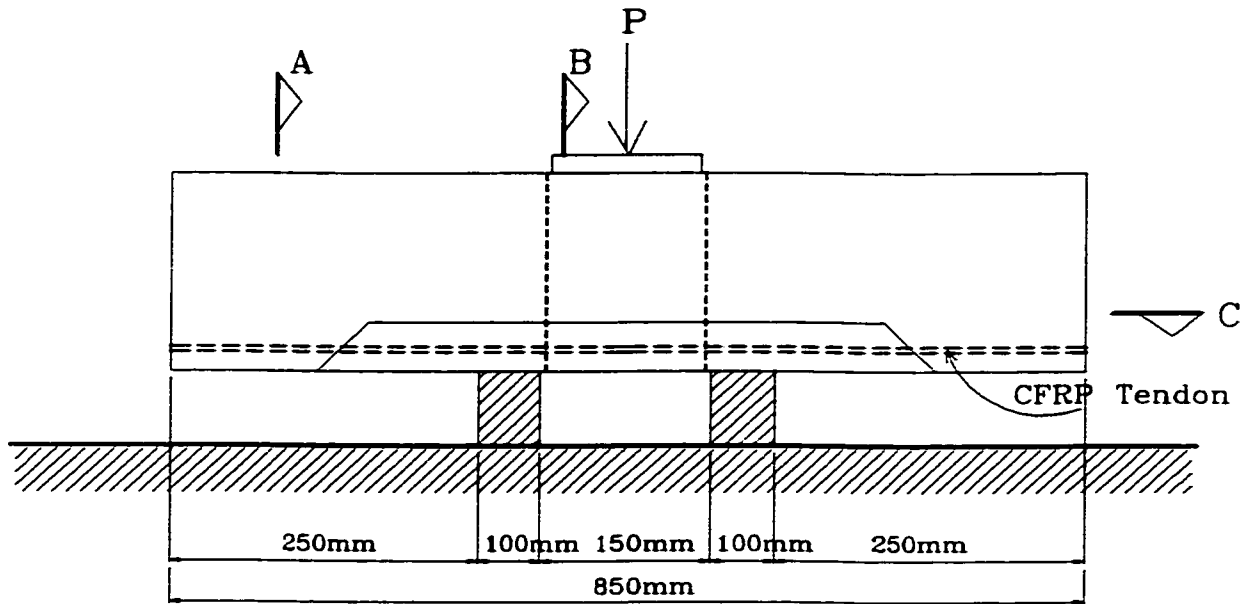
(a) Longitudinal Elevation.
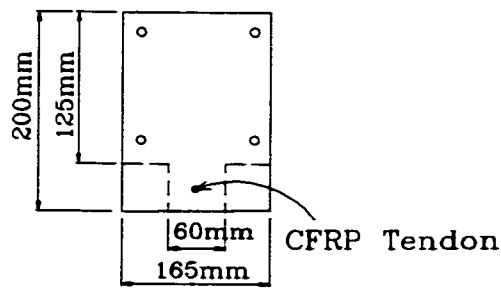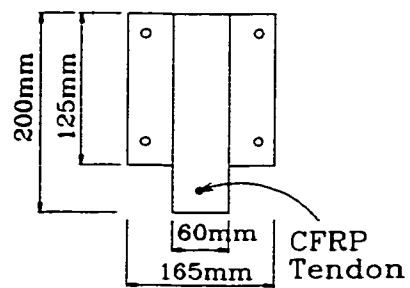
(b) Section A–A.   *(c) Section B–B.*
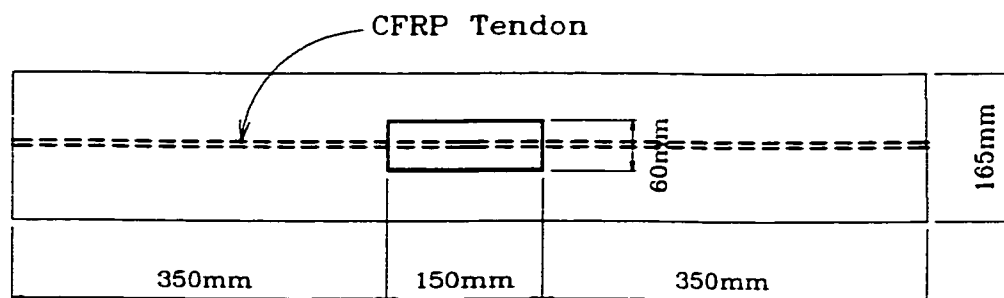
(d) Section C–C.

Fig. 2-6: Specimen Configuration and Test Set-up, (Park and Naaman 1999a).

33

CHAPTER 3

EXPERIMENTAL WORK

3.1 General

The experimental program discussed herein was carried out at the University of Windsor in two phases. The first phase was dedicated to the determination of the mechanical properties of the CFRP bars used in this experimental work (e.g. modulus of elasticity and tensile strength) (Abdel-Sayed et al. 1998). Bar samples of different diameters were also tested under direct shear loads to investigate their properties in the transverse direction. The test set-up as well as the relationship between the applied shear load and the corresponding shear displacement are shown in Figs. 3-1 to 3-4.

The bond characteristics between CFRP bars and concrete were also investigated through testing concrete beams reinforced in flexure with CFRP bars. These beams were designed and tested with special provisions to accommodate the gauges required to record the initiation of the bond failure between bars and concrete up to the complete failure of the beam. The main conclusion for the bond strength of these bars has been expressed as follows (Abdel-Sayed et al. 1998):

$$u_{u,f} = (I_{b,f} \ \sqrt{f_c'}) \ / \ d_b \leq \ 3.2 \ \text{MPa (470 psi)} \qquad (3\text{-}1)$$

where the FRP bars bond strength index, $I_{b,f}$, was obtained as 2.45 for the tested bars.

The second phase of the experimental program was the main part related to the present study and it is discussed in detail throughout this chapter. This phase was conducted to evaluate the behaviour and strength of both prestressed and nonprestressed concrete beams reinforced in flexure with CFRP bars under static loading conditions.

The main parameters investigated in this study were the geometry of crack path, crack width, and the properties of FRP bars in their transverse direction. The influence of varying other parameters such as shear span to depth ratio and shear reinforcement ratio were also investigated.

3.2 Test Specimens

3.2.1 Design of the Specimens

A total of eighteen concrete T-beams were tested in this phase: seventeen beams were reinforced in flexure with CFRP bars, and one beam with conventional steel bars. Regarding the prestressing and the shear reinforcement conditions, five beams were neither prestressed nor provided with shear reinforcement, six beams were not prestressed but provided with shear reinforcement, three beams were prestressed but not provided with shear reinforcement, and four beams were both prestressed and provided with shear reinforcement (Table 3-1).

While all of them were simply supported, fifteen beams were 3.66 m (12.0 ft.)

long, and two beams were 1.83 m (6.0 ft.) long. The clear span between supports was varied corresponding to the over-hung beam portions at beam ends in order to satisfy the designed shear span to depth ratio and/or the bond requirements of the reinforcing bars. The typical cross section dimensions and reinforcement details of the tested beams are shown in Fig. 3-5 and listed in Table 3-1. It should be mentioned that the beams missing from Table 3-1 (e.g. beam # 1 and 4 to 7) were the beams tested for bond during phase (I) in order to achieve the relationship expressed by Equation 3-1.

Beam # 24 was a special beam, as it was neither prestressed nor provided with shear reinforcement while it was reinforced in flexure with two bottom CFRP bars, besides an additional longitudinal CFRP bar at a height of 139.7 mm (5.5 in) measured from beam bottom. The idea behind this test was to study the effect of having longitudinal reinforcement of CFRP bars at different levels on the beam behaviour, in general, the crack formation characteristics, and the dowel action of the longitudinal reinforcement, in particular. In addition, the test would give an indication about the behaviour of concrete beams both prestressed and reinforced in flexure with CFRP bars.

3.2.2 Loading Set-up

Fig. 3-6 illustrates the loading set-ups selected for the tested beams. Set-up (I) for one concentrated load at mid-span and set-up (II) for two concentrated loads symmetrical about mid-span section. The corresponding values of the dimensions a, b, and Lp shown in Fig. 3-6 are listed in Table 3-1.

3.3 Material Properties

3.3.1 Concrete

The early strength concrete mix was designed for a compressive strength that ranged between 30 MPa (4.4 ksi) and 45 MPa (6.5 ksi) at 7 days after the concrete was cast. Three standard cylinders of the same concrete mix were tested in compression on the day of beam testing for nonprestressed beams, and on the day of releasing the tendons for prestressed beams (Fig. 3-7).

3.3.2 CFRP Bars

The mechanical properties of the CFRP bars used as flexural reinforcement in sixteen tested beams were evaluated during the first phase of the experimental program (Abdel-Sayed et al. 1998). These properties were as follows: the modulus of elasticity equals 158 GPa (23,000 ksi), and the tensile strength is 1655 MPa (240 ksi). The bond strength between these bars and concrete is 3.2 MPa (470 psi). The shear strength is 110 MPa (16 ksi) which corresponds to an ultimate shear displacement of 2.0 mm (0.078 in).

3.3.3 Mild Steel Bars

The stirrups as well as the top bars, i.e. stirrup hangers, were made of mild steel bars for beams provided with shear reinforcement. The stirrups were of diameters 10.0 mm (0.39 in) and 6.0 mm (0.24 in) while the hangers were of diameter 10.0 mm (0.39 in). The same type of bars were used as flexural reinforcement for beam # 21 (Table 3-1). The tensile strength of these bars was obtained in the laboratory as 413 MPa (60 ksi).

3.3.4 High Tensile Steel Bars

The tendons used for prestressed beams were high tensile steel bars, diameter 6.0 mm (0.24 in). Three samples of these bars were tested under tensile forces in the laboratory and the average value of their tensile strength was 1860 MPa (270 ksi).

3.4 Fabrication of the Specimen

3.4.1 Preparation of the Form

The beam forms were fabricated at the workshop of the University of Windsor. The form with its full size was used for most of the beams tested in the second phase of this experimental program. The same form can be divided into two similar forms of half span of the full size. The smaller forms were used for the beams tested to evaluate the bond characteristics between CFRP bars and concrete during the first phase of the program, as well as for beam # 35 and # 36.

Before placing the reinforcement, the form was cleaned and lubricated with proper release agent. When a beam was provided with shear reinforcement, stirrups were tied to the top bars at the designed spacing. The steel cage was placed in the form resting on steel spacers to achieve the required concrete cover, then the flexural reinforcement was inserted from pre-punched holes in the form end sides through the cage to allow for an exposed part of each bar of about 100 mm (4 in) outside each beam end. The flexural reinforcement was tied to the stirrups to ensure uniform spacing and verticality of the stirrups during concrete casting (Fig. 3-8).

3.4.2 Concrete Casting and Curing

The concrete ingredients were mixed by a concrete mixer in the laboratory of the University of Windsor. Concrete vibrators were used while casting, to avoid any surface voids or honeycombing. At the same time, standard size concrete cylinders were cast of the same mix. Both beams and cylinders were cured by moistening the concrete twice a day. Thereafter, the concrete was covered with plastic sheets.

3.4.3 Prestressing Procedure

The prestressing was applied to high tensile steel tendons located at the centroid of the beam cross section. The reason behind that was to place the tendon as far as possible from the beam bottom level in order to limit the interference between the dowel action of the steel tendons and that of the CFRP bars used as flexural reinforcement.

The tendon was inserted in the form through pre-punched holes in the form sides, then it was anchored from one end and the jacking force was applied from the other end by means of hydraulic jack. This force, i.e. initial prestressing, corresponded to 70% of the tendon tensile strength. The prestressing platform is shown in Fig. 3-9. The jacking force was checked by the pressure gauge of the hydraulic pump and the strain gauges attached to the tendon. Three standard cylinders of the same concrete mix were tested after seven days of casting to make sure that the specified compressive strength had been developed. Once this condition was satisfied, the jacking force was released.

3.5 Testing Procedure

3.5.1 Test Set-up

After the formwork was removed, the beam was moved to the testing platform. For all the tested beams, except for beam #3, # 35, and # 36, the beam rested from both sides on solid steel cylinders. At one side, the cylinder lay in a v-notch groove in a steel base plate. At the other side, the cylinder was able to roll on a horizontal flat base plate. Each base plate was fixed to a steel block underneath, which was also fixed to the testing platform. The loading system included a load cell of 222.4 kN (50.0 kips) capacity that was placed between the machine actuator and the spherical loading head. A thick steel plate, with a proper groove to accommodate the loading head, was used to transfer the load from the head to the beam below. For beams with set-up (I), this plate was located on the top of the beam flange and centred with the beam mid-span section.

In order to apply the load on beams with set-up (II) at the designed loading points, a system of a steel spreader beam and two steel pins was used. The loading head plate was placed on the spreader beam while the pins were in-between the bottom of this beam and the top of the tested beam flange. The proper alignment of the tested beam, the supports, and the loading system with respect to the axis of the testing machine was achieved during the test set-up. For safety purposes, some of the tested beams were provided with lateral supports from each side at the beam mid-span.

For beams # 3, # 35, and # 36, special supports were designed and fabricated to simulate the supports when the beam was hung by ties, see Figs. 3-12, 3-27, and 3-28. This set-up has been selected to study the effect of changing support conditions on crack geometry and bond between flexural reinforcement and concrete as well as on the overall beam behaviour and strength.

3.5.2 Test measurements

3.5.2.1 Strain Measurements

For prestressed beams, two strain gauges were attached to the tendon before applying any prestressing to make sure of attaining the required jacking force during the prestressing process.

3.5.2.2 Crack Progress Measurements

The path profile of the major cracks was recorded by measuring the coordinates of the points on the crack path profile with respect to a Cartesian system of coordinates that originates at the bottom corner of the nearest beam end to the developed crack.

3.5.2.3 Other measurements

Dial gauges were fixed to each of the exposed portions of flexural reinforcement bars at each beam end as shown in Fig. 3-10. The gauge sliding pin was oriented in a parallel position to the bars, allowing its free end to contact the concrete surrounding the bars. The function of these dial gauges was to measure any relative displacement between the bars and concrete, indicating any initiation of a bond failure of the flexural reinforcement. The maximum crack width, W_{max}, has been measured for the flexure cracks formed in beam # 35 and # 36 by a digital vernier with an accuracy of 0.01 mm.

3.5.3 Testing

Each beam was properly aligned and levelled, strain gauges were connected to the strain reading monitors and checked before the beginning of the test (Fig. 3-10). Static loading was applied to the beam through the hydraulic loading jack, and the load value was checked by the load cell monitor. The load was applied through increments of 4.45 kN (1.0 kip) and the time between two successive increments was about two minutes.

This time was required to record the measurements, to mark up the crack tip with the applied load value, to specify the crack tip location, to measure the maximum crack width for some beams, and to record the overall cracking pattern by means of photographs. The dial gauges connected to the exposed portion of the reinforcing bars

were continuously monitored to check for any possible slip. The loading rate was reduced into smaller increments of 2.22 kN (0.5 kip) when either one of the major cracks approached the beam flange or the applied load approached an expected failure load

3.6 Observed Behaviour

3.6.1 Beam # 2

Flexure cracks initiated at an applied load of 17.8 kN (4.0 kips), at the beam mid-span. Increasing the applied load, shear-flexure cracks were developed within the shear span (i.e. distance Lp). When the load reached 31.2 kN (7.0 kips), one of the flexure-shear cracks became a major crack, i.e. it widened and progressed faster with respect to the neighbouring cracks. This crack initiated at a distance 1097 mm (43.0 in) from the nearest beam edge.

The crack almost reached the flange at a load of 40.1 kN (9.0 kips) and suddenly at a load of 44.5 kN (10.0 kips), the CFRP bars crossing the crack ruptured in a brittle failure mode. As soon as the CFRP bars failed, a complete separation between the beam segments on both sides the crack took place as shown in Fig. 3-11. At the failure crack location, the bars had an appearance similar to the samples tested under direct shear loads.

3.6.2 Beam # 3

A behaviour similar to that of beam # 2 was observed for this beam except that the major crack initiated at a distance 685 mm (27.0 in) from the nearest beam edge. At a load of 44.5 kN (10.0 kips), a new crack started from the original crack profile at the level of the flexural reinforcement, progressing towards the nearest support.

As the applied load was increased, the concrete cover underneath the reinforcing bars crossing the major crack was pushed out. The beam failed at a load of 53.4 kN (12.0 kips) in the same mode as beam #2. Fig. 3-12 shows a complete separation between the beam portions on both sides of the failure crack.

3.6.3 Beam # 8

As the load was applied, flexure cracks started to appear within the constant moment zone, followed by shear-flexure cracks formed within the shear span. A major crack initiated at a distance 812.8 mm (32.0 in) from the nearest beam edge. This crack, apparently, limited the development length of the CFRP bars beyond the crack.

The dial gauges attached to the exposed portion of the CFRP bars at the nearest beam edge indicated the initiation of a bond failure at a load of 71.2 kN (16.0 kips). As the applied load was increased, the major crack gap increased greatly while the crack itself progressed vertically towards the beam flange (Fig. 3-13). A complete bond failure

between the CFRP bars and concrete took place at a load of 80.1 kN (18.0 kips) which was also confirmed by the reading of the dial gauges, followed immediately by an overall failure of the tested beam.

3.6.4 Beam # 15

At a load of 26.7 kN (6.0 kips), flexure cracks initiated within the constant moment zone. The cracks progressed vertically and they were almost uniformly spaced at 178 mm (7.0 in) which is the same spacing of the stirrups. At an applied load of 35.6 kN (8.0 kips), shear-flexure cracks developed within shear span. One of these cracks that initiated at a distance 381 mm (15.0 in) from the nearest beam edge became a major crack. While the crack was progressing towards the beam flange, the dial gauges attached to the exposed portion of the CFRP bars at the same beam edge indicated an initiation of a slip of the bars at a load of 115.7 kN (26.0 kips). The cracking pattern at this location is shown in Fig. 3-14. Thereafter, a gradual unloading process of the tested beam took place in order to start testing the beam with different load set-up that enables decreasing the tensile force in the CFRP bars and avoiding such bond failure.

3.6.5 Beam # 15'

After unloading beam #15, The unloaded beam was tested under new configurations and the name " beam #15' " as given in Table 3-1. The existing cracking pattern remained unchanged until the applied load reached a value of 48.9 kN (11.0 kips).

At this loading level, the existing flexure cracks started to continue their progress. New ones were also initiated near mid-span.

As the applied load was increased beyond 62.3 kN (14.0 kips), one of the flexure cracks became a major crack and progressed towards the beam flange. While crackling of the bars fibres crossing the crack was clearly heard, the bars suddenly ruptured at a load of 66.7 kN (15.0 kips). The failure crack location is shown in Fig. 3-15.

3.6.6 Beam # 16

For this set-up, the over-hung beam portion was increased to 610 mm (24.0 in) as shown in Table 3-1. This set-up was designed to increase the development length of the flexural reinforcing CFRP bars in order to avoid any bond failure. As the applied load increased, a shear-flexure became a major crack which initiated at distance 1283 mm (50.5 in) from the nearest beam edge.

A failure similar to that of beam #15′ was observed when this crack almost reached the beam flange. Crackling of the CFRP bars was heard at load at of 102.4 kN (23.0 kips). Increasing the load to 106.8 kN (24.0 kips), the bars crossing the crack suddenly ruptured. Fig. 3-16 shows the crack location after beam failure.

3.6.7 Beam # 17

Flexure cracks initiated at an applied load of about 17.8 kN (4.0 kips), at the beam mid-span. As the applied load was increased, shear-flexure cracks developed within the shear span. When the load reached 35.6 kN (8.0 kips), one of the shear-flexure cracks, initiated at a distance 813 mm (32.0 in) from the nearest beam edge, became a major crack. While this crack was progressing, at a load of 44.5 kN (10.0 kips), a new crack started from the original crack profile at the level of the flexural reinforcement, progressing towards the nearest support.

A relative transverse displacement was observed on both sides of the crack at the same level. When the major crack almost intersected the flange, at a load of 55.6 kN (12.5 kips), the CFRP bars crossing the crack were suddenly sheared, and the beam failed in a manner similar to that of beams #2 and #3. The failure crack is shown in Fig. 3-17.

3.6.8 Beam # 21

This beam was reinforced in flexure with mild steel bars. The bars were selected to introduce approximately the same tensile strength of the CFRP bars used to reinforce the other beams. This test was carried out to compare the behaviour, in general, and the crack formation characteristics, in particular, for FRP-reinforced concrete beams with those of steel-reinforced concrete beams. Since mild steel bars enabled the introduction of end hooks, the over-hung portion was reduced to 76 mm (3.0 in).

Flexure cracks initiated at an applied load of about 13.4 kN (3.0 kips), at the beam mid-span. Increasing the applied load, shear-flexure cracks developed within the shear span. Increasing the applied load, one of these cracks that initiated at a distance of 457 mm (18.0 in) from the nearest beam edge became a major crack. As soon as the crack reached the beam flange, at a load of about 57.8 kN (13.0 kips), the concrete above the crack within the beam flange failed in shear (i.e. diagonal tensile failure). The crack progressed immediately towards the loading point as shown in Fig. 3-18.

3.6.9 Beam # 24

Both flexure and shear-flexure cracks initiated at an approximately uniform spacing of 127 mm (5.0 in) through out the beam span as if the beam was provided with stirrups at this spacing. At a load of 31.2 kN (7.0 kips), one of the flexure-shear cracks that initiated at a distance 787 mm (31.0 in) from the nearest beam edge became a major crack.

When the crack approached the beam flange, all the CFRP bars crossing the crack suddenly ruptured at almost the same time at a load of 53.4 kN (12.0 kips). The crack progressed towards the loading point, resulting in a complete separation of the beam segments on both sides of the crack as shown in Fig. 3-19.

3.6.10 Beam # 25

Flexure cracks initiated at an applied load of about 17.8 kN (4.0 kips), at the beam mid-span. As the applied load was increased, shear-flexure cracks developed within the shear span. When the load reached 35.6 kN (8.0 kips), one of the flexure-shear cracks which initiated at a distance 812.8 mm (32.0 in) from the nearest beam edge became a major crack. At a load of 44.5 kN (10.0 kips), a new crack started from the original crack profile at the level of the flexural reinforcement, progressing towards the nearest support.

The progress of the major crack was accompanied by a relative transverse displacement on both sides of the crack at the flexure reinforcement level. When the major crack almost intersected the flange, at a load of 48.9 kN (11.0 kips), the concrete cover underneath the bars crossing the crack was pushed out, and the crack progressed towards the loading point causing a complete split of the concrete along the crack profile (Fig. 3-20). It can be seen that the beam segments on both sides of the crack were connected with the flexural reinforcement only.

3.6.11 Beam # 26

The behaviour and failure of this beam were almost identical to those of beam #25, except that the major crack initiated at a distance 724 mm (28.5 in) from the nearest beam edge, and the failure took place at a load of 40.0 kN (9.0 kips). The failure crack is shown in Fig. 3-21.

3.6.12 Beam # 29

The beam developed its first flexure crack at an applied load of 13.4 kN (3.0 kips), near the beam mid-span. Thereafter, more flexure cracks initiated as well as flexure-shear cracks that developed within the shear span. When the applied load was increased, none of the existing shear-flexure cracks was observed to be a major crack while the flexure cracks were progressing towards beam flange.

As the applied load was increased, beyond 75.7 kN (17.0 kips), one of the flexure cracks became a major crack. As this crack was progressing within the beam flange, crackling of the CFRP bars was heard. The bars crossing the crack suddenly ruptured at a load at of 88.9 kN (20.0 kips). The failure crack is shown in Fig. 3-22.

3.6.13 Beam # 30

The behaviour and failure of this beam were similar to those of beam #29, except that the failure took place at a load of 91.2 kN (20.5 kips). The failure crack is shown in Fig. 3-23.

3.6.14 Beam # 31

The behaviour of this beam was similar to that of beam #29 and #30 up to a load of about 66.8 kN (15.0 kips) until the following differences were observed: Two shear-

flexure cracks became major cracks. The first crack initiated, within one of the shear spans, at 660 mm (26.0 in) from the nearest beam edge while the second crack initiated, within the other shear span, at 965 mm (38.0 in) from the other beam edge.

While the first crack was progressing, at a load of 80.1 kN (18.0 kips), a relative transverse displacement was observed on both sides of the crack at the level of the flexural reinforcement. Crackling of the CFRP bars was heard at a load of 84.5 kN (19.0 kips). Thereafter, the bars crossing the second major crack ruptured at a load of 93.4 kN (21.0 kips) as can be seen from Fig. 3-24.

3.6.15 Beam # 32

The developed flexural, as well as shear-flexure cracks initiated at almost uniform spacing which was equal to the spacing of the stirrups provided. The beam experienced three major shear-flexure cracks. Two of them were initiated within the same shear span at distances of 610 mm (24 in) and 787 mm (31 in) from the nearest beam edge.

The third crack developed within the other shear span and started far from the other edge by 737 mm (29 in). While the three cracks were approaching the beam flange at an applied load of 129.0 kN (29.0 kips), the CFRP bars crossing the second major crack ruptured. The failure location is shown in Fig. 3-25.

3.6.16 Beam # 34

The behaviour and failure of this beam were almost identical to that of beam #32. Two flexure-shear cracks that initiated within the same shear span at distances of 787 mm(31.0 in) and 156 mm (37.0 in) from the nearest beam edge became major cracks. Another crack developed within the other shear span and started far from the other edge by 1040 mm (41.0 in) became a major crack as well. While the three cracks were approaching the beam flange at an applied load of 133.4 kN (30.0 kips), the CFRP bars crossing the third crack ruptured. The failure location is shown in Fig. 3-26.

3.6.17 Beam # 35

The behaviour and failure of this beam were similar to those of beam #25 and #26, except that the first flexure crack formed at a load of 26.7 kN (6.0 kips). Three major shear-flexure cracks initiated at a distances of 279 mm (11.0 in), 495 mm (19.5 in), and 610 mm (24.0 in) from the nearest beam edge, and the failure took place at a load of 53.4 kN (12.0 kips). The failure crack is shown in Fig. 3-27.

3.6.18 Beam # 36

Flexure cracks initiated at an applied load of 26.7 kN (6.0 kips), at beam mid-span. As the applied load was increased, shear-flexure cracks developed within shear span. A major shear-flexure crack initiated at a distance of 533 mm (21.0 in) from the

nearest beam edge. While this crack was progressing, a relative transverse displacement was observed on both sides of the crack. At a load of 104.5 kN (23.5 kips), the CFRP bars crossing the crack suddenly ruptured as shown in Fig. 3-28.

3.7 Summary of the Observed Behaviour

The observed behaviour of the tested beams can be summarised as follows:

I - Cracks began to appear at the mid-span of the beams for loading set-up (I) and within the constant moment zone, i.e. distance (b), for loading set-up (II). These cracks started from the bottom of the web and continued to progress vertically towards the flange, due to flexural tensile stresses. As the applied load increased, new cracks appeared within the shear spans, i.e. distance (Lp) on both sides of the beam. They started vertically and took a curved path when progressing in the beam web due to combined shear and flexural stresses.

II - As the applied load was increased, one or more of the cracks became major as they were progressing and widening significantly with respect to the other cracks.

III - For beams with low ratio of shear reinforcement, the following behaviour was observed as the major crack approached the beam flange:

- A relative rotation took place between the two beam segments on both

sides of the crack about its tip. This rotation was accompanied by a transverse displacement in the longitudinal reinforcement crossing the crack. At the same time, a new longitudinal crack developed as a branch of the existing major crack profile, along the flexural reinforcement level, progressing towards the nearest support as shown in Figs. 3-12 and 3-17.

- This new longitudinal crack formed due to the relative transverse displacement of the bars on both sides of the crack. In the beam segment attached to the nearest support, the bars pushed the concrete cover downward. When the tensile stresses in concrete exceeded the modulus of rupture, this longitudinal crack initiated and progressed towards the nearest support.

- For some beams that were not provided with stirrups (e.g. beam #25 and #26), this crack progressed quickly to the degree that a considerable portion of the concrete cover underneath was pushed off, exposing the CFRP bars for a certain distance that ranged between 152 mm (6.0 in) and 305 mm (12.0 in). As the bars lost their contact with the concrete, the major crack progressed suddenly through the beam flange, splitting the concrete on both sides the crack completely as can be seen in Figs. 3-20 and 3-21.

This behaviour may be explained as follows: when the bars crossing the major crack lost their contact with concrete, the shear resistance provided by these

bars was suddenly eliminated. Since the beam was not provided with stirrups, the concrete above the crack had to compensate for the sudden drop of shear resistance along the crack path. As a result, the shear stress induced in the concrete increased, and the principal tensile stresses at crack tip exceeded the concrete modulus of rupture all the way through the flange.

IV - For some of the beams with a relatively high ratio of shear reinforcement (e.g. beams # 29 and # 30) it was observed that shear reinforcement had a significant influence on prevention of the dowel failure of the CFRP bars, i.e. shear-tension failure of bars within shear span. For other beams with higher ratio of shear reinforcement (e.g. beams # 15' and # 16), the beams failed due to the dowel failure of CFRP bars. However, the stirrups were able to keep the bars in position under the induced transverse displacement without pushing the concrete cover underneath until the CFRP bars completely ruptured. This behaviour can be explained since the ratio of shear reinforcement is not the only parameter governing the possibility of the dowel failure of FRP bars. Other parameters such as the stirrups spacing, the crack path geometry, and the crack width affect the dowel action of FRP bars (the influence of these parameters will be explained in detail through the following chapters).

V — For all the tested beams (except beams # 35 and # 36), no cracks developed within a distance of 300 mm (12 in) from each support. This distance is approximately equal to the beam depth, d, as this zone is mainly subjected to compressive stresses due to the transfer of the reaction between beam and support. For beams # 3, # 35 and # 36, the

provided supports simulated the beam when hung by ties (Figs. 3-12, 3-27 and 3-28). In this case, the reaction between beam and support is transferred mainly by tension, allowing for crack formation within this zone.

VI - For the concrete beams reinforced with steel bars (e.g. beam # 21) similar cracking behaviour and crack geometry were observed as outlined by Leet (1991) and Ferguson and Cowen (1981). Fig. 3-18 shows the failure crack of beam # 21.

Table 3-1: Specimen Configurations, dimensions are in mm (inch).

Beam # (1)	Setting Type (2)	Settings, mm (in)			Flexure Bars (6)	Prestressing Condition (7)	Shear Reinforcement (8)	Failure Load kN (kips) (9)
		a (3)	Lp (4)	b (5)				
2	I	76.0 (3.0)	1753.0 (69.0)	-	2-CFRP bars, diam. 8 (0.31)	Nonprestressed	No Stirrups	44.5 (10.0)
3	I	76.0 (3.0)	1753.0 (69.0)	-	2-CFRP bars, diam. 8 (0.31)	Nonprestressed	No Stirrups	53.4 (12.0)
8	II	76.0 (3.0)	839.0 (33.0)	1829.0 (72.0)	2-CFRP bars, diam. 8 (0.31)	Nonprestressed	Steel Stirrups, diam. 10 (0.39) @ 178 (7)	71.2 (16.0)
15	II	76.0 (3.0)	839.0 (33.0)	1829.0 (72.0)	2-CFRP bars, diam. 8 (0.31)	Prestressed	Steel Stirrups, diam. 10 (0.39) @ 178 (7)	115.7 (26.0)
15'	I	76.0 (3.0)	1753.0 (69.0)	-	2-CFRP bars, diam. 8 (0.31)	Prestressed	Steel Stirrups, diam. 10 (0.39) @ 178 (7)	66.7 (15.0)
16	II	610.0 (24.0)	914.0 (36.0)	610.0 (24.0)	2-CFRP bars, diam. 8 (0.31)	Nonprestressed	Steel Stirrups, diam. 10 (0.39) @ 178 (7)	106.8 (24.0)
17	I	305.0 (12.0)	1524.0 (60.0)	-	2-CFRP bars, diam. 8 (0.31)	Prestressed	No Stirrups	55.6 (12.5)
21	I	305.0 (12.0)	1524.0 (60.0)	-	5-Steel bars, diam. 10 (0.39)	Nonprestressed	No Stirrups	57.8 (13.0)
24	I	305.0 (12.0)	1524.0 (60.0)	-	2-CFRP bars, diam. 8 (0.31)	Nonprestressed	No Stirrups	53.4 (12.0)
25	I	305.0 (12.0)	1524.0 (60.0)	-	2-CFRP bars, diam. 8 (0.31)	Prestressed	No Stirrups	48.9 (11.0)
26	I	305.0 (12.0)	1524.0 (60.0)	-	2-CFRP bars, diam. 8 (0.31)	Prestressed	No Stirrups	40.0 (9.0)
29	II	305.0 (12.0)	1219.0 (48.0)	610.0 (24.0)	2-CFRP bars, diam. 8 (0.31)	Nonprestressed	Steel Stirrups, diam. 6 (0.24) @ 102 (4)	88.9 (20.0)
30	II	305.0 (12.0)	1219.0 (48.0)	610.0 (24.0)	2-CFRP bars, diam. 8 (0.31)	Nonprestressed	Steel Stirrups, diam. 6 (0.24) @ 152 (6)	91.2 (20.5)
31	II	305.0 (12.0)	1219.0 (48.0)	610.0 (24.0)	2-CFRP bars, diam. 8 (0.31)	Nonprestressed	Steel Stirrups, diam. 6 (0.24) @ 203 (8)	93.4 (21.0)
32	II	305.0 (12.0)	914.0 (36.0)	1219.0 (48.0)	2-CFRP bars, diam. 8 (0.31)	Prestressed	Steel Stirrups, diam. 6.0 (0.24) @ 152 (6)	129.0 (29.0)
34	II	1219.0 (48.0)	914.0 (36.0)	1219.0 (48.0)	2-CFRP bars, diam. 8 (0.31)	Prestressed	Steel Stirrups, diam. 6.0 (0.24) @ 102 (4)	133.4 (30.0)
35	II	76.0 (3.0)	686.0 (27.0)	1219.0 (48.0)	2-CFRP bars, diam. 8 (0.31)	Nonprestressed	No Stirrups	53.4 (12.0)
36	I	76.0 (3.0)	839.0 (33.0)	-	2-CFRP bars, diam. 8 (0.31)	Nonprestressed	Steel Stirrups, diam. 6 (0.24) @ 203 (8)	104.5 (23.5)

Beam height is 356 mm (14.0 in) for all the tested beams
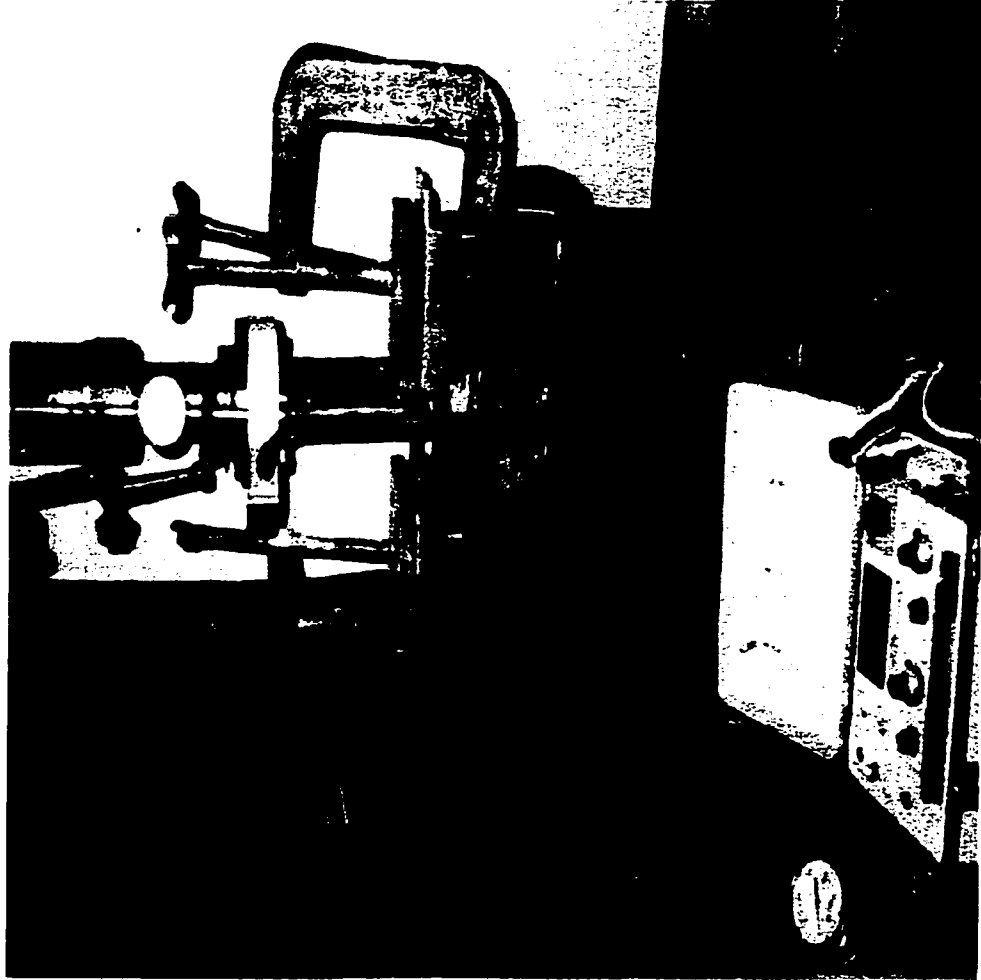
Fig. 3-1: Set-up and Instrumentation for Testing CFRP Bars under Shear.

Applied load

Section I—I   Section II—II
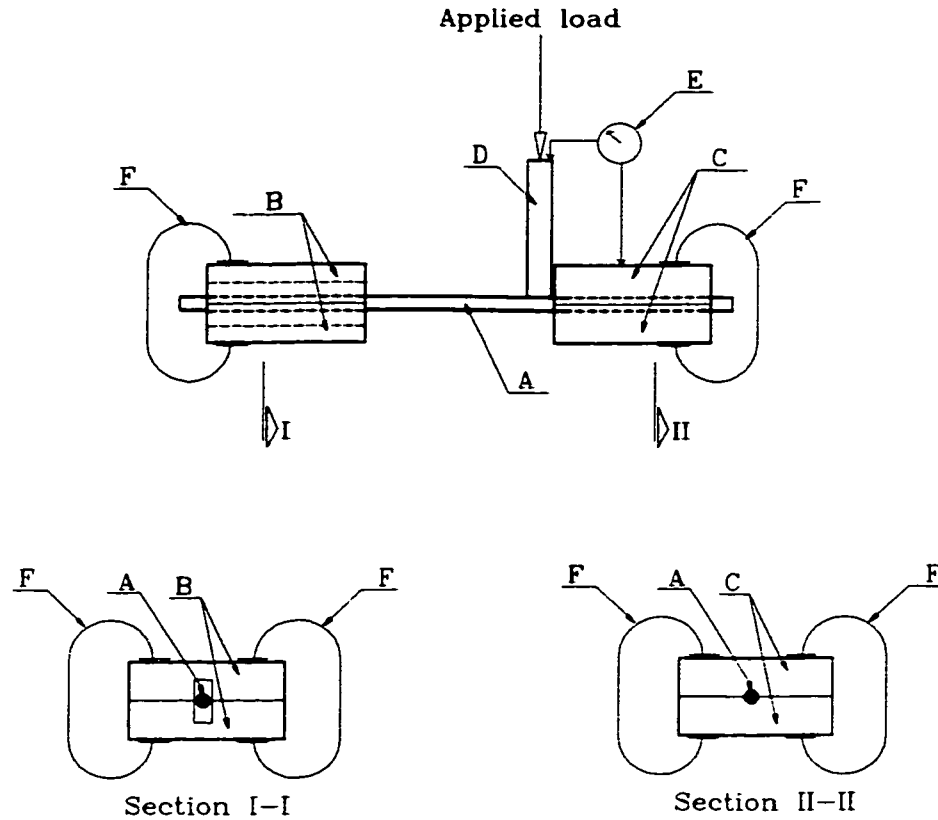
(A) CFRP Bar Sample to be Tested.

(B) Two Metal Parts to Provide an Alignment for the Specimen.
(Not to Provide any kind of Support. See Sec. I—I)

(C) Two Metal Parts to Provide Full Fixation of the Specimen. See Sec. II—II.

(D) Rigid Steel Plate to Apply the Load on the Specimen.

(E) Dial Gauge to Measure the Specimen Shear Displacement.

(F) Clamps to Keep the Set—up Parts in Position.

Fig. 3-2: The Set-up Components for Testing CFRP Bars under Shear.

59
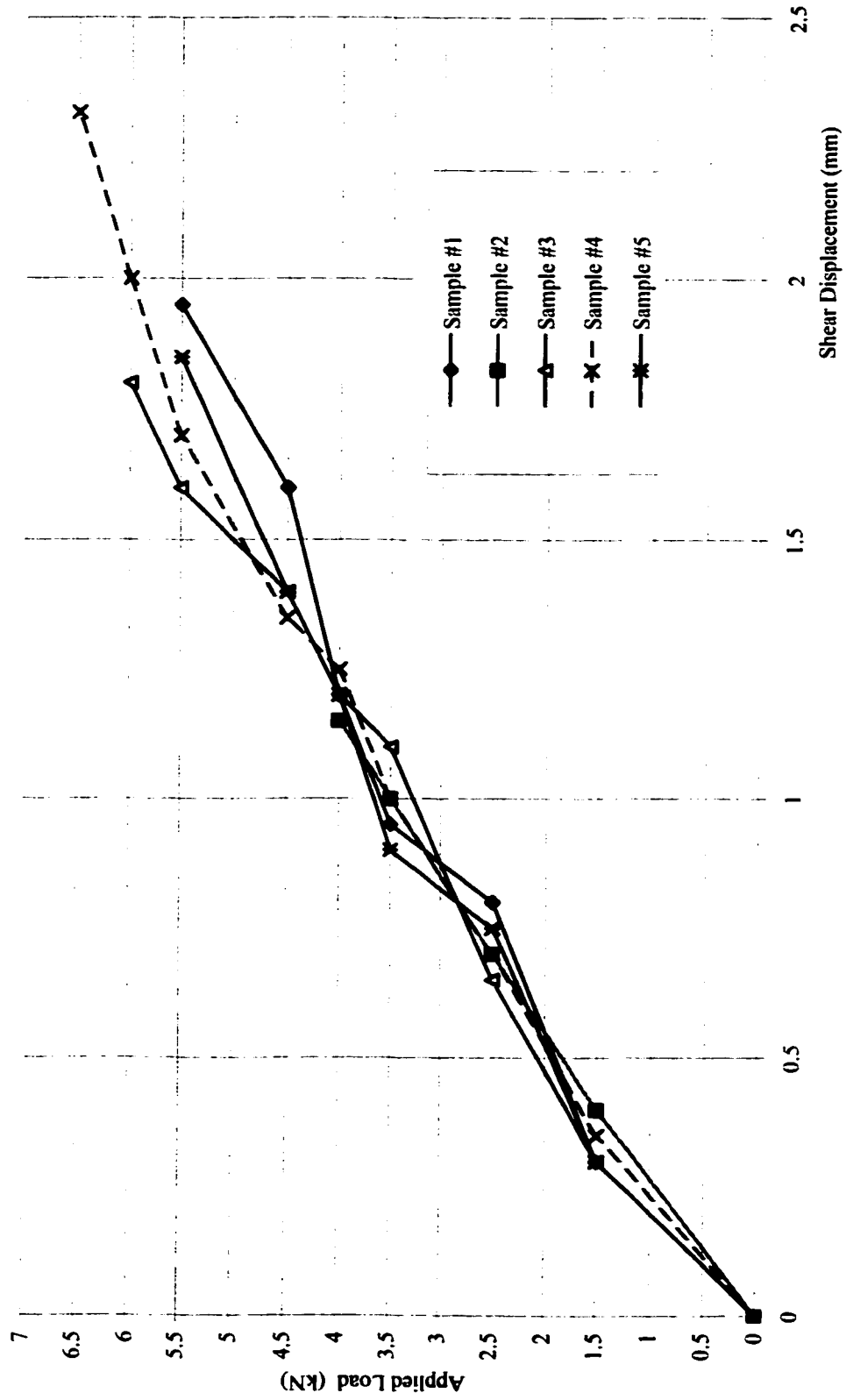
Fig. 3-3: Applied Shear Load vs Shear Displacement for CFRP Bars (8mm diameter).
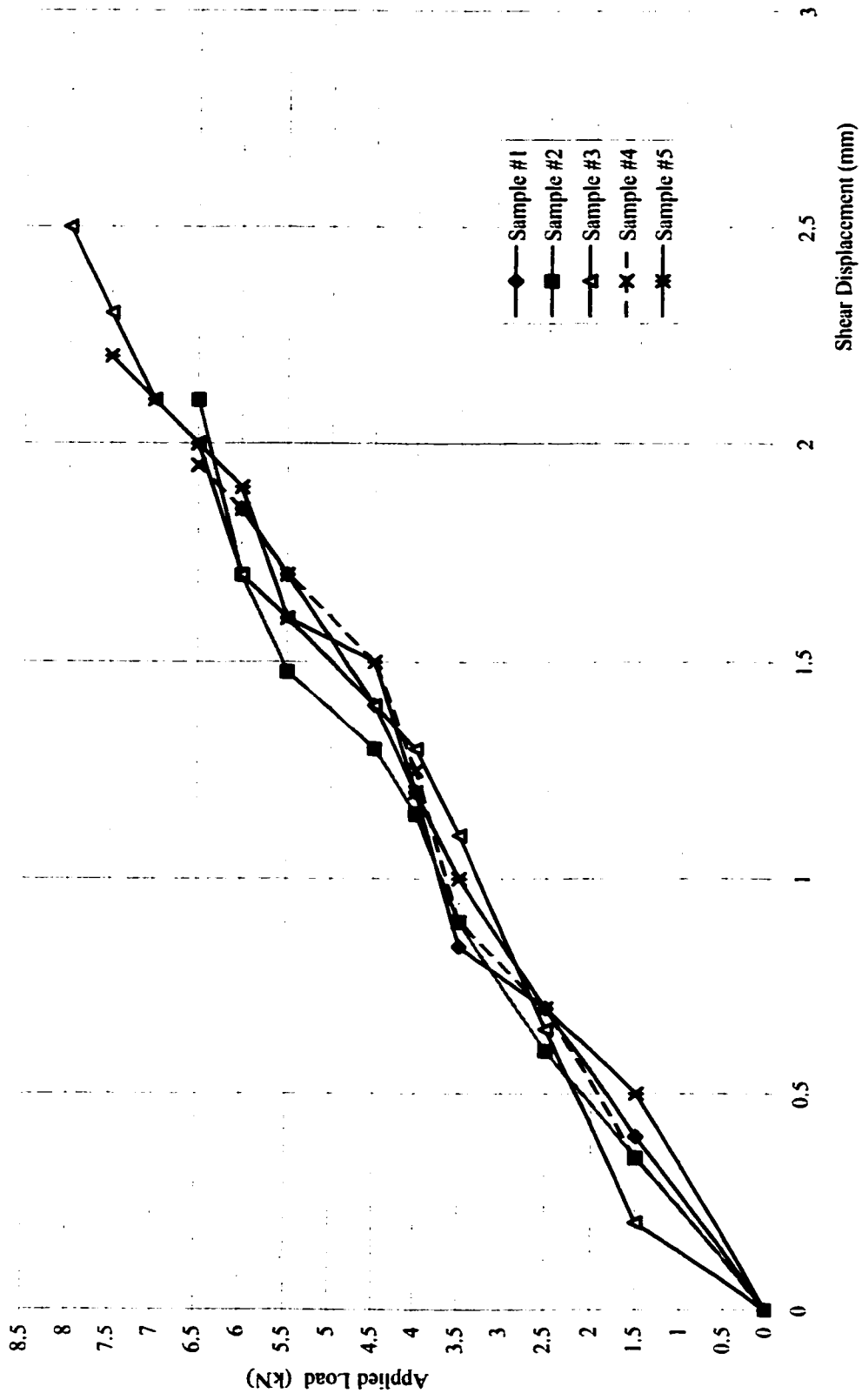
Fig. 3-4: Applied Shear Load vs. Shear Displacement for CFRP Bars (10mm diameter).

2 Steel bars
(when Stirrups exist)

U-shape Stirrups
(when Shear Reinforcement
is provided)

Prestressing Tendon
(if provided)

Flexural Reinforcement

254.0mm
10.00"

76.2mm
3.00"

279.4mm
11.00"

211.6mm
8.33"

88.9mm
3.50"

114.3mm
4.50"

(b) Typical Cross Section I–I.

1828.8mm or 3657.6mm (see Table 3–1)
72.00" or 144.00"

76.2mm
3.00"

279.4mm
11.00"

355.6mm
14.00"
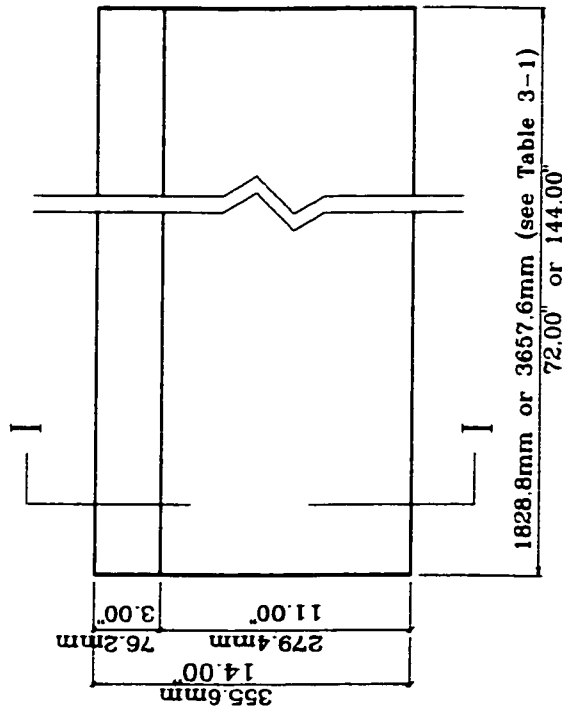
(a) Longitudinal Elevation.
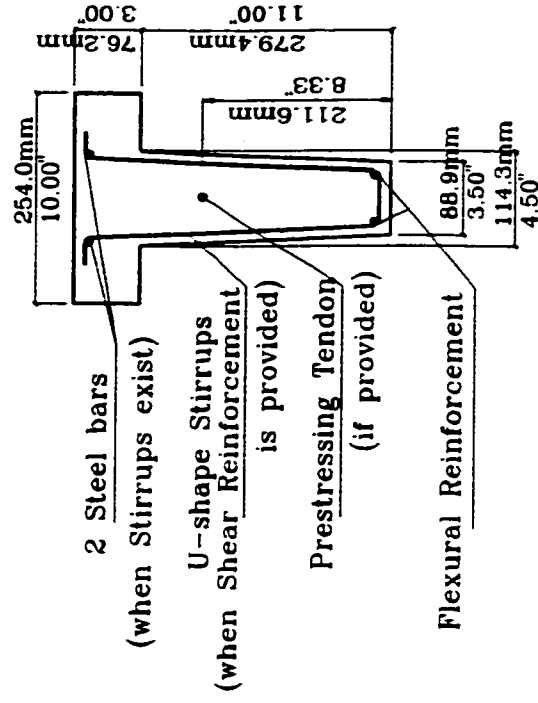
Fig. 3-5: Typical Details of the Specimens.

62

Applied Load (P)

Lp | b | Lp

a | | a

(b) Set-up Type (II).

Applied Load (P)

Lp | Lp

a | a
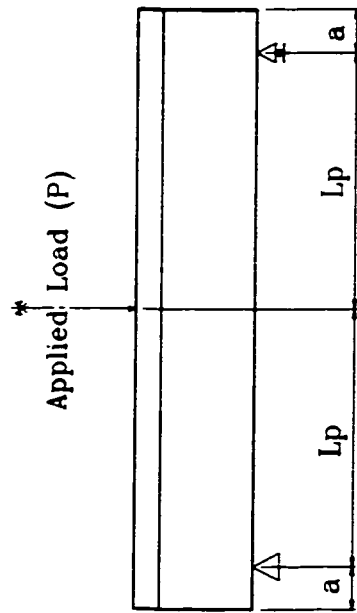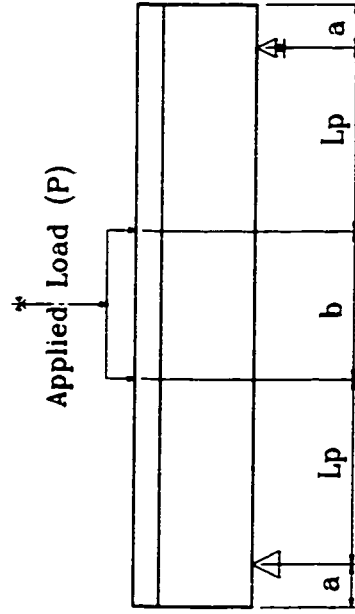
(a) Set-up Type (I).

Fig. 3-6: Loading Set-ups.
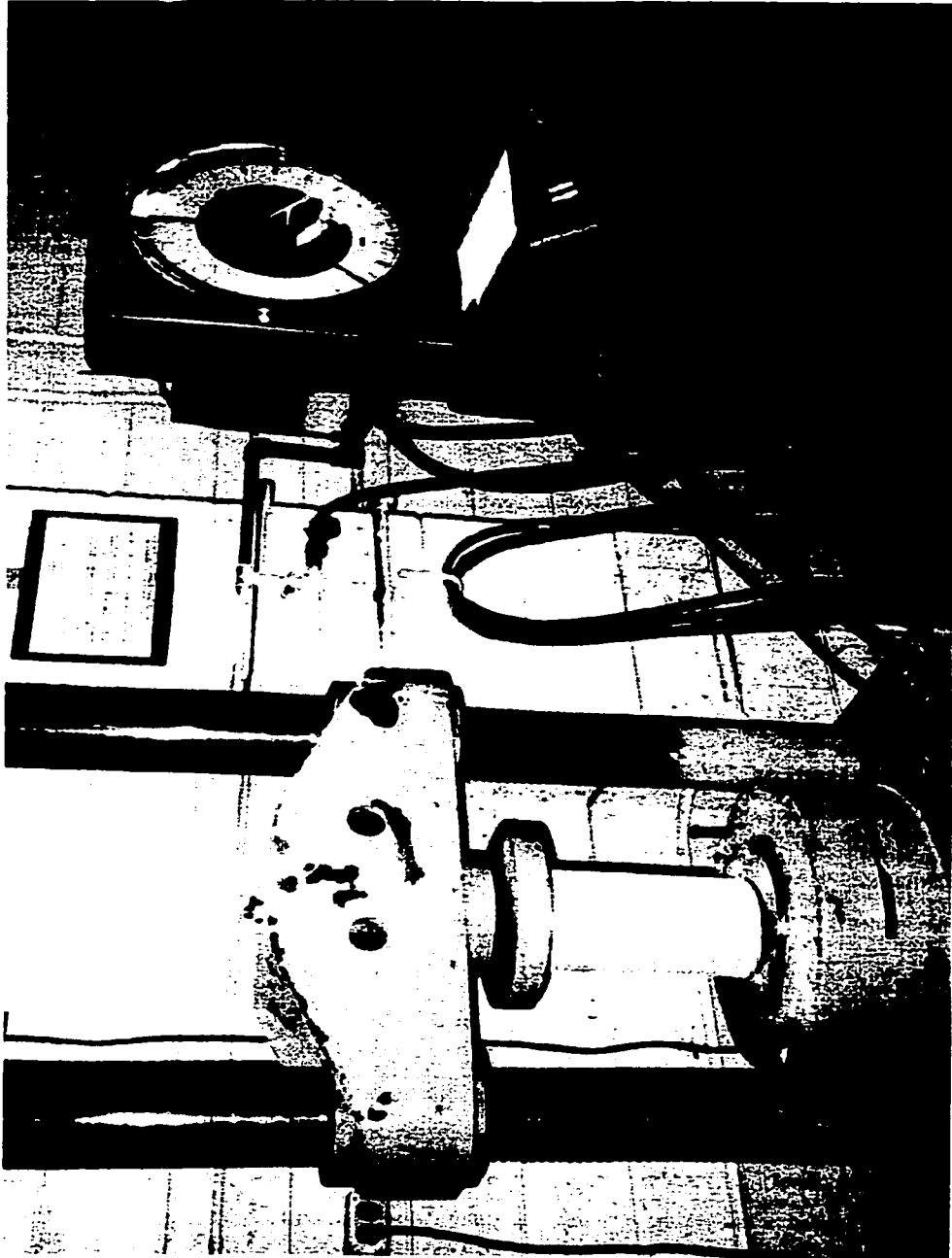
Fig. 3-7: Testing of Standard Concrete Cylinders.

Fig. 3-8: Beam Formwork.

Fig. 3-9: Prestressing Platform.

Fig. 3-10: Beam Set-up and Instrumentation.
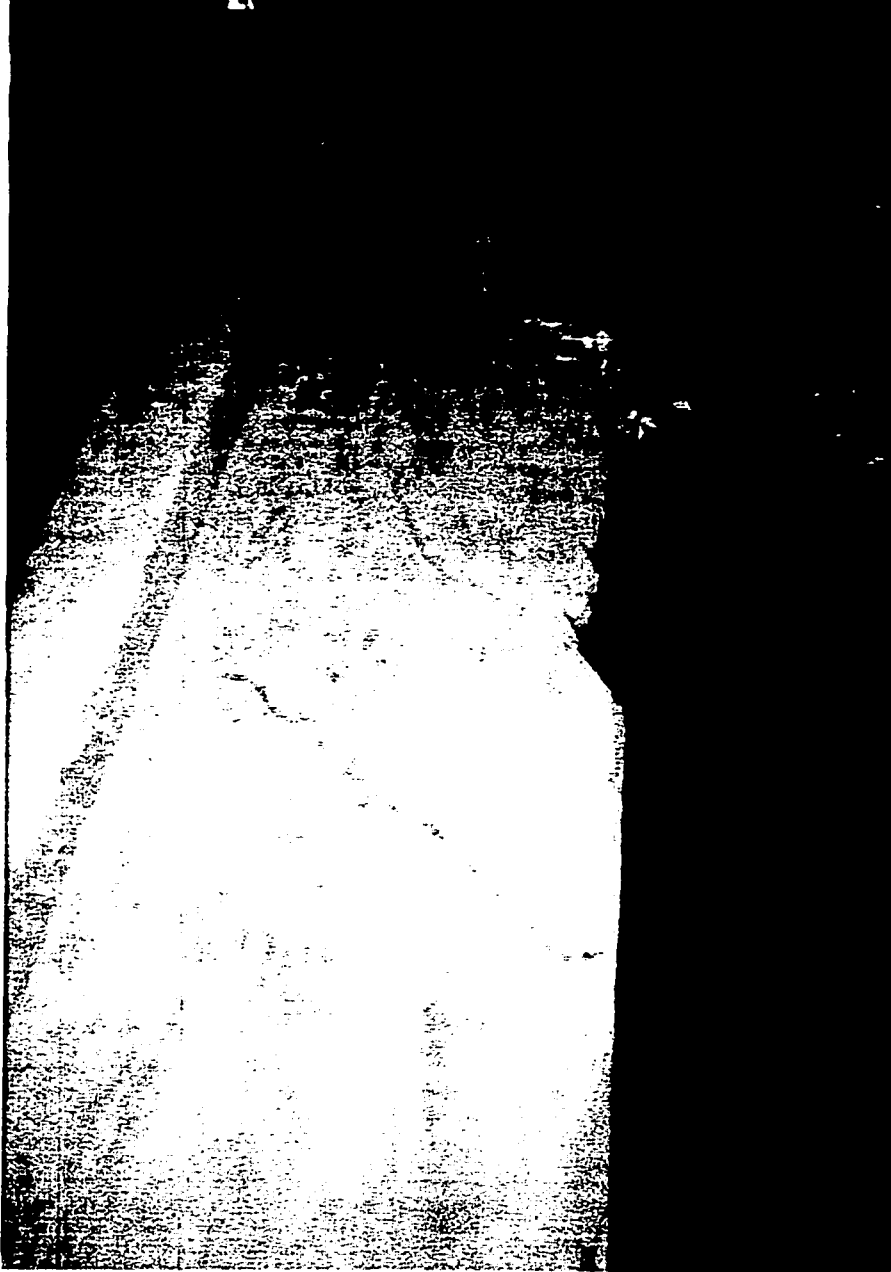
Fig. 3-11: Failure Crack of Beam # 2.
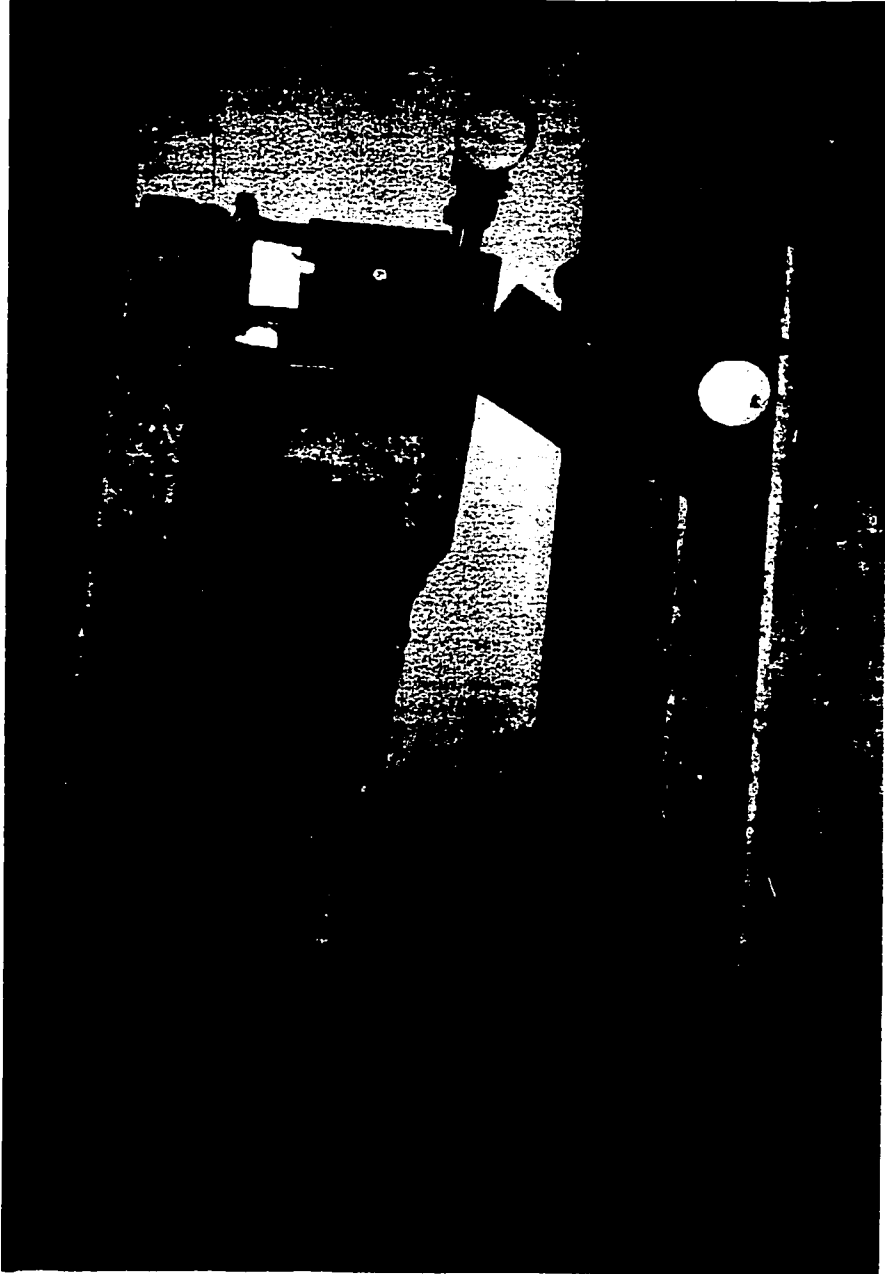
Fig. 3-12: Failure Crack of Beam # 3.

69
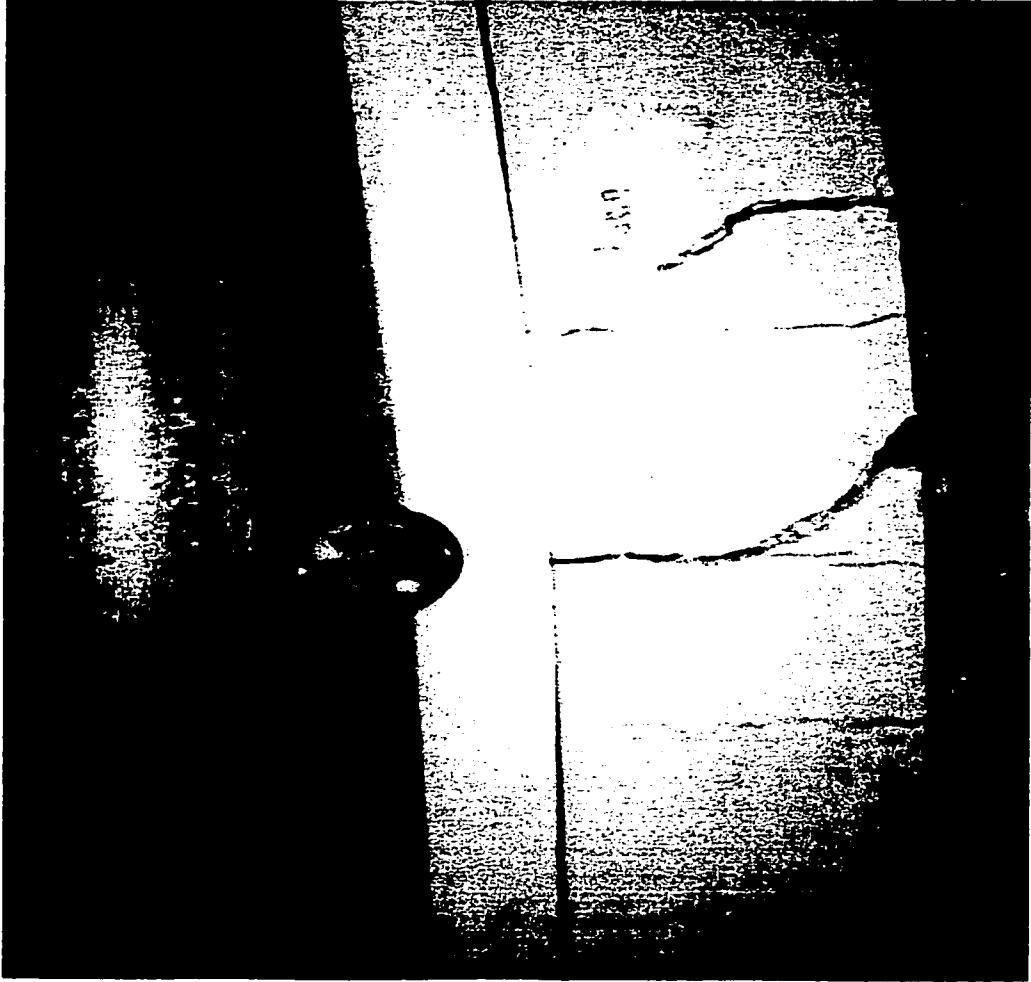
Fig. 3-13: Failure Crack of Beam # 8.
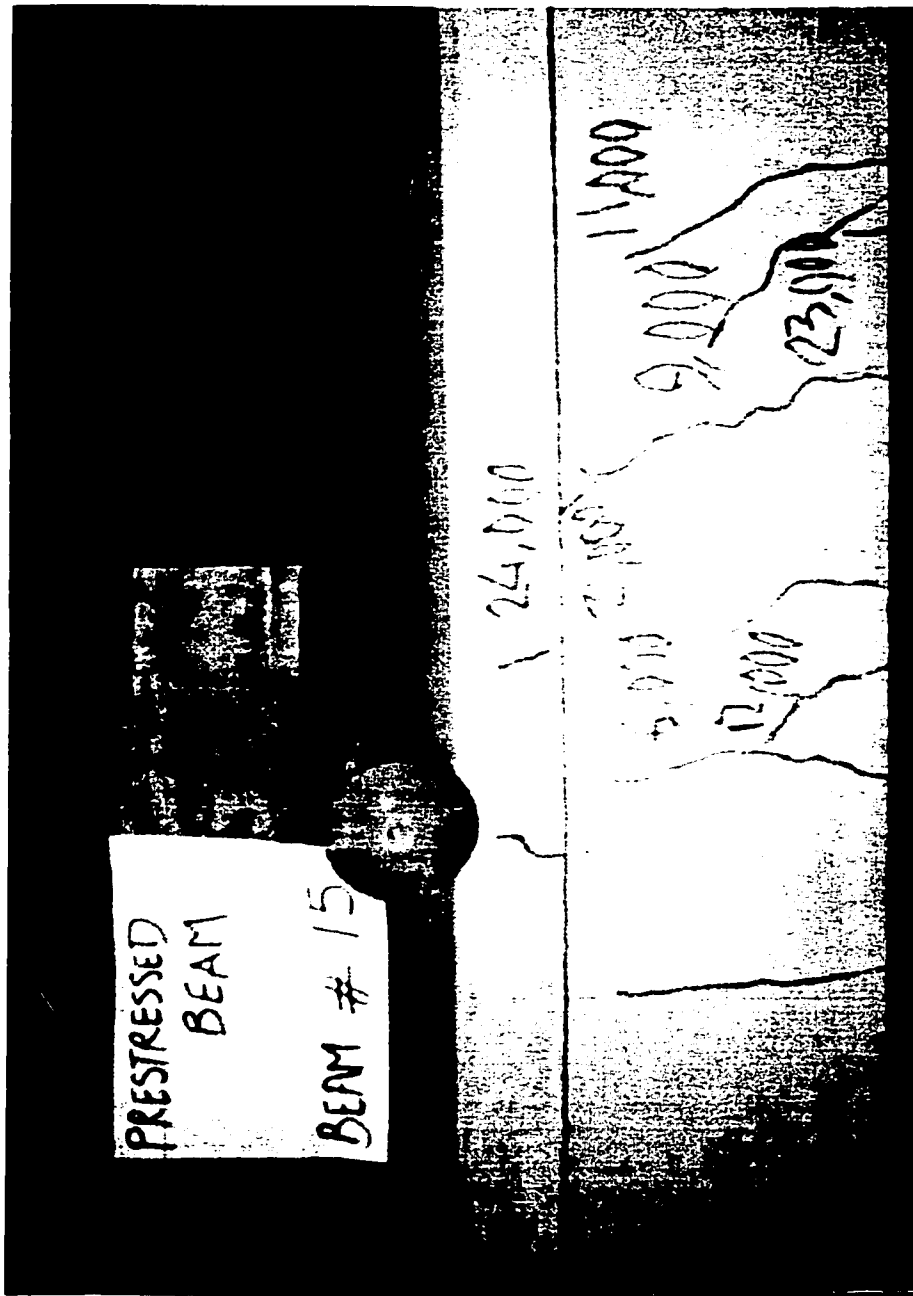
Fig. 3-14: Cracking Pattern of Beam # 15.
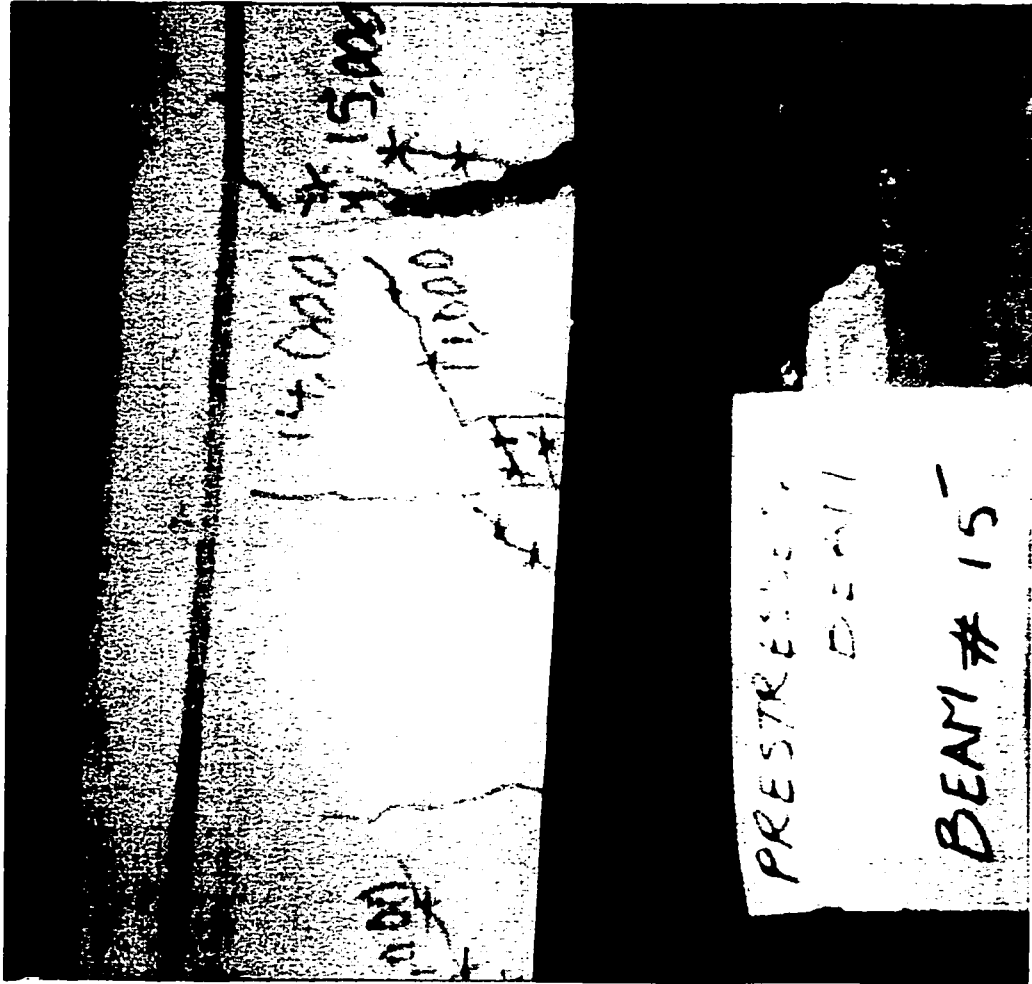
Fig. 3-15: Failure Crack of Beam #15.
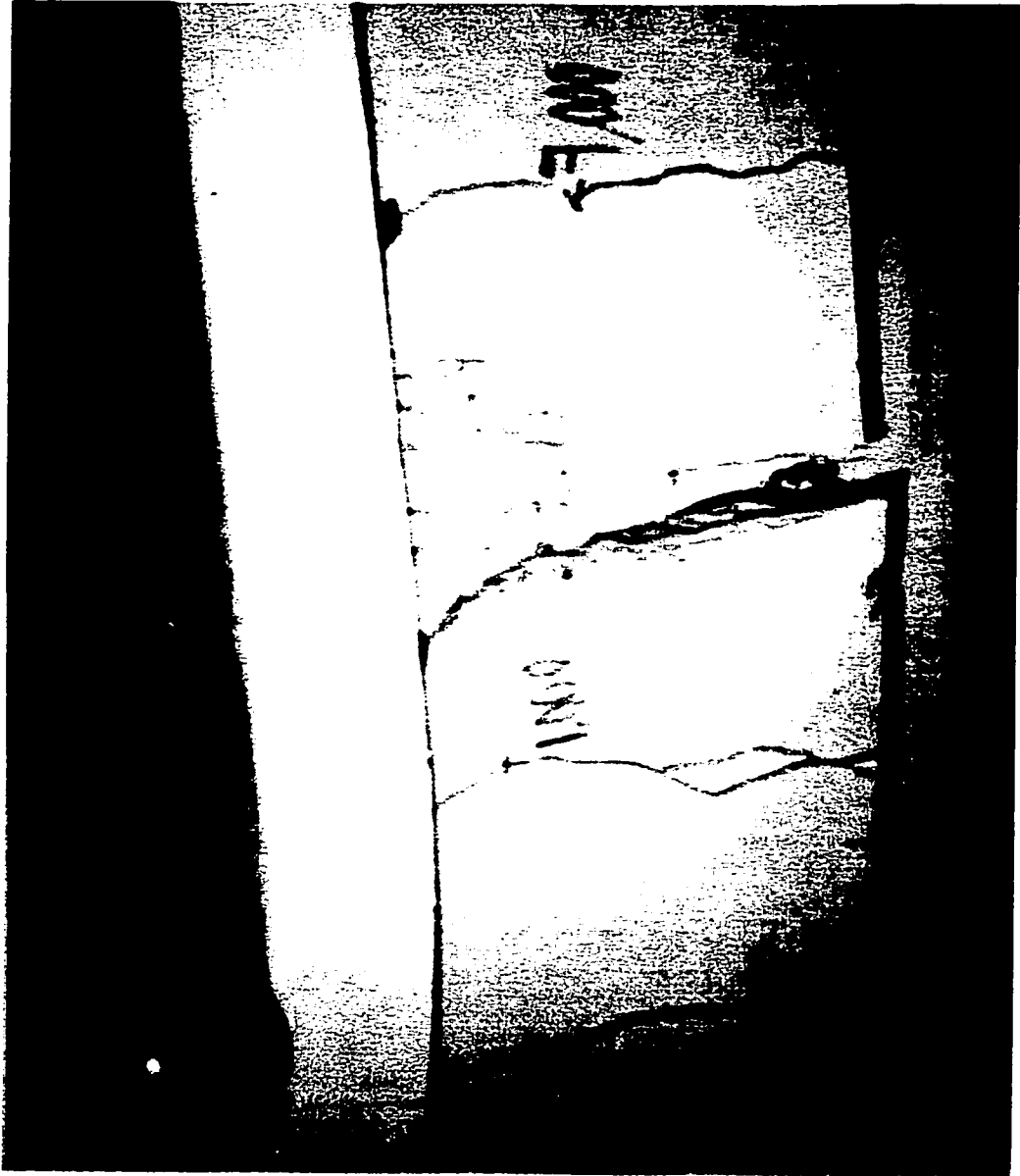
Fig. 3-16: Failure Crack of Beam # 16.
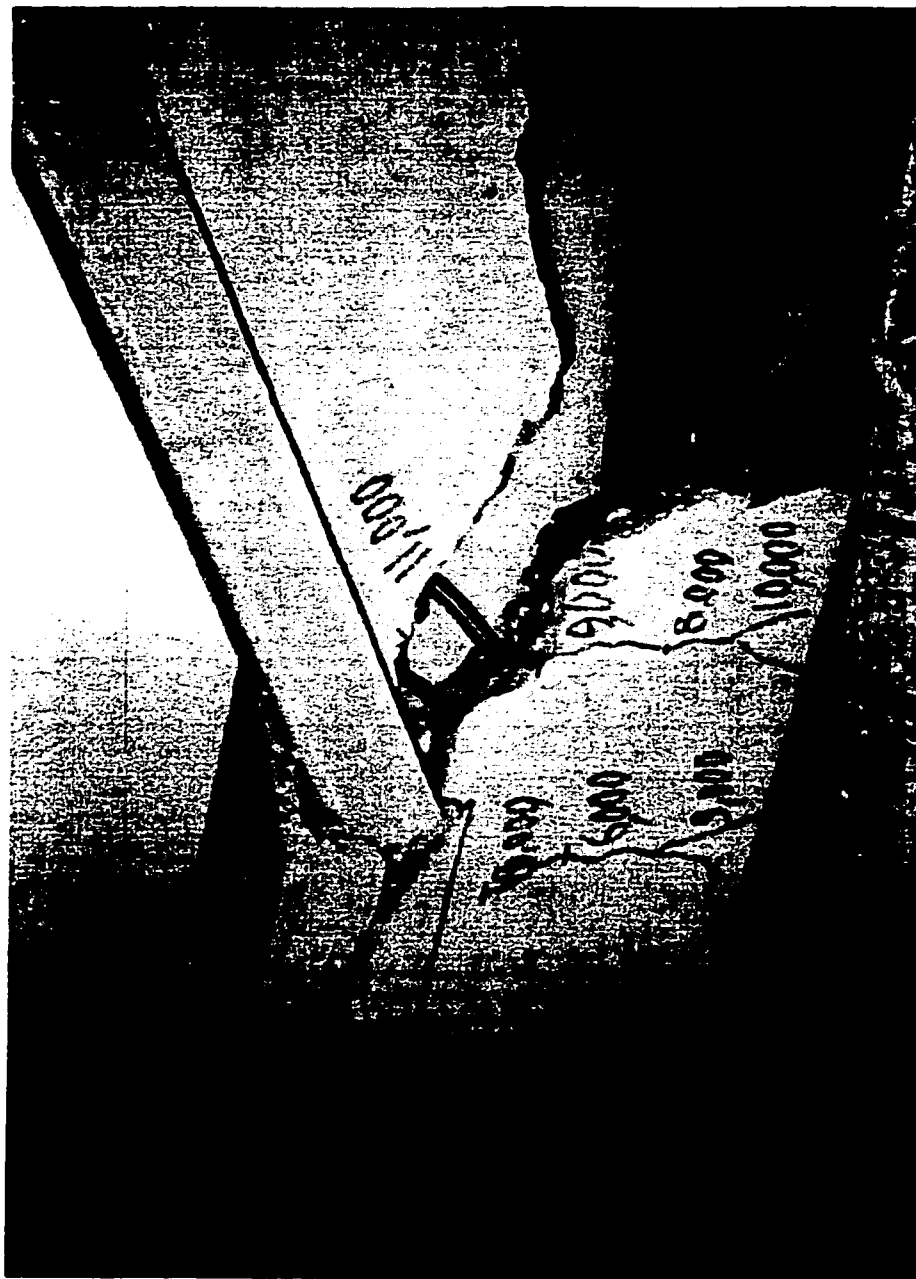
Fig. 3-17: Failure Crack of Beam # 17.

Fig. 3-18: Failure Crack of Beam # 21.

Fig. 3-19: Failure Crack of Beam # 24.

Fig. 3-20: Failure Crack of Beam # 25.

77
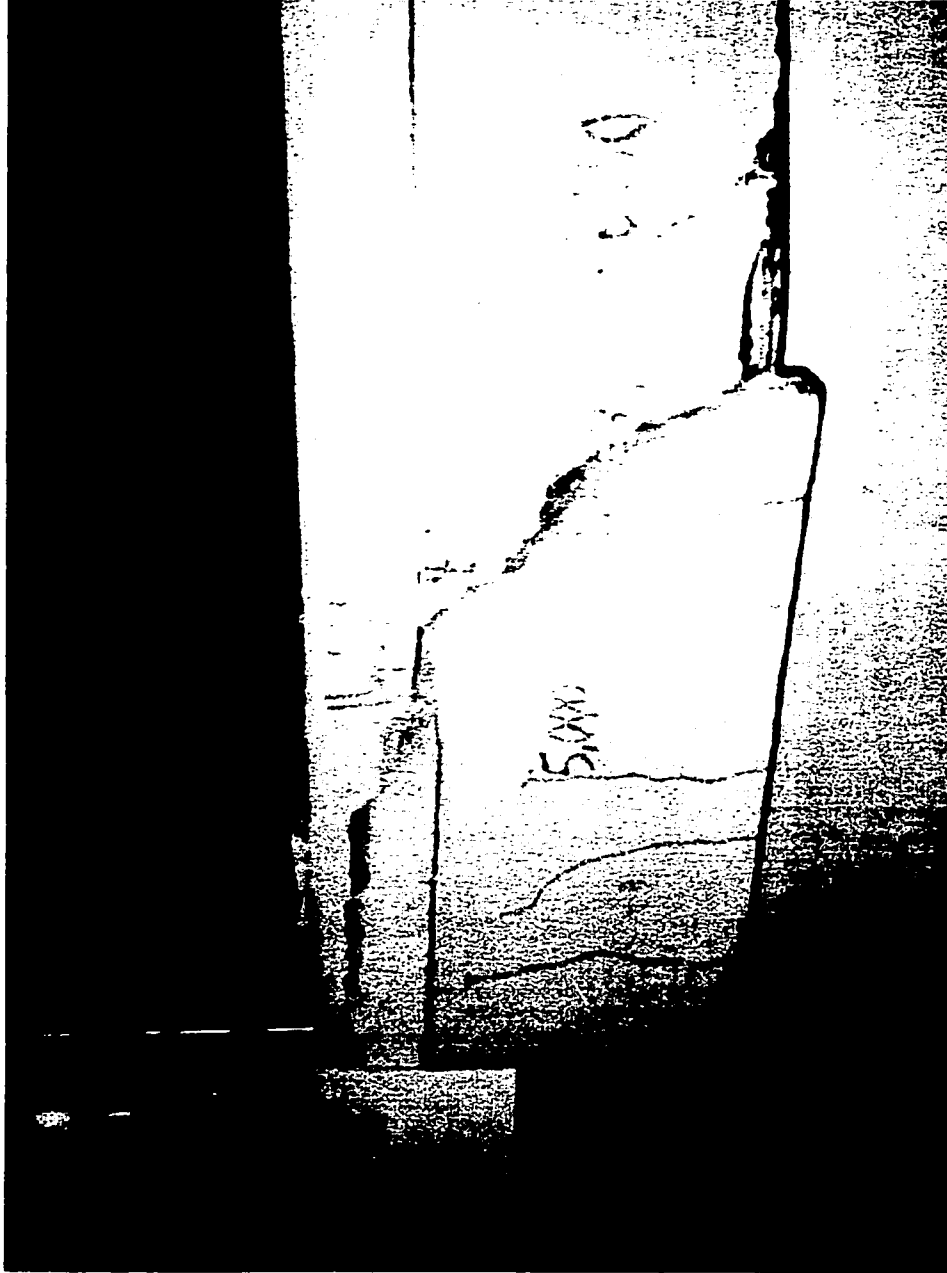
Fig. 3-21: Failure Crack of Beam # 26.

Fig. 3-22: Failure Crack of Beam # 29.
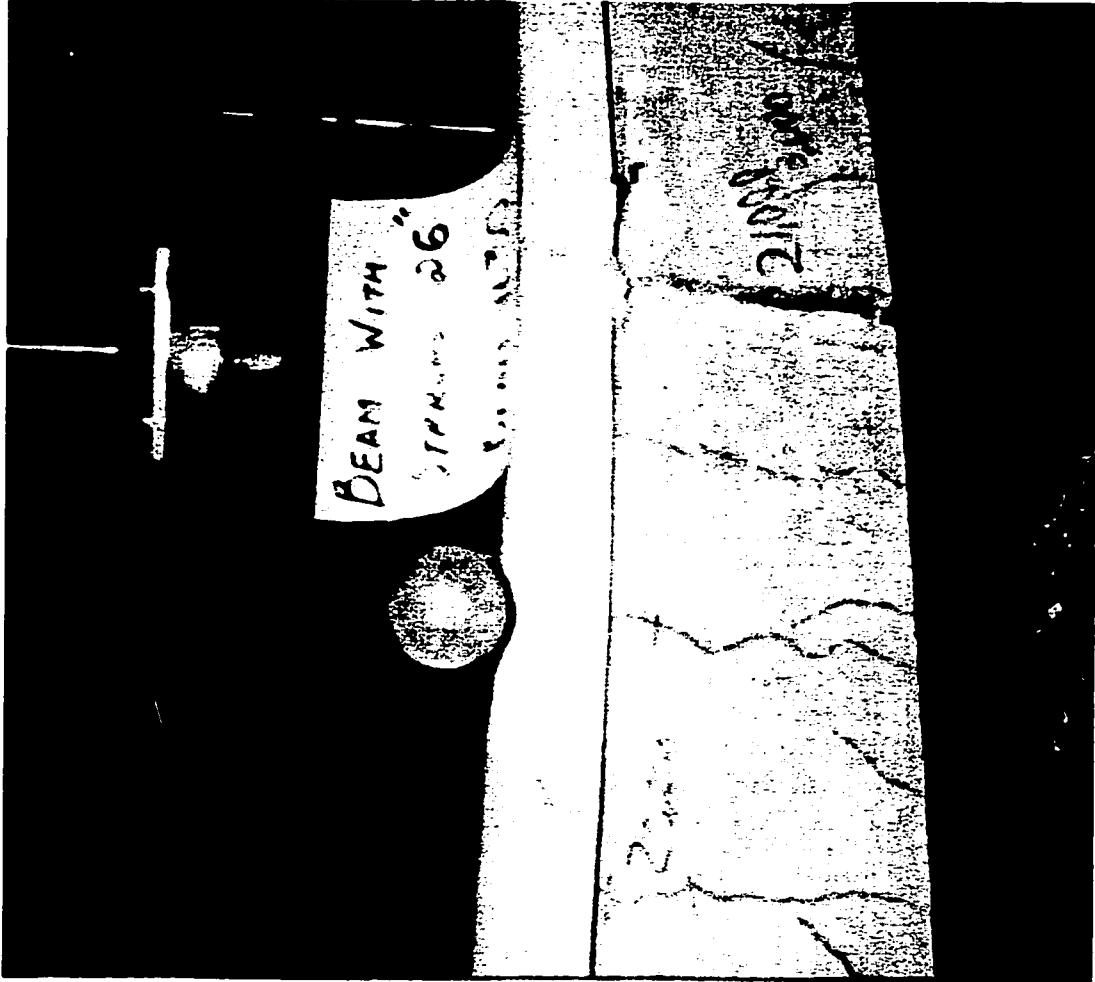
Fig. 3-23: Failure Crack of Beam # 30.
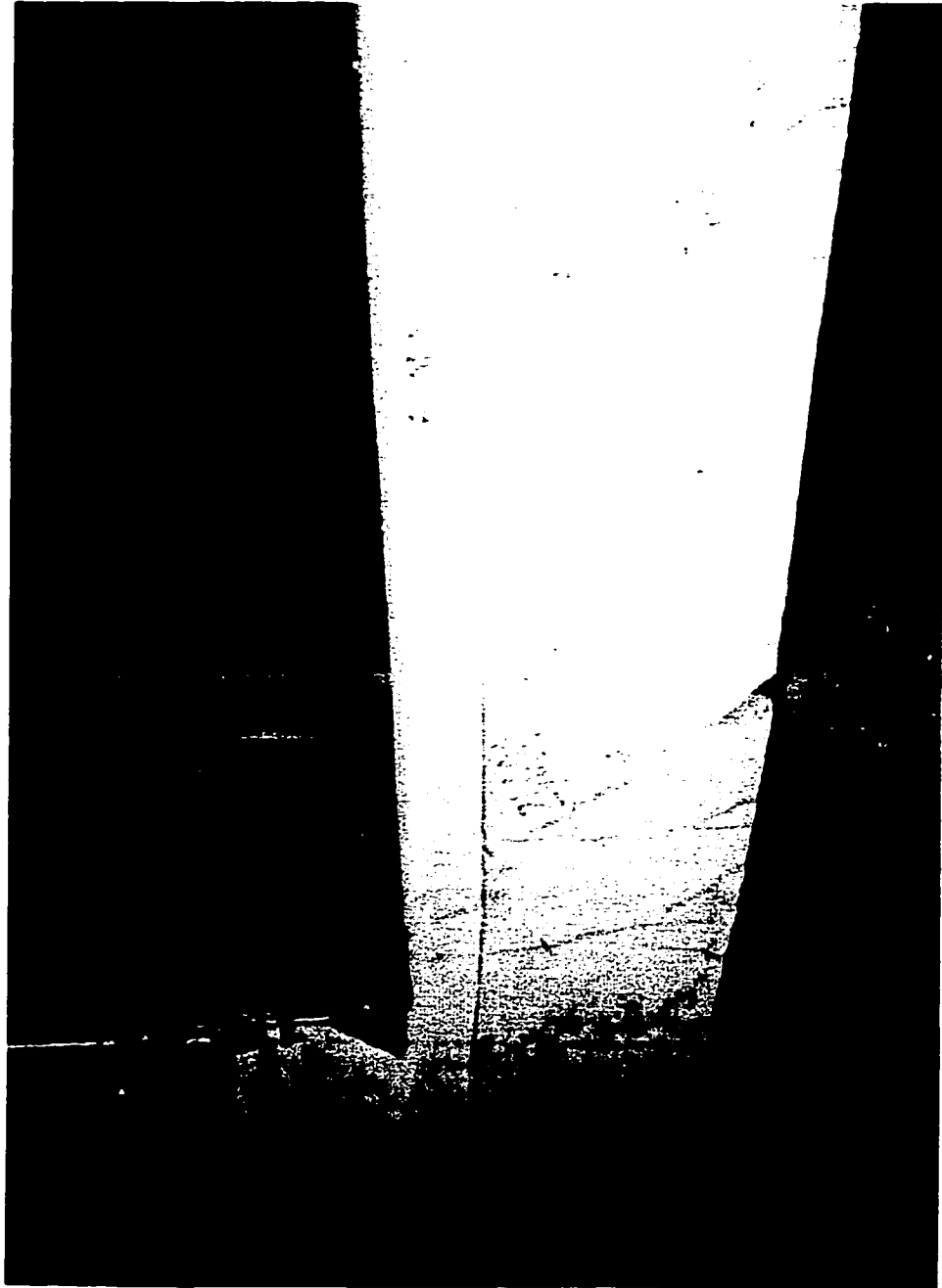
Fig. 3-24: Failure Crack of Beam # 31.

Fig. 3-25: Failure Crack of Beam # 32.
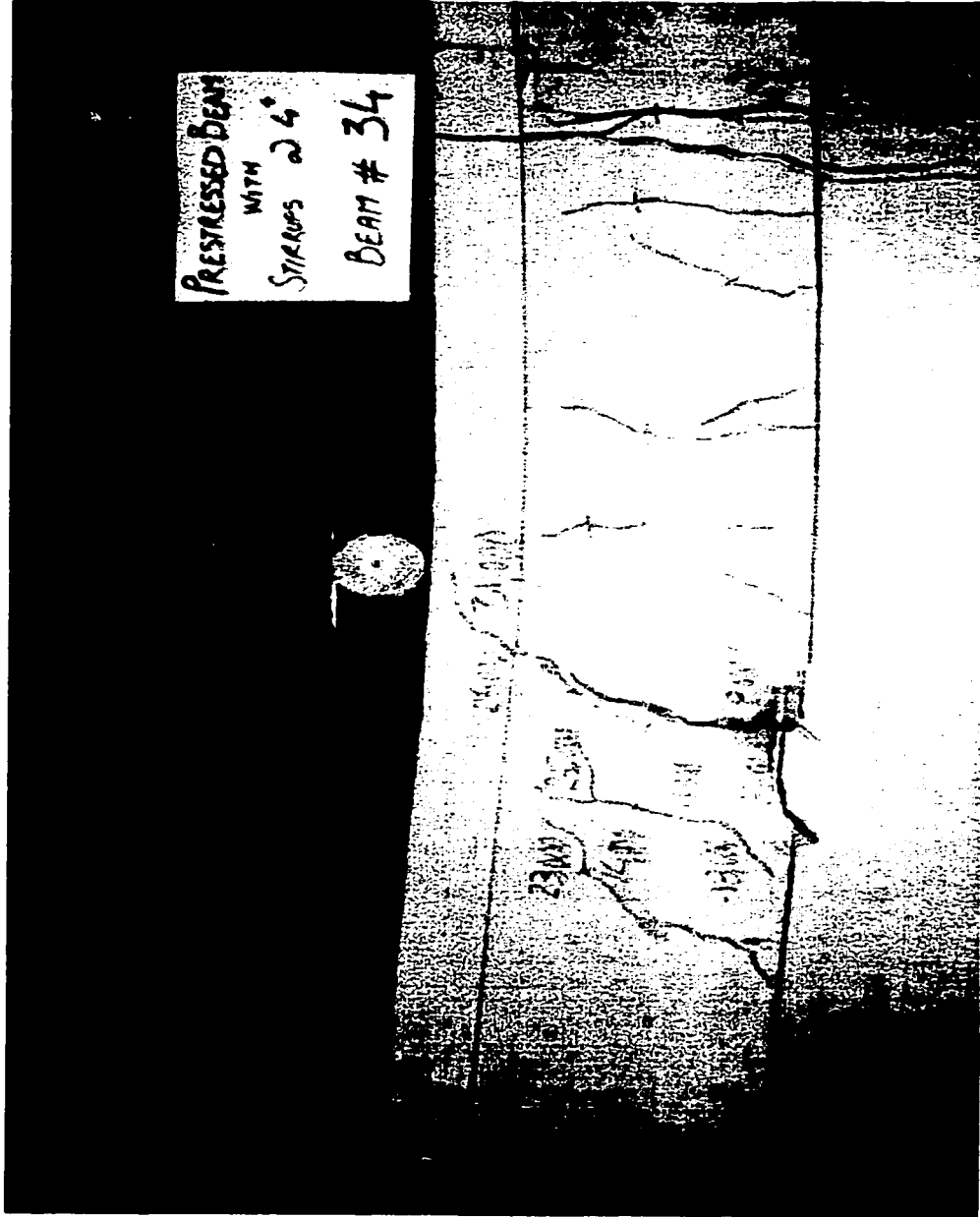
Fig. 3-26: Failure Crack of Beam # 34.

Fig. 3-27: Failure Crack of Beam # 35.

84
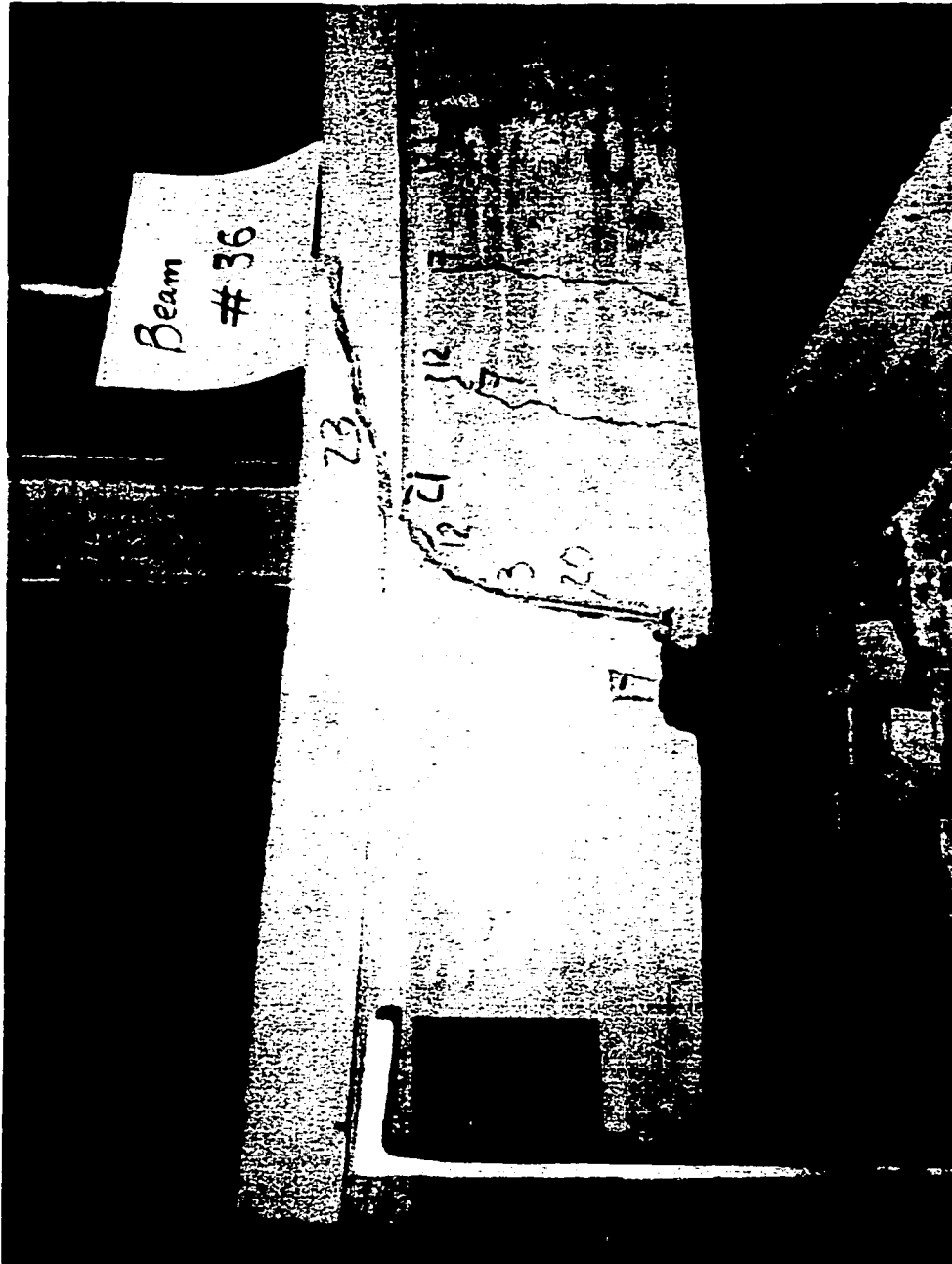
Fig. 3-28: Failure Crack of Beam # 36.

CHAPTER 4

ANALYTICAL MODELLING OF CRACK PATH GEOMETRY

4.1 General

The corrosion resistance of FRP bars highlights the possibility of allowing for wider and deeper cracks in FRP-reinforced concrete beams. However, it has been observed during the conducted experimental program (Chapter 3) that the crack formation characteristics, e.g. crack geometry and crack width, have a significant effect on the behaviour and strength of the tested beams. Therefore, this chapter presents an analytical modelling of crack geometry for concrete beams reinforced with FRP or steel bars as a step to quantifying the effect of crack formation not only on beam serviceability but also on beam behaviour and strength.

Fig. 4-1 illustrates the proposed model of crack path geometry versus the common simplified model as a line connecting point (f) with the nearest loading point (pt) (Jenq and Shah 1989). In order to determine the forces developed in the concrete portion above crack tip at the beam cross section I-I, the crack tip located at point (i) by the proposed model is relocated at point (j) by the line model. It can be seen that based on point (j), the depth of the concrete above the crack is significantly more than the actual one, leading to an inaccurate prediction of the shear/compressive forces developed in concrete.

Consequently, the shear/tension forces developed in both longitudinal and shear reinforcement crossing the crack, which must be in equilibrium with the forces developed in concrete, will be inaccurate as well. Furthermore, the error in locating point (i), which is the centre of rotation of the beam segments on both sides of the crack, will be reflected in an error in estimating the shear displacement induced in the bars crossing the crack (Fig. 3-30). Also, the significance of having an accurate model for crack path geometry has been demonstrated in detail in Chapter 8 by investigating the effect of the model accuracy on the predicted beam strength.

4.2 Analytical Modelling

The main parameter that defines the crack path in concrete is the direction of the principal stresses/strains. Assuming that the directions of principal stresses coincide with those of the principal strains, when the crack reaches a certain point, the perpendicular to the crack path at this point has the same direction of the principal tensile stress and the tangent to the path has the same direction of the principal compressive stress.

At the crack starting point (st) (Fig. 4-1) the shear stress equals zero and consequently the direction of the principal tensile stress at this point coincides with that for the longitudinal tensile stress at the extreme bottom of the beam web. Similarly, approaching point (pt), the crack path tends to be tangential to X-axis (Ferguson and Cowen 1981; Leet 1991; Salib et al. 1999b). In fact, these directions will be affected by the local stresses resulting from the applied load at point (pt). However, the zone of this

effect is limited and the crack approaches point (pt) governed by the same principal stresses concept until, actually or virtually, it reaches this point. Therefore, the boundary conditions of the relationship between X_i and Y_i can be easily determined and mathematically expressed. The first and second of these conditions represent that the crack starts vertically at a distance D from the nearest support, i.e. from the origin of the coordinate system (Fig. 4-2) as follows:

$$X = D \quad at \quad Y = 0.0 \tag{4-1}$$

$$(dX/dY) = 0.0 \quad at \ (X = D \ \& \ Y = 0.0) \tag{4-2}$$

Similarly, the third and fourth boundary conditions can be presented as follows:

$$X = Lp \quad at \quad Y = H \tag{4-3}$$

$$(dY/dX) = 0.0 \quad at \ (X = Lp \ \& \ Y = H) \tag{4-4}$$

Hence, the relationship between X and Y can be expressed as follows:

$$\left(\frac{L_P - X}{L_P - D}\right)^2 + \left(\frac{Y}{H}\right)^2 = 1 \qquad ; \ 0.0 \leq Y \leq H \ ; \ D \leq X \leq Lp \tag{4-5}$$

It can be seen that this relationship is represented by the equation of a quarter of an ellipse that connects point (st) and point (pt).

4.3 Analytical Modelling vs. Experimental Results

The comparison between the actual crack geometry and that obtained by Equation 4-5 indicated that this equation provides a good accuracy up to $Y \leq H/4$. Then gradually, as Y increases, the corresponding X-coordinate calculated by the equation is less than the

actual ones. As can be seen from Fig. 4-2, while the crack progresses towards the nearest loading point, it is shifted to follow a new elliptical path of a starting point that is further from the support than that of the original elliptical path expressed by Equation 4-5. Hence, the new elliptical path may be expressed as follows (Fig. 4-3):

$$\left(\frac{L_p - X}{C_D \, (L_P - D)}\right)^2 + \left(\frac{Y}{H}\right)^2 = 1 \qquad ; \ 0.0 \leq Y \leq H \ ; \ D \leq X \leq Lp \qquad (4\text{-}6)$$

where: C_D = dimensionless coefficient used to locate the starting point of the new elliptical path

$$C_D = \left(\frac{(C_o - C_{Lp})(L_P - D)}{L_P}\right) + C_{Lp} \qquad (4\text{-}7)$$

$$C_o = 1.0 \qquad (4\text{-}8)$$

$$C_{Lp} = 0.5 * (Lp/d - 1.5) \qquad\qquad ; \ 1.0 \geq C_{Lp} \geq 0.0 \quad (4\text{-}9)$$

Equation 4-9 has been selected based on the least squares method when applied to the difference between the actual crack geometry for few of the major cracks formed in beams #34 and #35 and the corresponding modelled geometry obtained under different values and expressions of C_{Lp} (Tables 4-1 to 4-4). The square root of the summation of $\{ [(X_i)_{mod} - (X_i)_{exp}] / (X_i)_{exp} \}^2$ is listed at the last row of these tables, corresponding to the assumed value of C_{Lp}.

In order to provide a smooth transition between Equation 4-5 and 4-6, the analytical modelling has been proposed as follows (Fig. 4-3):

89

- For $0.0 \leq Y \leq H/4$, the analytical model is presented by Equation 4-5.

- For $H/4 \leq Y \leq 3H/4$, the analytical model is presented by this equation:

$$X = \frac{\left[\left(\dfrac{3H}{4} - Y\right)*(Equation\ 4-5) + \left(Y - \dfrac{H}{4}\right)*(Equation\ 4-6)\right]}{H/2} \tag{4-10}$$

- For $3H/4 \leq Y \leq H$, the analytical model is presented by Equation 4-6.

The results obtained by the analytical model have been compared with the corresponding results of the tested beams. The actual geometry of the major/failure cracks formed in beams # 2, 3, 21, 25, 26, 31, 34 and 35 are presented in Figs. 4-4 to 4-14 respectively, as well as the corresponding crack geometry obtained by the analytical model. It should be mentioned that beam # 21 was reinforced in flexure with steel bars (Table 3-1).

Since beam failure was observed for most cases to be initiated when one of the major cracks approached the beam flange, the X-Coordinate of point (fl) (Fig. 4-1) calculated by the analytical model, $(X_{fl})_{mod}$, has been compared with the corresponding measured distance, $(X_{fl})_{exp}$, for all the major/failure cracks formed in the tested beams. The values of both $(X_{fl})_{mod}$ and $(X_{fl})_{exp}$ are listed in Table 4-5 accompanied with the percentage of error, %e, which has been calculated as follows:

$$\%e = \left(\frac{(X_{fl})_{mod} - (X_{fl})_{exp}}{(X_{fl})_{exp}}\right)*100 \tag{4-11}$$

It can be realised that the values of %e ranges between - 5.0 % and + 9.7 % with an absolute mean value of 3.4 %.

It should be also noted that for some beams, the difference in a crack point location introduced by the model and that actually measured in the laboratory may be attributed to the roughness of the actual crack surface. The concrete fracture occurs at the interface between the cement-fine aggregate matrix and the coarse aggregate where the crack progresses bounded by the neighbouring coarse aggregates introducing a corrugated path (Surendra et al. 1995).

Although, the geometrical characteristics of the crack path for reinforced concrete beams, in general, and for prestressed ones, in particular, have not been reported in detail yet, the published photos of the failure cracks formed in the FRP-prestressed concrete beams tested by Park and Naaman (1999c) demonstrate similar geometrical characteristics to those outlined by Ferguson and Cowen (1981), Leet (1991), and Salib et al. (1999b) as well as to the present analytical modelling. Therefore, this modelling (Equations 4-5, 4-6, and 4-10), which has been verified for both prestressed and non-prestressed concrete beams tested in the present experimental program (Chapter 3), is assumed to be valid for both prestressed and non-prestressed concrete beams.

Table 4-1: *Calculated Path Co-ordinates for a major Crack in Beam # 34 using Different Formulas of C_{Lp}, dimensions are in mm (in).*

Y mm (in)	$X_{(exp)}$ mm (in)	$X_{(mod)}$ mm (in)					
		$C_{Lp} =$ 0.5	$C_{Lp} =$ 0.5(Lp/d-0.5)	$C_{Lp} =$ 0.5(Lp/d-1.0)	$C_{Lp} =$ 0.5(Lp/d-1.5)	$C_{Lp} =$ 0.5(Lp/d-2.0)	$C_{Lp} =$ 0.5(Lp/d-2.5)
(1)	(2)	(3)	(4)	(5)	(6)	(7)	(8)
0 (0.0)	635 (25.00)	635.0 (25.00)	635.0 (25.00)	635.0 (25.00)	635.0 (25.00)	635.0 (25.00)	635.0 (25.00)
25 (1.0)	640 (25.20)	635.8 (25.03)	635.8 (25.03)	635.8 (25.03)	635.8 (25.03)	635.8 (25.03)	635.8 (25.03)
51 (2.0)	650 (25.60)	637.8 (25.11)	637.8 (25.11)	637.8 (25.11)	637.8 (25.11)	637.8 (25.11)	637.8 (25.11)
76 (3.0)	653 (25.70)	641.6 (25.26)	641.6 (25.26)	641.6 (25.26)	641.6 (25.26)	641.6 (25.26)	641.6 (25.26)
102 (4.0)	662.9 (26.10)	653.3 (25.72)	646.7 (25.46)	647.9 (25.51)	651.5 (25.65)	654.8 (25.78)	658.1 (25.91)
127 (5.0)	676 (26.60)	672.8 (26.49)	653.5 (25.73)	657.9 (25.90)	667.5 (26.28)	677.4 (26.67)	687.1 (27.05)
152 (6.0)	687 (27.05)	693.4 (27.30)	661.9 (26.06)	669.1 (26.34)	684.8 (26.96)	700.8 (27.59)	716.0 (28.19)
178 (7.0)	706 (27.80)	714.8 (28.14)	672.3 (26.47)	682.2 (26.86)	703.1 (27.68)	724.4 (28.52)	744.9 (29.33)
203 (8.0)	719 (28.30)	736.6 (29.00)	685.0 (26.97)	696.9 (27.44)	722.6 (28.45)	748.3 (29.46)	773.7 (30.46)
229 (9.0)	737 (29.00)	759.2 (29.89)	700.3 (27.57)	713.9 (28.11)	743.2 (29.26)	772.7 (30.42)	801.4 (31.55)
254 (10.0)	757 (29.80)	782.3 (30.80)	718.8 (28.30)	733.6 (28.88)	764.8 (30.11)	797.1 (31.38)	828.0 (32.60)
280 (11.0)	775 (30.50)	802.1 (31.58)	741.7 (29.20)	755.7 (29.75)	785.4 (30.92)	816.9 (32.12)	845.3 (33.28)
$\sqrt[2]{\sum_{Y=0}^{Y=1}\left(\dfrac{X_{mod}-X_{exp}}{X_{exp}}\right)^2}$		0.071	0.122	0.084	0.039	0.108	0.191

Table 4-2: *Calculated Path Co-ordinates for the First Major Crack of Beam # 35 using Different Formulas of C_{Lp}, dimensions are in mm (in).*

Y mm (in) (1)	$X_{(exp)}$ mm (in) (2)	$X_{(mod)}$ mm (in)					
		$C_{Lp} = 0.5$ (3)	$C_{Lp} = 0.5(Lp/d-0.5)$ (4)	$C_{Lp} = 0.5(Lp/d-1.0)$ (5)	$C_{Lp} = 0.5(Lp/d-1.5)$ (6)	$C_{Lp} = 0.5(Lp/d-2.0)$ (7)	$C_{Lp} = 0.5(Lp/d-2.5)$ (8)
0 (0.0)	419 (16.50)	419.1 (16.50)	419.1 (16.50)	419.1 (16.50)	419.1 (16.50)	419.1 (16.50)	419.1 (16.50)
25 (1.0)	419 (16.50)	419.6 (16.52)	419.6 (16.52)	419.6 (16.52)	419.6 (16.52)	419.6 (16.52)	419.9 (16.53)
51 (2.0)	419 (16.50)	421.9 (16.61)	421.9 (16.61)	421.9 (16.61)	421.9 (16.61)	421.9 (16.61)	421.9 (16.61)
76 (3.0)	432 (17.00)	425.2 (16.74)	425.2 (16.74)	425.2 (16.74)	425.2 (16.74)	425.2 (16.74)	425.2 (16.74)
102 (4.0)	457 (18.00)	435.9 (17.16)	432.6 (17.03)	435.4 (17.14)	438.2 (17.25)	440.9 (17.36)	17.47 (17.47)
127 (5.0)	464 (18.25)	453.1 (17.84)	443.5 (17.46)	17.85 (17.85)	459.9 (18.11)	467.9 (18.42)	476.3 (18.75)
152 (6.0)	476 (18.75)	471.4 (18.56)	455.9 (17.95)	468.9 (18.46)	482.6 (19.00)	495.6 (19.51)	508.5 (20.02)
178 (7.0)	502 (19.75)	490.7 (19.32)	469.6 (18.49)	487.4 (19.19)	505.7 (19.91)	522.7 (20.58)	540.5 (21.28)
203 (8.0)	530 (20.85)	510.5 (20.10)	485.1 (19.10)	506.7 (19.95)	528.8 (20.82)	21.64 (21.64)	571.3 (22.49)
229 (9.0)	564 (22.20)	531.4 (20.92)	502.2 (19.77)	526.8 (20.74)	542.8 (21.37)	575.8 (22.67)	600.5 (23.64)
254 (10.0)	589 (23.20)	552.9 (21.77)	521.5 (20.53)	547.9 (21.57)	575.3 (22.65)	600.9 (23.66)	627.6 (24.71)
280 (11.0)	615 (24.20)	572.0 (22.52)	542.0 (21.34)	568.2 (22.37)	593.3 (23.36)	617.7 (24.32)	642.6 (25.32)
$\sqrt{\dfrac{1}{2}\sum_{Y=0}^{Y=1}\left(\dfrac{X_{mod}-X_{exp}}{X_{exp}}\right)^2}$		0.129	0.238	0.145	0.066	0.086	0.171

Table 4-3: Calculated Path Co-ordinates for the Second Major Crack in Beam # 35 using Different Formulas of C_{Lp}, dimensions are in mm (in).

Y mm (in)	$X_{(exp)}$ mm (in)	$X_{(mod)}$ mm (in)					
		$C_{Lp} =$ 0.5	$C_{Lp} =$ 0.5(Lp/d-0.5)	$C_{Lp} =$ 0.5(Lp/d-1.0)	$C_{Lp} =$ 0.5(Lp/d-1.5)	$C_{Lp} =$ 0.5(Lp/d-2.0)	$C_{Lp} =$ 0.5(Lp/d-2.5)
(1)	(2)	(3)	(4)	(5)	(6)	(7)	(8)
0 (0.0)	533 (21.00)	533.4 (21.00)	533.4 (21.00)	533.4 (21.00)	533.4 (21.00)	533.4 (21.00)	533.4 (21.00)
25 (1.0)	540 (21.25)	533.9 (21.02)	533.9 (21.02)	533.9 (21.02)	533.9 (21.02)	533.9 (21.02)	533.9 (21.02)
51 (2.0)	546 (21.50)	534.9 (21.06)	534.9 (21.06)	534.9 (21.06)	534.9 (21.06)	534.9 (21.06)	534.9 (21.06)
76 (3.0)	551 (21.70)	536.9 (21.14)	536.9 (21.14)	536.9 (21.14)	536.9 (21.14)	536.9 (21.14)	536.9 (21.14)
102 (4.0)	554 (21.80)	543.6 (21.40)	541.5 (21.32)	543.3 (21.39)	545.6 (21.48)	547.6 (21.56)	549.7 (21.64)
127 (5.0)	572 (22.50)	555.2 (21.86)	548.4 (21.59)	554.5 (21.83)	560.3 (22.06)	566.2 (22.29)	572.3 (22.53)
152 (6.0)	584 (23.00)	567.2 (22.33)	556.0 (21.89)	565.7 (22.27)	575.3 (22.65)	584.9 (23.03)	594.4 (23.40)
178 (7.0)	597 (23.50)	579.4 (22.81)	564.6 (22.23)	577.6 (22.74)	590.3 (23.24)	603.3 (23.75)	615.9 (24.25)
203 (8.0)	603 (23.75)	592.1 (23.31)	573.8 (22.59)	589.5 (23.21)	605.3 (23.83)	621.0 (24.45)	636.5 (25.06)
229 (9.0)	610 (24.00)	604.8 (23.81)	583.9 (22.99)	601.9 (23.70)	619.8 (24.40)	637.8 (25.11)	655.6 (25.81)
254 (10.0)	622 (24.50)	617.7 (24.32)	595.4 (23.44)	614.7 (24.20)	633.9 (24.96)	653.3 (25.72)	672.6 (26.48)
280 (11.0)	654 (25.75)	628.1 (24.73)	607.1 (23.90)	625.3 (24.62)	643.6 (25.34)	662.2 (26.07)	680.5 (26.79)
$\sqrt[2]{\sum_{Y=0}^{Y=1}\left(\frac{X_{mod}-X_{exp}}{X_{exp}}\right)^2}$		0.078	0.140	0.084	0.055	0.085	0.139

94

Table 4-4: Calculated Path Co-ordinates for the Failure Crack of Beam # 35 using Different Formulas of C_{Lp}, dimensions are in mm (in).

Y mm (in)	$X_{(exp)}$ mm (in)	$X_{(mod)}$ mm (in)					
		$C_{Lp} =$ 0.5	$C_{Lp} =$ 0.5(Lp/d-0.5)	$C_{Lp} =$ 0.5(Lp/d-1.0)	$C_{Lp} =$ 0.5(Lp/d-1.5)	$C_{Lp} =$ 0.5(Lp/d-2.0)	$C_{Lp} =$ 0.5(Lp/d-2.5)
(1)	(2)	(3)	(4)	(5)	(6)	(7)	(8)
0 (0.0)	203 (8.00)	203.2 (8.00)	203.2 (8.00)	203.2 (8.00)	203.2 (8.00)	203.2 (8.00)	203.2 (8.00)
25 (1.0)	203 (8.00)	204.5 (8.05)	204.5 (8.05)	204.5 (8.05)	204.5 (8.05)	204.5 (8.05)	204.5 (8.05)
51 (2.0)	203 (8.00)	208.0 (8.19)	208.0 (8.19)	208.0 (8.19)	208.0 (8.19)	208.0 (8.19)	208.0 (8.19)
76 (3.0)	216 (8.50)	214.4 (8.44)	214.4 (8.44)	214.4 (8.44)	214.4 (8.44)	214.4 (8.44)	214.4 (8.44)
102 (4.0)	241 (9.50)	227.8 (8.97)	225.3 (8.87)	227.8 (8.97)	230.1 (9.06)	232.7 (9.16)	235.2 (9.26)
127 (5.0)	267 (10.50)	249.4 (9.82)	241.0 (9.49)	248.2 (9.77)	255.5 (10.06)	262.4 (10.33)	269.2 (10.60)
152 (6.0)	292 (11.50)	273.0 (10.75)	259.6 (10.22)	271.0 (10.67)	282.7 (11.13)	294.1 (11.58)	305.8 (12.04)
178 (7.0)	324 (12.75)	299.2 (11.78)	280.9 (11.06)	296.4 (11.67)	311.9 (12.28)	327.4 (12.89)	342.9 (13.5)
203 (8.0)	349 (13.75)	327.9 (12.91)	305.8 (12.04)	324.6 (12.78)	343.4 (13.52)	362.2 (14.26)	381.5 (15.02)
229 (9.0)	356 (14.00)	359.7 (14.16)	334.5 (13.17)	355.9 (14.01)	377.4 (14.86)	399.0 (15.71)	420.6 (16.56)
254 (10.0)	406 (16.00)	394.9 (15.55)	367.8 (14.48)	390.9 (15.39)	414.3 (16.31)	437.4 (17.22)	461.0 (18.15)
280 (11.0)	444 (17.50)	431.8 (17.00)	406.2 (15.99)	427.9 (16.85)	450.3 (17.73)	472.2 (18.59)	494.8 (19.48)
305 (12.0)	635 (25.00)	474.5 (18.68)	452.9 (17.83)	471.2 (18.55)	489.7 (19.28)	508.0 (20.00)	526.8 (20.74)
330 (13.0)	660 (26.00)	533.7 (21.01)	517.9 (20.39)	531.1 (20.91)	544.6 (21.44)	557.8 (21.96)	570.9 (22.48)
356 (14.0)	686 (27.00)	685.8 (27.00)	685.8 (27.00)	685.8 (27.00)	685.8 (27.00)	685.8 (27.00)	685.8 (27.00)
$\sqrt[2]{\sum_{Y=0}^{Y=14}\left(\dfrac{X_{mod}-X_{exp}}{X_{exp}}\right)^2}$		0.352	0.456	0.365	0.304	0.306	0.357

Table 4-5: Measured and Calculated Crack Coordinates, dimensions are in mm (in).

Beam # (1)	D (2)	$(X_{fl})_{mod}$ (3)	$(X_{fl})_{exp}$ (4)	%e (5)
2	1016 (40.0)	1296.9 (51.06)	1298 (51.1)	-0.1
3	610 (24.0)	974.6 (38.37)	1026 (40.4)	-5.0
21	381 (15.0)	745.9 (29.37)	737 (29.0)	1.2
24	483 (19.0)	815.3 (32.10)	836 (32.9)	-2.4
25	838 (33.0)	1057.2 (41.62)	1054 (41.5)	0.3
26	724 (28.5)	772.2 (30.40)	737 (29.0)	4.8
31	356 (14.0)	647.4 (25.49)	640 (25.2)	1.2
32	305 (12.0)	582.4 (22.93)	531 (20.9)	9.7
	432 (17.0)	669.5 (26.36)	635 (25.0)	5.4
	483 (19.0)	700.5 (27.58)	666 (26.2)	5.3
33	305 (12.0)	582.4 (22.93)	534 (21.0)	9.1
	330 (13.0)	599.9 (23.62)	554 (21.8)	8.3
	610 (24.0)	771.1 (30.36)	762 (30.0)	1.2
34	483 (19.0)	700.5 (27.58)	663 (26.1)	5.6
	635 (25.0)	784.6 (30.89)	775 (30.5)	1.2
	737 (29.0)	837.4 (32.97)	838 (33.0)	-0.1
35	203 (8.0)	452.9 (17.83)	445 (17.5)	1.8
	419 (16.5)	604.5 (23.80)	605 (23.8)	0.0
	533 (21.0)	642.6 (25.30)	653 (25.7)	-1.9
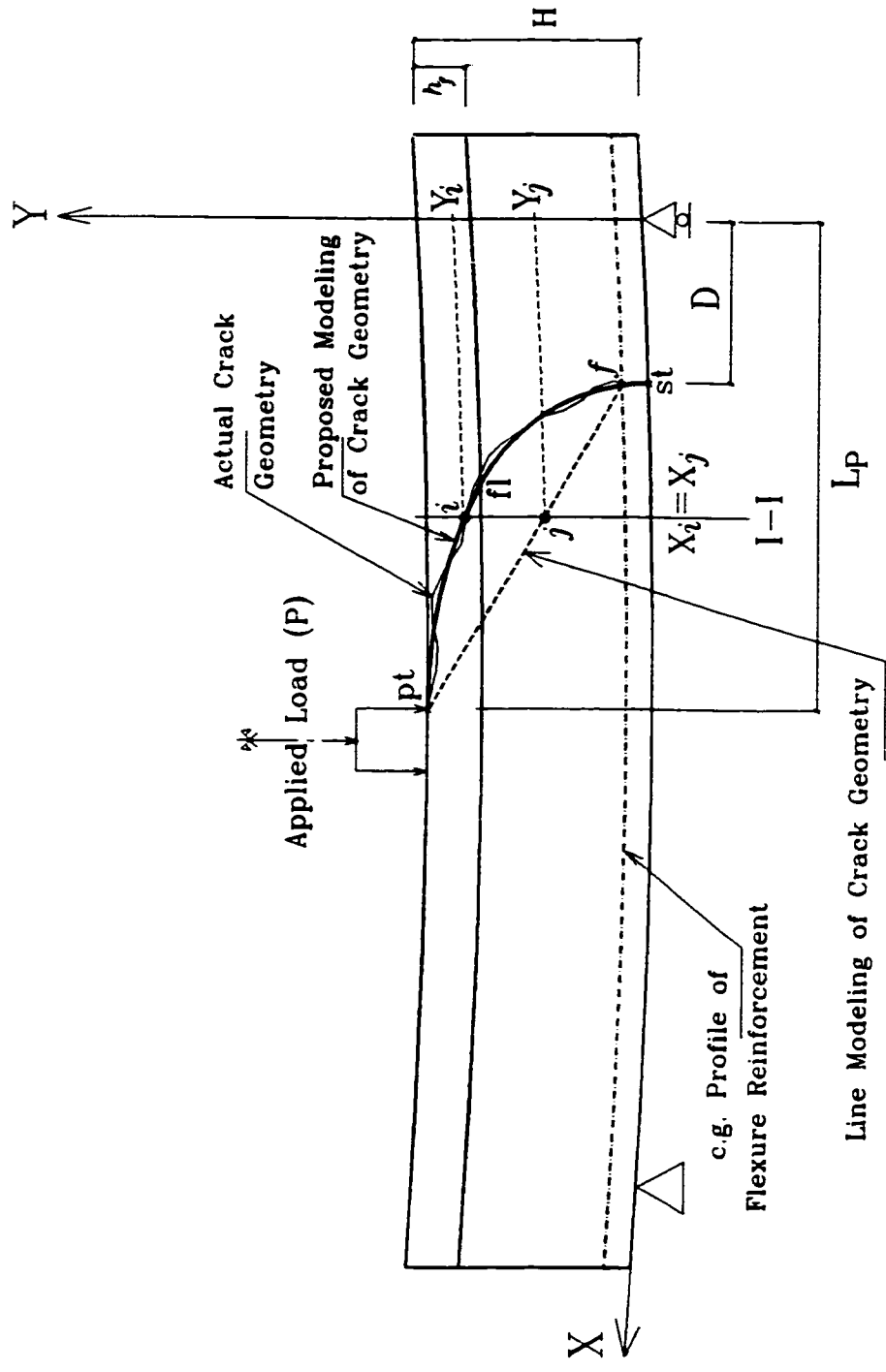
Fig. 4-1: Crack Path Geometry.
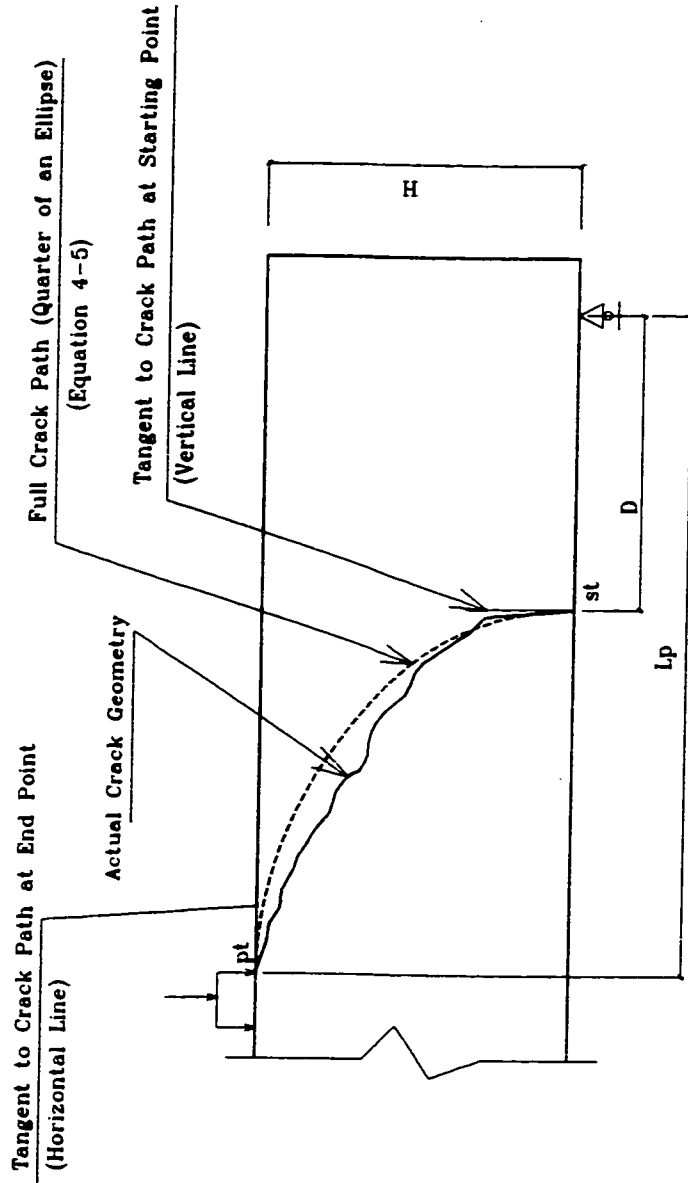
Fig. 4-2: Analytical Modelling of Crack Path Geometry Based on Equation 4-5.
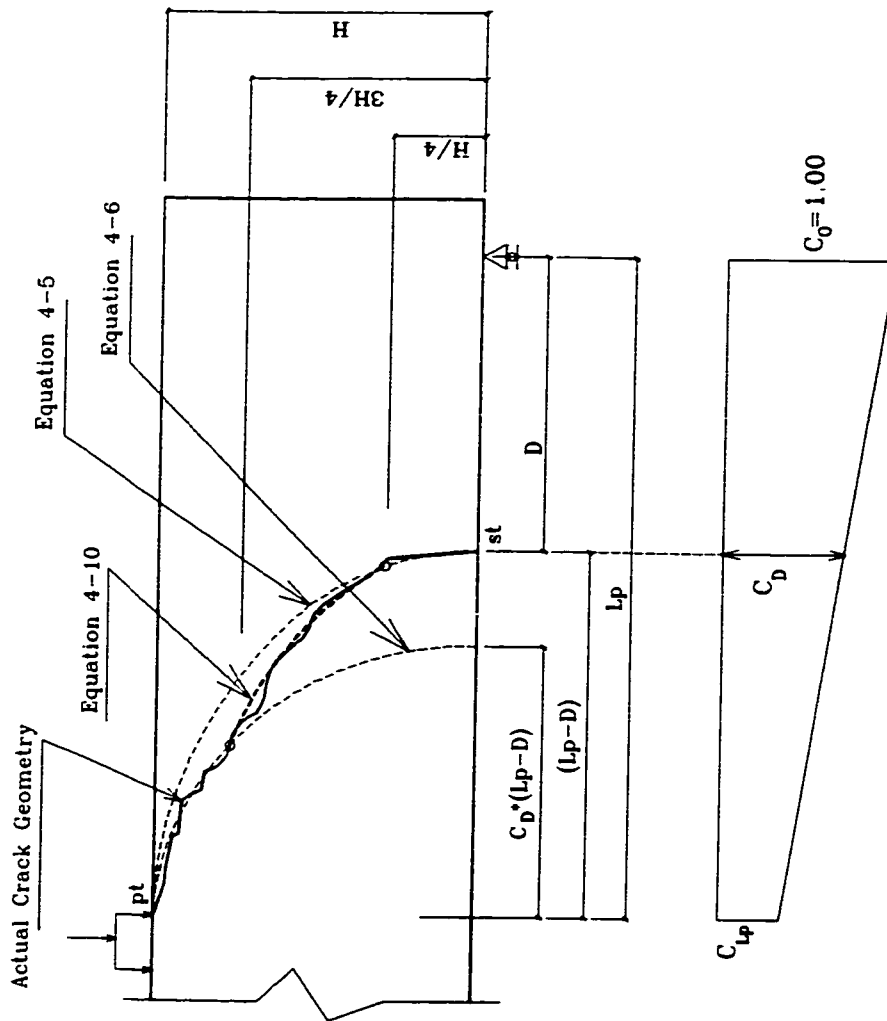
Fig. 4-3: *Analytical Modelling of Crack Path Geometry Based on Equations 4-5, 4-6 & 4-10.*
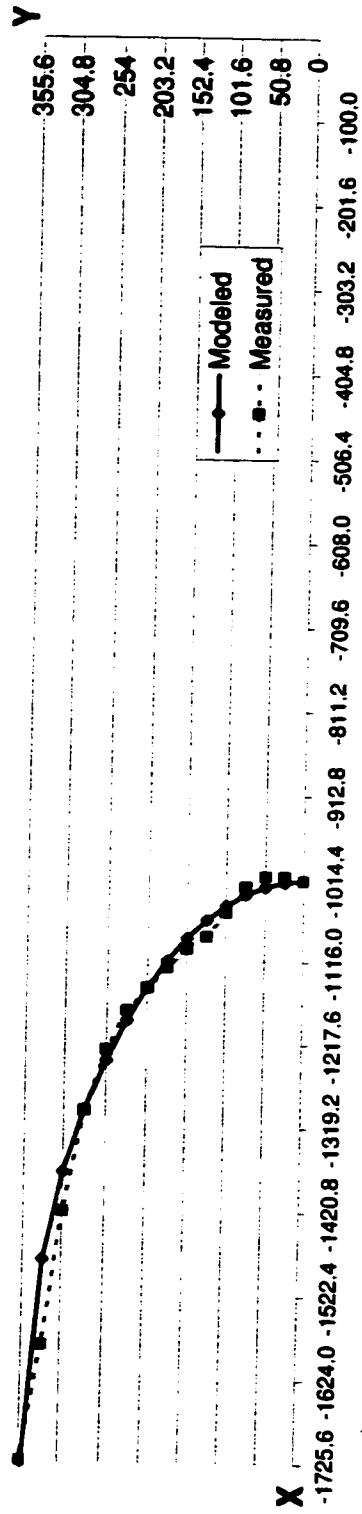
Fig. 4-4: Measured and Modeled Failure Crack Geometry of Beam # 2, (Dimensions are in mm).
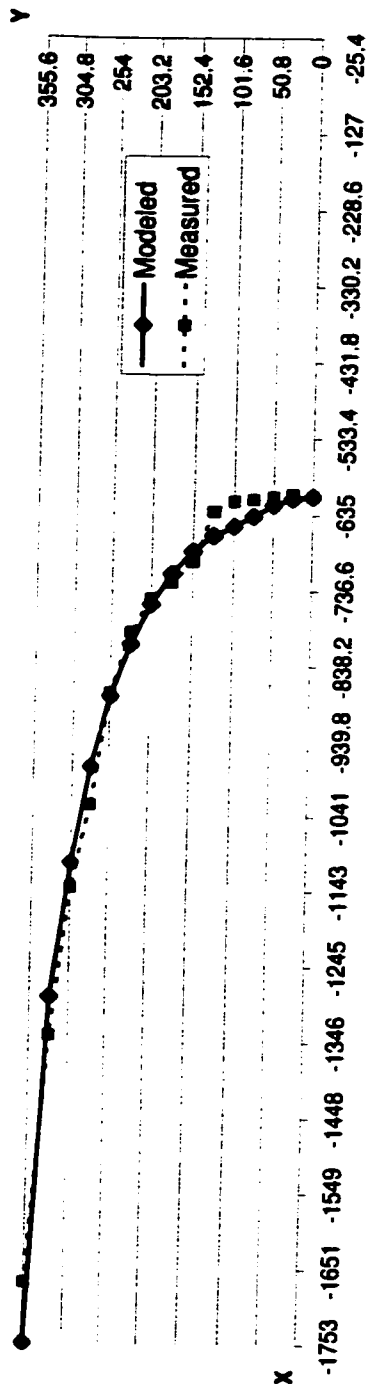
Fig. 4-5: Measured and Modeled Failure Crack of Beam # 3, (Dimensions are in mm).
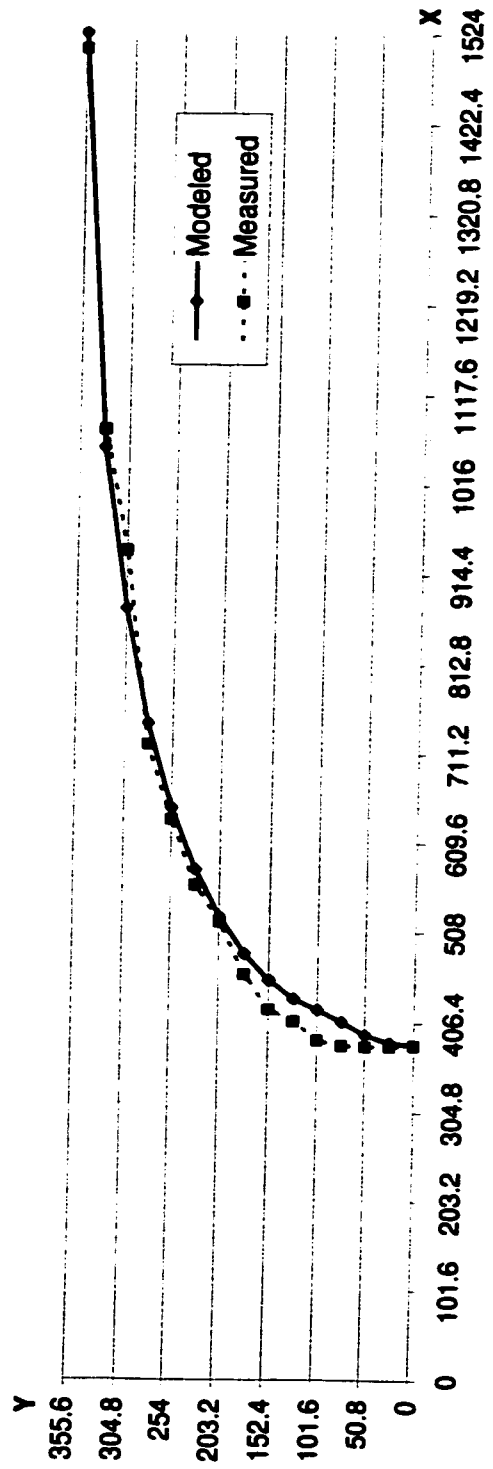
Fig. 4-6: Measured and Modeled Failure Crack Geometry of Beam # 21, (Dimensions are in mm).
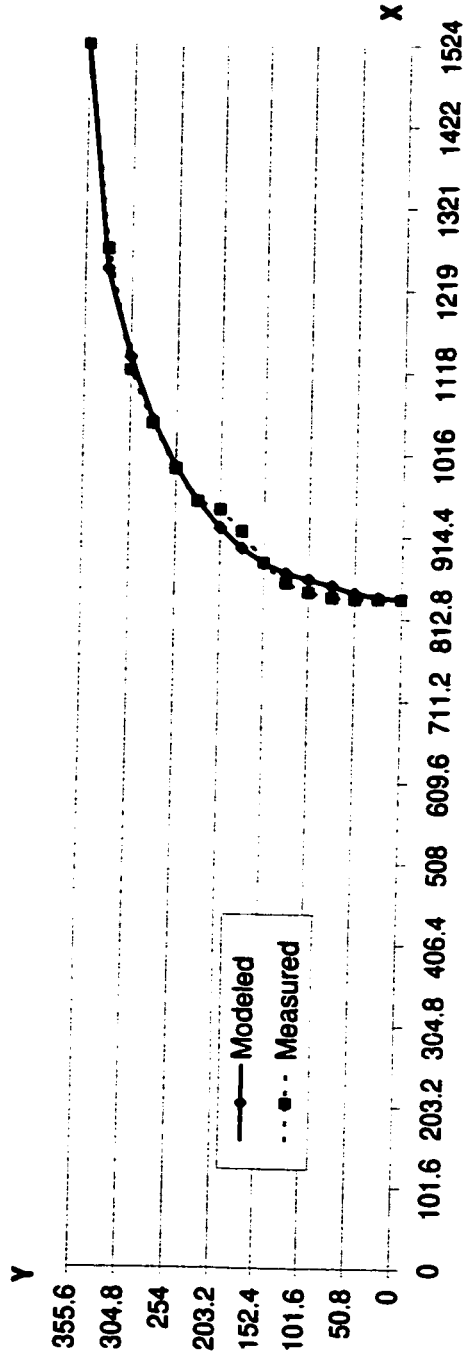
Fig. 4-7: Measured and Modeled Failure Crack Geometry of Beam # 25, (Dimensions are in mm).
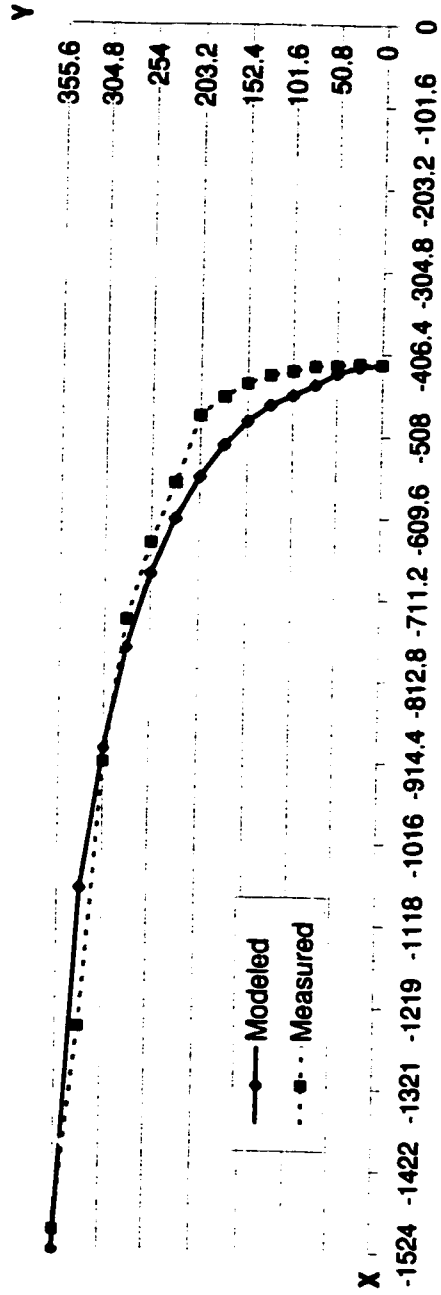
Fig. 4-8: Measured and Modeled Failure Crack Geometry of Beam # 26. (Dimensions are in mm).
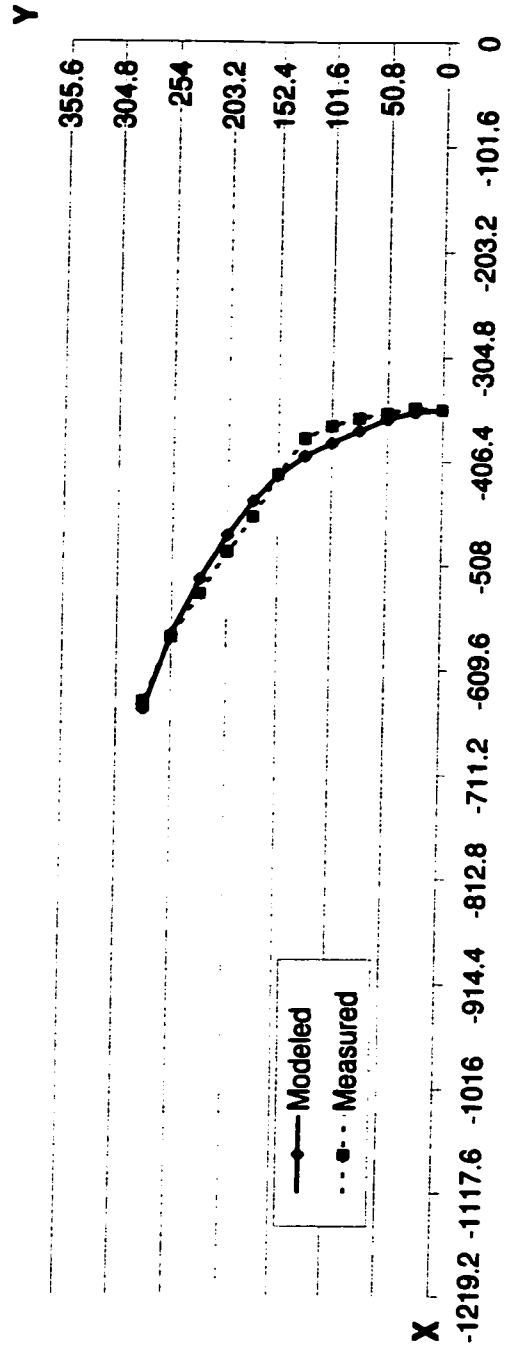
Fig. 4-9: Measured and Modeled Geometry of a Major Crack of Beam # 31, (Dimensions are in mm).
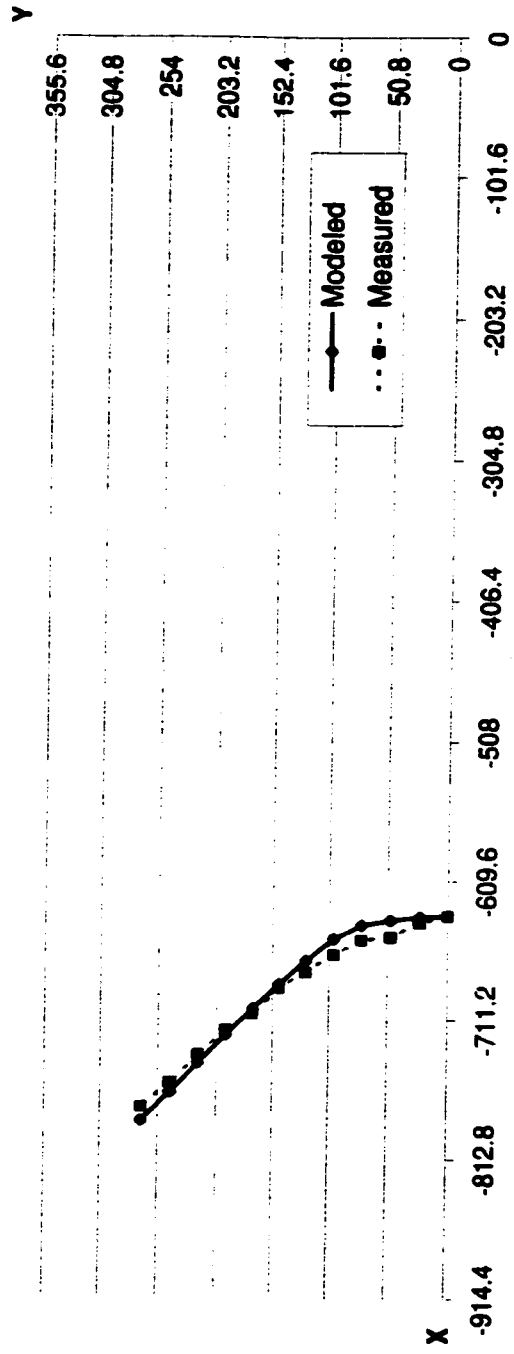
Fig. 4-10: Measured and Modeled Geometry of a Major Crack of Beam # 34, (Dimensions are in mm).
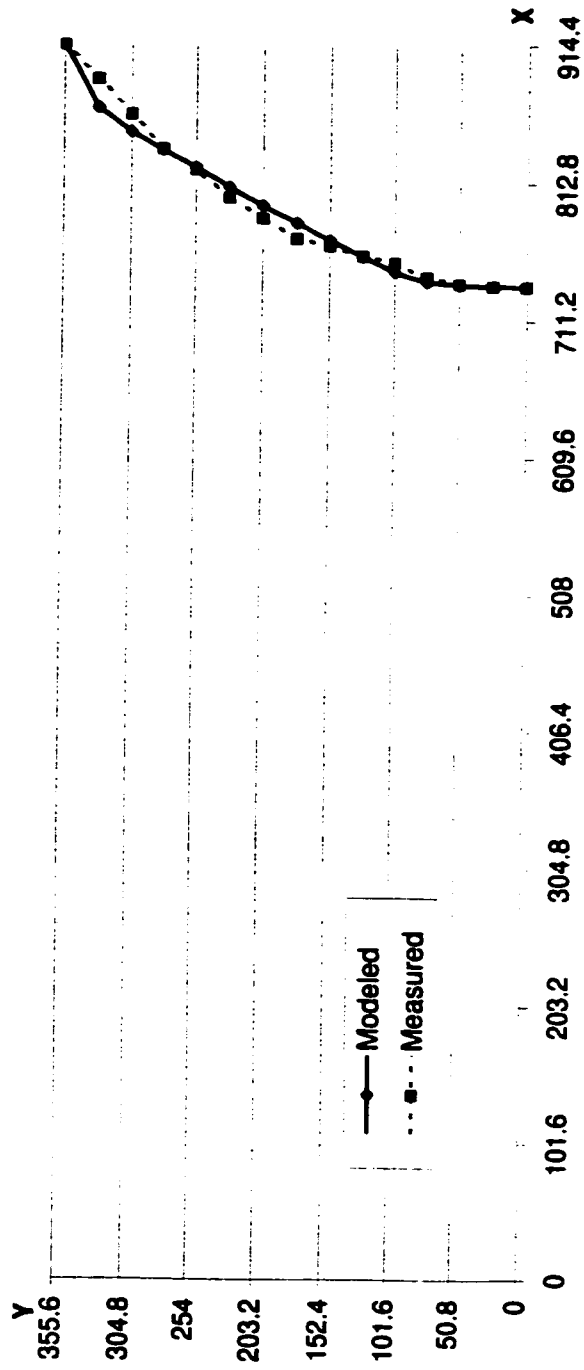
Fig. 4-11: Measured and Modeled Failure Crack Geometry of Beam # 34, (Dimensions are in mm).
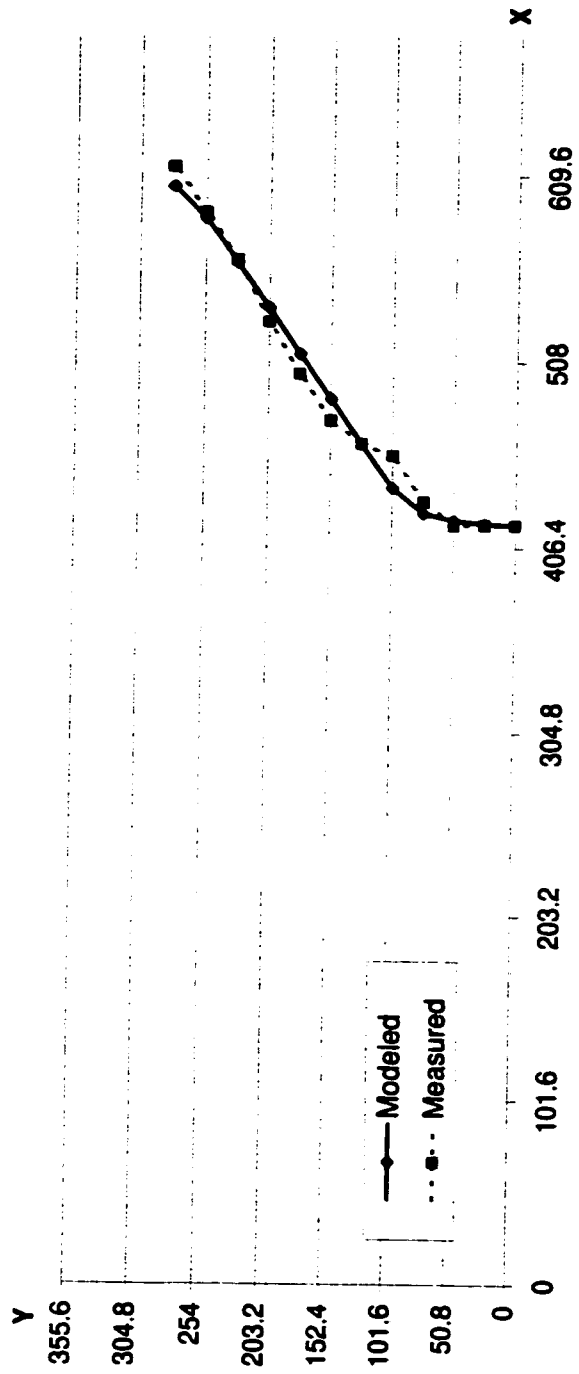
Fig. 4-12: Measured and Modeled Geometry of a Major Crack of Beam # 35, (Dimensions are in mm).
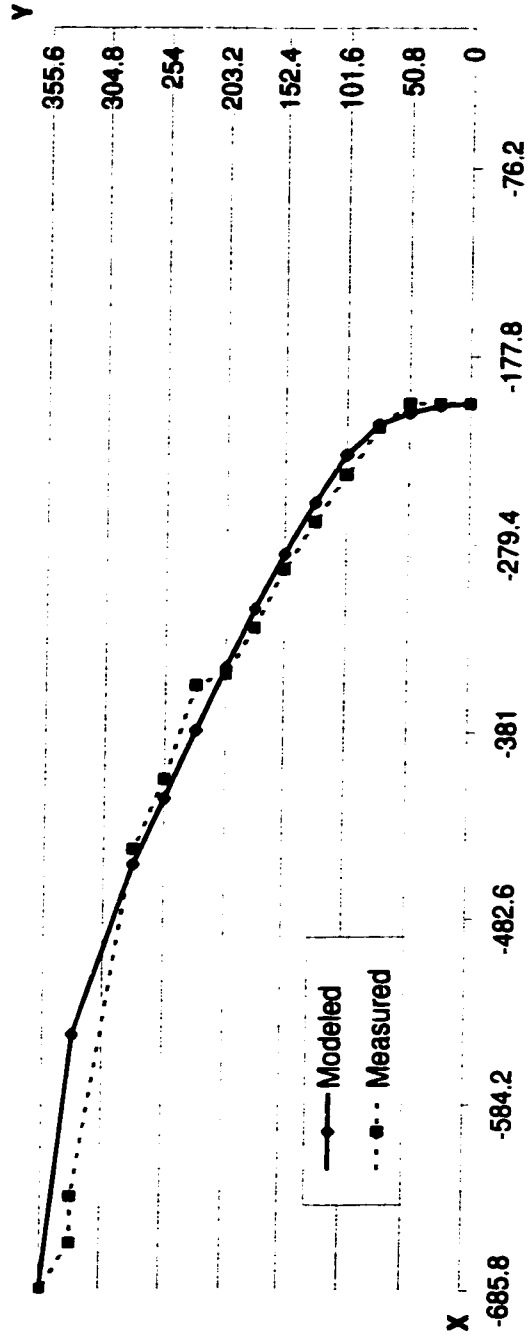
Fig. 4-13 Measured and Modeled Failure Crack Geometry of Beam # 35, (Dimensions are in mm).

CHAPTER 5

MAXIMUM CRACK WIDTH

5.1 General

The non-corrosive properties of FRP bars provide better durability of reinforced concrete structures. However, any recommendation towards relaxing the limits of the maximum allowable crack width should be re-examined. Based on the observed behaviour of FRP-reinforced concrete beams, the shear displacement of the reinforcing bars crossing a crack is significantly affected by the induced crack width. Furthermore, due to the low strength and brittle failure of FRP bars subjected to shear stresses, crack width becomes an important parameter that influences not only the beam serviceability but also the beam strength and its mode of failure. Therefore, in this chapter, one of the most common formulas used to predict crack width for steel-reinforced concrete beams has been modified for FRP-reinforced concrete beams. The versatility of the proposed modifications to update other conventional crack width formulas to be valid for FRP reinforcement has also been investigated.

5.2 Proposed Formula

The modifications proposed herein for the formula developed by Gergely and Lutz (1968), Equation 2-22, transform the FRP-reinforced concrete beam into an equivalent (virtual) beam reinforced with conventional steel bars for which this equation was established. In order to achieve an accurate and reliable transformation, the

difference between FRP and steel bars regarding the mechanical properties, as well as the bond characteristics should be represented in the equivalent beam. In this case, Equation 2-22 can be set in the following form:

$$W_{max} = 0.076 \times 10^{-3} \beta \, f_{eq} \, \sqrt[3]{d_{c,eq} \, A_{1,eq}} \qquad ; \text{(kip-inch units)} \qquad (5\text{-}1)$$

where f_{eq} = equivalent tensile stress in longitudinal bars; $d_{c,eq}$ = equivalent concrete cover; and $A_{1,eq}$ = equivalent tension area per bar.

$$f_{eq} = f \cdot (E_s / E_f) \qquad (5\text{-}2)$$

Considering the number of FRP bars is (N_f) with diameter (d_b) and bond strength $(u_{u,f})$. The equivalent number of steel bars, (N_{eq}), that have the same diameter and a bond strength $(u_{u,s})$ can be obtained as follows:

$$u_{u,f} = (I_{b,f} \, \sqrt{f_c'}) / d_b \qquad (5\text{-}3)$$

$$u_{u,s} = (I_{b,s} \, \sqrt{f_c'}) / d_b \qquad (5\text{-}4)$$

$$N_{eq} = N_f \cdot (u_{u,f} / u_{u,s}) = N_f \, (I_{b,f} / I_{b,s}) \qquad (5\text{-}5)$$

where d_b = bar diameter; E_f = modulus of elasticity of FRP bars; E_s = modulus of elasticity of steel bars; f_c' = concrete compressive strength; $I_{b,f}$ = FRP bars bond strength index; $I_{b,s}$ = steel bars bond strength index; $u_{u,f}$ = FRP bars bond strength; and $u_{u,s}$ = steel bars bond strength.

Hence, the equivalent tension area per bar, $A_{1,eq}$, is calculated from the following equation:

$$A_{1,eq} = A_1 \, (I_{b,s} / I_{b,f}) \qquad (5\text{-}6)$$

111

Similar to the concept of stretching the concrete cover towards the nearest elastic bars if the extreme bottom ones are yielding (ACI Committee 224, 1972) (Section 2.15), consider a multi-layer reinforced concrete beam where the extreme bottom bars have an approximately zero bond strength. In this case, the effective concrete cover depends on the nearest bonded bars and consequently the following equation is proposed:

$$d_{c.eq} = d_c \ (I_{b,s} / I_{b,f})$$ (5-7)

5.3 Verification Process

The reliability of the proposed formula presented in Equation 5-1 has been verified in different ways. The values obtained by this formula have been compared with the corresponding crack width measured in the tested beams, as well as with the corresponding values calculated by different formulas developed by other researchers. The validity of the proposed modifications to be imposed into other formulas for steel-reinforced concrete beams to update them for FRP reinforcement also has been examined.

5.3.1 Part (I)

This part of the verification process presents the comparison between the maximum crack width measured for beams # 35 and # 36 and the corresponding values obtained from the modified formula, Equation 5-1, as well as the values calculated by the formulas of Equations 2-25 and 2-26. This comparison is presented in Tables 5-1 and 5-2.

It should be mentioned that the tensile stress in the bars corresponding to each applied load level has been calculated based on the location of the neutral axis, and the strain distribution over the beam cross section at the measured crack. The cracks under consideration are only pure flexure cracks, e.g. cracks formed within constant moment zone. In order to examine the proposed formula under different values of d_c, the concrete cover for the flexure reinforcement has been increased from 25.4 mm (1.0 in) in beam #35 to 50.8 mm (2.0 in) in beam #36.

5.3.2 Part (II)

A comparison between the mathematical form of Equation 2-22 and that of Equation 5-1 leads to the following:

$$Equation\ (5-1) = Equation\ (2-22) * \left(\frac{E_s}{E_f}\right)\left(\frac{I_{b.s}}{I_{b.f}}\right)^{2/3} \qquad (5\text{-}8)$$

In other words, the crack width for a concrete beam reinforced with FRP bars is the crack width of a similar beam but reinforced with steel bars of the same number and diameter as that of the FRP bars, multiplied by the term $\left(\frac{E_s}{E_f}\right)\left(\frac{I_{b.s}}{I_{b.f}}\right)^{2/3}$.

The formula recommended by the Euro Code 2-1991 (EC2-91) to calculate the maximum crack width in steel-reinforced concrete members subject to axial tension and/or bending moment (Ghali and Favre, 1994) is proposed as an example to examine this concept. This formula is as follows:

$$W_{max} = S_{rm} . \varepsilon_s . \zeta \qquad (5\text{-}9)$$

where S_{rm} = average spacing between cracks; ε_s = tensile strain of the longitudinal steel bars; and ζ = dimensionless coefficient between 0.0 and 1.0 representing the degree of participation of concrete in the tensioned zone.

Based on EC2-91, the average spacing between cracks, S_{rm}, can be calculated as follows:

$$S_{rm} = 50 + \frac{k_1\, k_2\, d_b}{4\, \rho_r} \quad \text{; (N-mm units)} \tag{5-10}$$

where k_1 = coefficient based on bond quality between concrete and bars (1.6 for plain bars and 0.8 for high bond bars); k_2 = coefficient based on strain distribution over the member cross section (0.5 for members subject to bending and 1.0 for members subject to axial tension); ρ_r = steel bars ratio based on the effective tension area of concrete surrounding the bars , A_{cef}; A_{cef} = (b_w * 2.5 (H-d)) or (b_w * (H-c)/3) whichever is smaller; b_w = width of beam web; and c = depth of compression zone.

According to Equation 5-8, the formula presented in Equation 5-9 can be transformed to predict the crack width for FRP reinforced concrete beams as follows:

$$S_{rm} = \left(50 + \frac{k_1\, k_2\, d_b}{4\, \rho_r}\right) \varepsilon_s\, \zeta \left(\frac{E_s}{E_f}\right)\left(\frac{I_{b,s}}{I_{b,f}}\right)^{2/3} \quad \text{; (N-mm units)} \tag{5-11}$$

The crack width calculated by Equations 2-25, 2-26, 5-1, and 5-11 together with the corresponding width obtained experimentally for beam #35 and #36 are presented in Tables 5-1 and 5-2. It should be noted that the values of k_1 and ζ were substituted as 1.0 and 0.75 based on deformed steel bars and neglecting 75% of the concrete in the tensioned zone.

Table 5-1: Crack Width Obtained Analytically and Experimentally for Beam # 35,
values are in mm (in).

Load kN (kip)	Measured Crack Width			Calculated Crack Width			
	Crack # 1	Crack # 2	Average	Equation # 5-1	Equation # 2-25	Equation # 2-26	Equation # 5-11
(1)	(2)	(3)	(4)	(5)	(6)	(7)	(8)
31.1 (7.0)	0.52 (0.020)	0.42 (0.016)	0.47 (0.018)	0.47 (0.018)	0.51 (0.020)	0.45 (0.017)	0.47 (0.018)
35.6 (8.0)	0.54 (0.021)	0.46 (0.018)	0.50 (0.019)	0.56 (0.022)	0.60 (0.024)	0.53 (0.021)	0.55 (0.022)
40.0 (9.0)	0.56 (0.022)	0.70 (0.027)	0.68 (0.026)	0.60 (0.024)	0.66 (0.026)	0.58 (0.023)	0.60 (0.023)
44.5 (10.0)	0.71 (0.028)	0.75 (0.029)	0.73 (0.029)	0.66 (0.025)	0.72 (0.028)	0.64 (0.025)	0.67 (0.026)
48.9 (11.0)	0.75 (0.029)	0.78 (0.030)	0.77 (0.03)	0.73 (0.029)	0.79 (0.31)	0.70 (0.027)	0.75 (0.030)

Table 5-2: Crack Width Obtained Analytically and Experimentally for Beam # 36,
values are in mm (in).

Load kN (kip)	Measured Crack Width	Calculated Crack Width			
		Equation # 5-1	Equation # 2-25	Equation # 2-26	Equation # 5-11
(1)	(2)	(3)	(4)	(5)	(6)
35.6 (8.0)	0.89 (0.035)	1.02 (0.040)	1.35 (0.053)	0.76 (0.030)	0.99 (0.039)
44.5 (10.0)	1.32 (0.052)	1.45 (0.057)	1.93 (0.076)	0.94 (0.037)	1.22 (0.048)
53.4 (12.0)	1.55 (0.061)	1.70 (0.067)	2.26 (0.089)	1.07 (0.042)	1.42 (0.056)
62.3 (14.0)	1.85 (0.073)	1.98 (0.078)	2.64 (0.104)	1.22 (0.048)	1.67 (0.066)
71.2 (16.0)	2.08 (0.082)	2.26 (0.089)	3.02 (0.119)	1.37 (0.054)	1.91 (0.075)
80.1 (18.0)	2.36 (0.093)	2.59 (0.102)	3.40 (0.134)	1.55 (0.061)	2.13 (0.084)

CHAPTER 6

STRENGTH OF CONCRETE BEAMS
REINFORCED AND/OR PRESTRESSED WITH FRP BARS

6.1 General

This chapter is directed at developing an analytical model for determining the strength of concrete beams reinforced and/or prestressed with FRP bars, taking into account some parameters which are usually neglected when dealing with the strength of steel-reinforced concrete beams as well as in the current design guidelines for FRP-reinforced concrete beams (ACI 1995; Surendra et al. 1995; CSA 1994; Leet 1991; CHBDC 2000; ACI 1999; and BIR 1997).

The first parameter is the crack path geometry which depends on several factors such as the location of starting point of crack, and the shear span to depth ratio. These factors have been considered through the analytical model established for crack geometry presented in Chapter 4.

The second parameter is the crack width at the level of the longitudinal reinforcing bars. The mechanical properties of these bars, as well as their bond characteristics with concrete, have a significant effect on the induced crack width as expressed in the proposed formula to calculate the maximum crack width in FRP-reinforced concrete beams (Chapter 5).

116

The third parameter is the dowel action of the longitudinal reinforcing bars, i.e. the induced shear force and the corresponding shear displacement of the flexural reinforcement and prestressing tendons if any. The fourth parameter is the rigid body rotation of the beam portions on both sides of the crack. This rotation affects the deformations and the stresses induced in both concrete and reinforcement at crack location.

The influence of the above-mentioned parameters on the behaviour and strength of concrete beams reinforced with FRP bars is presented herein and expressed through the following analytical model.

6.2 Steps of the Analytical Modelling

The analytical model proposed herein is presented in steps according to the sequence required to obtain the beam strength and the mode of failure, as well as the corresponding location of the crack tip at failure.

Step 1: Crack Formation

The analysis considers different possible crack paths, for which the location of crack initiation, D, can be as follows:

- The nearest crack to support initiates at $D = D_o$ where D_o equals 0.0 or d according to the support conditions (ACI 1995; CSA 1994).

- The shear-flexure cracks can be assumed to initiate at reasonable spacing within shear span, e.g. stirrups spacing if stirrups are provided or $d/2$ in other cases.

- The crack that develops vertically at the end of shear span, $D = Lp$, presents a pure flexure crack.

For each assumed crack, the analytical model is applied considering different crack tips along the crack path, starting from $Y = \Delta Y$ up to $Y \cong H$ with certain increment, e.g. $\Delta Y = H/10$. The relationship between X_i and Y_i, i.e. the geometry of the crack path, follows the analytical model described in Chapter 4 (Equations 4-5, 4-6 & 4-10).

While the crack is progressing, a gap (iAB) is created bounded by the crack sides (iA) and (iB) (Fig. 6-1a). Each of the beam portions on both sides of the crack experiences a rigid body rotation about the crack tip (i). The shear displacement of the longitudinal reinforcement that accompanies this rotation is shown in Figs. 6-1b and 6-1c. The original position of the flexural reinforcement coincided on the line fF and due to the rotation of the crack sides about crack tip, point (F) is shifted to point (F') where the distance fF is the longitudinal crack gap component, $W_{lf,i}$, (the crack width induced by the tensile stress in this reinforcement) and the distance FF' is the transverse crack gap component, W_{nf}, (the shear displacement induced by the rotation of the beam portions on both sides of the crack about the crack tip).

Since point (i) is the centre of rotation and the distance fF' is very small compared to the distance if, it can be considered that the radius if is perpendicular to the line fF' and that the angle ($fF'F$) equals the angle (ife), equals to $\varphi_{f,i}$.

Accordingly, the relationship between $W_{tf,i}$ and $W_{nf,i}$ is:

$$W_{nf,i} = W_{tf,i} \cdot \cot \varphi_{f,i} \tag{6-1}$$

In which $\cot \varphi_{f,i} = (X_i - X_f)/(Y_i - Y_f) \tag{6-2}$

Similarly, the relation between the crack gap component along the prestressing tendons, $W_{tp,i}$, and the crack gap component normal to this tendon, $W_{np,i}$, can be calculated as follows:

$$W_{np,i} = W_{tp,i} \cdot \cot \varphi_{p,i} \tag{6-3}$$

Where:

$$W_{tp,i} = W_{tf,i} (Y_i - Y_p) / (Y_i - Y_f) \tag{6-4}$$

$$\cot \varphi_{p,i} = (X_i - X_p)/(Y_i - Y_p) \tag{6-5}$$

(X_f, Y_f) and (X_p, Y_p) are the coordinates of the intersection between the crack profile and the centroid of the flexural reinforcement, point (f), and centroid of the prestressing tendons, point (p), respectively; and $\varphi_{p,i}$ = the angle between X-axis and the line connecting point (i) with point (p).

The crack gap component in the longitudinal direction, $W_{tf,i}$, can be expressed as follows (Fig. 6-1):

$$W_{tf,i} = W_{max,i} (Y_i - Y_f) / (Y_i) \tag{6-6}$$

119

where the value of $W_{max,i}$ is obtained by the formula proposed in Chapter 5, Equation 5-1, that takes into account the effect of both the bond characteristics and the mechanical properties of the FRP bars on the induced crack width.

Step 2: Conditions of Equilibrium

Step 2.1: Equilibrium Equations (Set #1)

The location of the neutral axis and the distribution of the strains over the beam cross section, see Fig. 6-2a, can be obtained by applying the Moment-Curvature principles for concrete beams reinforced and/or prestressed by bonded bars (Lin and Burns 1981; Gaylord et al. 1997), based on the following equilibrium equations:

Corresponding to the equilibrium in the longitudinal direction:

$$T_{fv,i} + T_{pv,i} = C_{v,i} \tag{6-7}$$

Taking the moment about the point which has the coordinates $(X_i, 0)$:

$$C_{v1,i}.\overline{Y_{c1}} - C_{v2,i}.\overline{Y_{c2}} - T_{pv,i}.Y_p - T_{fv,i}.Y_f = R_i.X_i - P_{ow,v,i}.\frac{(X_i + a)}{2} \tag{6-8}$$

Where:

$$C_{v,i} = C_{v1,i} - C_{v2,i} \quad (6\text{-}9); \qquad R_i = P_{ow,v,i} + \frac{P_{1,i}}{2} \tag{6-10}$$

$$\varepsilon_{fv,i} = \varepsilon_{c,top,i} \frac{(Y_{NA} - Y_f)}{(H - Y_{NA})} \quad (6\text{-}11); \qquad \varepsilon_{pv,i} = \varepsilon_{fv,i} \frac{(Y_{NA} - Y_p)}{(Y_{NA} - Y_f)} \tag{6-12}$$

$$T_{fv,i} = \varepsilon_{fv,i} \, A_f \, E_f \quad (6\text{-}13); \qquad T_{pv,i} = \varepsilon_{pv,i} \, A_p \, E_p + (T_{po} - T_{pl}) \tag{6-14}$$

$C_{v,i}$ = resultant of the concrete compressive force at the beam vertical section passing through point (i); E_p = modulus of elasticity of tendons; $T_{fv,i}$ and $T_{pv,i}$ = tensile force of the flexural reinforcement and tendons that acts at the beam vertical cross section which passes through point (i); T_{pl} = loss of initial prestressing force; T_{po} = initial prestressing force; $P_{l,i}$ = applied load required to maintain the equilibrium of the beam segment under study ;$P_{ow,v,i}$ = own weight of the beam segment under study; Y_f and Y_p = Y-coordinate of the centroid of flexural reinforcement and tendons; $\overline{Y}_{c1}$ and $\overline{Y}_{c2}$ = Y-coordinate of the point of action of the compressive force $C_{v1,i}$ and $C_{v2,i}$; Y_{NA} = Y-coordinate of the neutral axis; $Z_{v,i}$ = effective beam depth at the beam vertical cross section which passes through point i;and $\varepsilon_{fv,i}$ and $\varepsilon_{pv,i}$ = tensile strain of the flexural reinforcement and tendons that acts at the beam vertical cross section which passes through point (i).

In order to solve the equilibrium equations (Equations 6-7 and 6-8), the same procedure followed by Lin and Burns (1981) has been adopted herein as follows:

i-   Assume the location of the neutral axis, Y_{NA}, and the compressive strain induced in concrete at the top of beam flange, $\varepsilon_{pv,i}$.

ii-   The compressive stress-strain relationship (Fig 2-2) can be expressed as follows (Lin and Burns 1981; Vecchio and Collins 1986):

$$f_c = f_c^{'}\left[\frac{2\varepsilon_c}{\varepsilon_c^{'}} - \left(\frac{\varepsilon_c}{\varepsilon_c^{'}}\right)^2\right] \tag{6-15}$$

iii-   Substituting:

$$\varepsilon_c = \theta\, Y'; \theta = \frac{\varepsilon_{c,top,i}}{(H - Y_{NA})}; Y' = (Y - Y_{NA}); c_1 = (H - Y_{NA}); c_2 = (H - h_f - Y_{NA})$$

For $Y_{NA} < (H - h_f)$:

$$C_{v1,i} = \int_0^{c1} f_c\, b_f\, dY' = b_f\, f_c'\, \frac{\theta\, c_1^2}{\varepsilon_c'}\left[1 - \frac{\theta\, c_1}{3\varepsilon_c'}\right] \qquad (6\text{-}16)$$

$$C_{v2,i} = \int_0^{c2} f_c\, (b_f - b_w)\, dY' = (b_f - b_w)\, f_c'\, \frac{\theta\, c_2^2}{\varepsilon_c'}\left[1 - \frac{\theta\, c_2}{3\varepsilon_c'}\right] \qquad (6\text{-}17)$$

$$\overline{Y_{c1}} = Y_{NA} + c_1\left[\frac{8\varepsilon_c' - 3\theta\, c_1}{12\varepsilon_c' - 4\theta\, c_1}\right] \qquad (6\text{-}18)$$

$$\overline{Y_{c2}} = Y_{NA} + c_2\left[\frac{8\varepsilon_c' - 3\theta\, c_2}{12\varepsilon_c' - 4\theta\, c_2}\right] \qquad (6\text{-}19)$$

For $Y_{NA} \geq (H - h_f)$:

$$C_{v1,i} = \int_0^{c1} f_c\, b_f\, dY' = b_f\, f_c'\, \frac{\theta\, c_1^2}{\varepsilon_c'}\left[1 - \frac{\theta\, c_1}{3\varepsilon_c'}\right] \qquad (6\text{-}20)$$

$$C_{v2,i} = 0.0 \qquad (6\text{-}21)$$

iv-   Calculate $\varepsilon_{fv,i}$ and $\varepsilon_{pv,i}$ (Equations 6-11 and 6-12).

v-   Calculate $T_{fv,i}$ and $T_{pv,i}$ (Equations 6-13 and 6-14).

vi-   Check that Equation 6-7 is satisfied otherwise repeat the above-mentioned procedure starting with step i.

vii-   Calculate $P_{l,i}$ (Equation 6-8) required to maintain the equilibrium of the beam segment under study.

122

Step 2.2: Equilibrium Equations (Set #2)

The free body diagram for the beam segment between support and one of the cracks that progressed up to point (i) at a total applied load P_i is presented in Fig. 6-2b. The equilibrium of this beam segment is governed by three equations as follows:

Taking the moment about the point of action of the concrete compressive force, C_i, i.e. point (c):

$$R_i \cdot X_i = \{T_{sh,i} (X_i - D)/2 + V_{f,i} (X_i - X_f) + V_{p,i} (X_i - X_p) + T_{f,i} \cdot Z_i$$

$$+ T_{p,i} (Z_i - Y_p + Y_f) + P_{ow,i} \cdot L_{ow,i}\}$$

$$(6\text{-}22)$$

Corresponding to the equilibrium in the longitudinal direction:

$$C_i = T_{f,i} + T_{p,i} \tag{6-23}$$

Corresponding to the equilibrium in the vertical direction:

$$R_i = V_{c,i} + V_{p,i} + V_{f,i} + T_{sh,i} + P_{ow,i} = (P_{2,i} + P_{ow,beam})/2 \tag{6-24}$$

where C_i = the compressive force induced in concrete above crack tip; L_{ow} = moment arm of P_{ow} about point (i); $P_{2,i}$ = applied load required to maintain the equilibrium of the beam segment under study; P_{ow} = resultant of the own weight of this beam segment; $P_{ow,beam}$ = total own weight of beam; $V_{c,i}$ = shear force induced in concrete; $V_{f,i}$ = shear force induced in flexural reinforcement; $V_{p,i}$ = shear force induced in prestressing tendon(s); R_i = total reaction at the nearest support to the developed crack; $T_{f,i}$ = tensile force induced in flexural reinforcement; $T_{p,i}$ = resultant tensile force induced

in tendon(s); $T_{sh,i}$ = tensile force induced in shear reinforcement; X_f and X_p = X-coordinate of the centroid of flexural reinforcement and tendon(s) respectively; and Z_i = effective beam depth.

Step 3: Internal Forces and Applied Load

Step 3.1: Compressive Force induced in Concrete

The value of C_i corresponds to the compressive stress-strain distribution above crack tip (Fig. 6-2b). The point of action (c) can be determined by subtracting the compressed portion between Y_i and Y_{NA} from the portion between Y_{NA} and H that corresponds to $C_{v,i}$.

Step 3.2: Tensile Force induced in Longitudinal Reinforcement

The tensile force induced in flexural reinforcement, $T_{f,i}$, as well as in tendons, $T_{p,i}$, can be expressed as follows (Fig. 6-2b):

$$T_{f,i} = f_{f,i} \, A_f \qquad (6\text{-}25)$$

$$T_{p,i} = \varepsilon_{p,i} \, A_p \, E_p + \left(T_{po} - T_{pl}\right) \qquad (6\text{-}26)$$

$$\varepsilon_{f,i} = f_{f,i} / E_f \qquad (6\text{-}27); \qquad \varepsilon_{p,i} = \varepsilon_{f,i} \frac{\left(Y_i - Y_p\right)}{\left(Y_i - Y_f\right)} \qquad (6\text{-}28)$$

where: $\varepsilon_{f,i}$ and $\varepsilon_{p,i}$ = tensile strain of the segments of flexural reinforcement and tendons crossing the crack.

Equations 6-25 and 6-26 can be substituted in Equation 6-23 to obtain $f_{f,i}$.

124

Step 3.3: Shear Force Carried by Longitudinal Reinforcement

Based on the observed behaviour of the CFRP bar samples tested under direct shear loads (Figs. 3-3 and 3-4), the relation between the shear stress induced in the flexural reinforcement, $v_{f,i}$, corresponding to $W_{nf,i}$ is assumed to be linear as follows:

$$v_{f,i} = v_f'. W_{nf,i} / W_{nfu} \tag{6-29}$$

Substituting Equations 6-1, 6-2 and 6-6 into 6-29, the value of $V_{f,i}$ can be expressed in the following way:

$$V_{f,i} = A_f.v_{f,i} = A_f.v_f'.\frac{W_{tf,i}}{W_{nfu}}.\frac{X_i - X_f}{Y_i - Y_f} = A_f.v_f'.\frac{W_{max,i}}{W_{nfu}}.\frac{X_i - X_f}{Y_i} \tag{6-30}$$

The shear force induced in FRP tendons, $V_{p,i}$, can be calculated in a manner similar to that of $V_{f,i}$ as follows:

$$v_{p,i} = v_p'. W_{np,i} / W_{npu} \tag{6-31}$$

Substituting Equations 6-4, 6-5 and 6-6 into 6-31, the value of $V_{f,i}$ can be expressed in the following way:

$$V_{p,i} = A_p.v_{p,i} = A_p.v_p'.\frac{W_{tp,i}}{W_{npu}}.\frac{X_i - X_p}{Y_i - Y_p} = A_p.v_p'.\frac{W_{max,i}}{W_{npu}}.\frac{X_i - X_p}{Y_i} \tag{6-32}$$

where: A_f and A_p = cross sectional area of flexural reinforcement and tendons; v_f' and v_p' = shear strength of the flexural reinforcement and tendons corresponding to W_{nfu} and W_{npu} respectively; and W_{nfu} and W_{npu} = ultimate shear displacement of the flexural reinforcement and tendons.

125

Based on the determined value of $f_{f,i}$, the values $W_{max,i}$ and $W_{tf,i}$ can be calculated (Equations 5-1 and 6-6). Consequently, the shear force developed in flexural reinforcement and prestressing tendons, $V_{f,i}$ and $V_{p,i}$ can be obtained (Equations 6-30 and 6-32).

Step 3.4: Tensile Force Developed by Stirrups

The relationship between the diagonal crack width, $W_{sh,i}$, and the tensile strain induced in the stirrups crossing the crack, $\varepsilon_{sh,i}$, expressed by Equation 2-19 has been adopted by the present analytical modelling.

The diagonal crack width, $W_{sh,i}$, can be calculated at crack mid-height, $Y_m = Y_i/2$, as follows (Fig. 6-3):

$$W_{sh,i} = \frac{W_{max,i}}{2}\sin(\varphi_{m,i}) \quad (6\text{-}33); \qquad \varphi_{m,i} = \tan^{-1}\left(\frac{dY}{dX}\right)_{(X_m,Y_m)} \quad (6\text{-}34)$$

It can be seen that the value of $W_{sh,i}$ and consequently the value of $\varepsilon_{sh,i}$, depend on $f_{f,i}$ and the geometry of the crack path profile. After $f_{f,i}$ is determined in step 6 and the crack path geometry is defined through Equations 4-5, 4-6 and 4-10, the value of $(\varepsilon_{sh,i})$ can be obtained (Equation 2-19), and the tensile force, $T_{sh,i}$, developed by the stirrups crossing the crack, $(= (X_i - D)/S)$, can be calculated as follows:

$$T_{sh,i} = \varepsilon_{sh,i}\, E_s\, (X_i - D)\, A_{sh}/S \qquad (6\text{-}35)$$

Step 3.5: Applied Load

As the values of $T_{f,i}$, $T_{p,i}$, $V_{f,i}$, $V_{p,i}$, and $T_{sh,i}$ have been determined through the previous steps, the value of the applied load $P_{2,i}$, required to maintain the equilibrium of the beam segment under study, can be obtained from Equation 6-22. This value should be equal to the value of the applied load $P_{1,i}$ obtained in step 3. A margin of tolerance $\pm 0.5\%$ of $P_{1,i}$ has been allowed in the present analysis. Exceeding this margin leads to repeat the analysis starting with step 3.

Step 3.6: Shear Force Developed by Concrete

The shear force induced in concrete including the interlocking/friction developed in-between the crack surfaces is presented by $V_{c,i}$ as shown in Figs. 6-2a and 6-2b. The value of $V_{c,i}$ can be obtained from Equation 6-24 based on the determined values of $V_{f,i}$, $V_{p,i}$, $P_{2,i}$ and $T_{sh,i}$. Thereafter, the combination of compressive/shear stresses induced in concrete at crack tip, point (i), can be checked to confirm the progress of crack up to this point as follows (Fig. 6-4):

$$f_{ct,i}'' = \sqrt{v_c^2 + \left(\frac{f_{c,i}}{2}\right)^2} - \left(\frac{f_{c,i}}{2}\right) \geq f_{ct}' \qquad (6\text{-}36)$$

where: $f_{c,i}$ = the compressive stress induced in concrete at point (i); f_{ct}'' = the principal tensile stress induced in concrete at point (i); f_{ct}' = the tensile strength of concrete = $0.6\sqrt{f_c'}$ (N-mm units) (CSA 1994); v_c = the average shear stress induced in the concrete portion above crack tip.

Step 4: Failure Mechanism

As the applied load and its corresponding shear force and bending moment are increased, the tensile stresses of the flexural reinforcement crossing the crack gap increase, the crack is widening, i.e. the gap components, $W_{tp.i}$ and $W_{tf.i}$, increase, and the tensile stresses of the shear reinforcement increase as well. At the same time, the crack progresses more away from its starting point, resulting in a reduction of the angles $\varphi_{p.i}$ and $\varphi_{f.i}$. According to Equation 6-1, as $W_{tp.i}$ and $W_{tf.i}$ increase while $\varphi_{p.i}$ and $\varphi_{f.i}$ decrease, the shear displacement of both the flexural reinforcement, $W_{nf.i}$, and the prestressing tendons, $W_{nf.i}$, increase, leading to an increase of the shear stresses induced in both flexural reinforcement and prestressing tendons. Also, the crack progress towards the beam flange shifts the crack tip upward and consequently reduces the depth of the concrete portion above crack resulting in an increase of the stresses induced in this portion. Hence, the failure at this crack location can be one of the following:

1- Tension and/or Shear failure of flexural reinforcement.

2- Compressive and/or Shear failure of concrete.

3- Tension and/or Shear failural of shear reinforcement.

The above mentioned failures will all be of the brittle type if the beam is reinforced in both flexure and shear with FRP. However, the concrete compressive failure has relative ductility when compared to FRP failure due to the softening phase before the concrete reaches its ultimate compressive strain, i.e. quasi-brittle material failure,

(Surendra et al. 1995). Although the sudden rupture of shear reinforcement has been avoided in the present experimental work by using mild steel stirrups, the developed analytical model has been extended and verified for the possibility of such failure when using FRP stirrups/FRP grids as will be discussed in Chapter 7. It should be noted that the bond failure of flexural and shear reinforcement has been excluded as the forces in the reinforcing bars were fully developed.

Step 5: Prediction of Beam Strength

The calculated stresses and strains induced in concrete and reinforcement, as described in the previous steps, are compared with their ultimate values to identify any possible failure as follows:

- $F_{f,i} = 1.00$ indicates tension/shear rupture of FRP flexural bars;

$$F_{f,i} = \sqrt{\left(\frac{v_{f,i}}{v_f^*}\right)^2 + \left(\frac{f_{f,i}}{f_f^*}\right)^2} \qquad (6\text{-}37)$$

Based on Equation 6-7, Equation 6-37 can be reformed as follows:

$$F_{f,i} = \sqrt{\left(\frac{W_{nf,i}}{W_{nuf}}\right)^2 + \left(\frac{f_{f,i}}{f_f^*}\right)^2} \qquad (6\text{-}38)$$

- $F_{p,i} = 1.00$ indicates tension/shear rupture of FRP tendons;

$$F_{p,i} = \sqrt{\left(\frac{v_{p,i}}{v_p^*}\right)^2 + \left(\frac{f_{p,i}}{f_p^*}\right)^2} \qquad (6\text{-}39)$$

Similarly, Equation 6-39 can be reformed as follows:

$$F_{f,i} = \sqrt{\left(\frac{W_{np,i}}{W_{nup}}\right)^2 + \left(\frac{f_{p,i}}{f_p^{'}}\right)^2}$$ (6-40)

- $\varepsilon_{c,top,i} = 0.0035$ indicates compressive failure of concrete (CSA 1994).

- $\varepsilon_{sh,i} = \varepsilon_y$ indicates yield of steel stirrups.

- $V_{c,i} = V_{cr}$ indicates shear failure of concrete; V_{cr} is calculated by Equation 2-10 where $K^{'}$ is obtained from Equation 2-13 which takes into account the effect of the flexural reinforcement ratio, ρ_f, and the modular ratio (E_f/E_s).

If any of the above-mentioned conditions is satisfied, the crack reaches a failure crack tip, point (f), and the calculated applied load is considered the beam strength corresponding to the crack under study, $P_{u,D}$. Steps 1 to 5 are repeated for the other cracks and the minimum failure load $(P_{u,D})_{min}$ is the overall beam strength. The flow chart of the steps of the analysis presented in this chapter is shown in Fig. 6-5.

6.3 Verification Process

6.3.1 Part (I)

The presented analytical model has been examined by analysing each tested beam along the failure crack path , i.e. at $D = D_{fail}$, according to the flow chart illustrated in Fig. 6-5. The coordinates of the failure crack tip, $(X_f, Y_f)_{mod}$, the failure load $(P_f)_{mod}$ and the strains and stresses induced in concrete and reinforcement obtained by the analytical model are listed in Tables 6-1 and 6-2, together with their corresponding experimentally obtained values $(X_f, Y_f)_{exp}$, and $(P_f)_{exp}$.

130

Considering beam #2 and #17 as examples, the analytical model indicated a dowel failure of CFRP bars in both beams at a load, $(P_f)_{mod}$, equals 42.3 kN (9.5 kips) and 60.0 kN (13.5 kips) respectively based on the calculated value of the failure factor, F_f =1.00. Both beams actually failed in the same mode, at the same location, and at a load, $(P_f)_{exp}$, equals 44.5 kN (10.0 kips) and 56.0 kN (12.5 kips) respectively.

As mentioned for beams #25 and #26, they were not provided with stirrups and the concrete cover underneath the CFRP bars crossing the failure crack was pushed out due to the relative transverse displacement on both sides of the crack, preventing the bars from being completely ruptured. Since the analytical model cannot handle concrete spalling, the failure mechanism at this crack location has been traced by the model considering the concrete cover to keep the bars in position to experience higher values of shear displacement. As can be seen in Tables 6-1 and 6-2, the analytical results indicate that if the latter case took place, these two beams would have sustained more loading before failing when the calculated value of the failure factor, F_f, reached 1.00 at a load, $(P_{fail})_{mod}$, of 62.3 kN (14.0 kips) instead of $(P_{fail})_{exp}$ which was 49.3 kN (11.0 kips) for beam # B25 and 60.0 kN (13.5 kips) instead of $(P_{fail})_{exp}$ which was 40.3 kN (9.0 kips) for beam # B26. These results show that the damage of concrete cover leads to pre-mature failure of beams. However, such failure is usually avoided by placing stirrups.

For the beams that failed in shear due to the dowel failure of FRP bars, i.e. shear-tension rupture of bars, the beam strength obtained by the present model and that calculated by Equations (2-2 to 2-4), (2-9 to 2-12), and (2-14 to 2-17) are illustrated in

Fig. 6-6 together with the actual beam strength (i.e. the beam failure load obtained experimentally). These equations are recommended by the Japanese (BIR), the American (ACI), and the Canadian (CHBDC) guidelines for RFP-reinforced concrete structures respectively. Also, Equations 2-9 to 2-12 have been applied after being modified by the value of K' calculated according to Equation 2-13 (ACI, modified). Herein it may be noted that the shear strength calculated by the above-mentioned equations has been multiplied by 2.0 to obtain the corresponding calculated beam strength. Also, the performance factors have been substituted as 1.0 (e.g. ϕ_c in Equations 2-14 and 2-15).

It can be realised that for beams without shear reinforcement, (beam # 2, 3, 17, 25 and 26), most of the shear strength values calculated according to the above-mentioned design guidelines are close to the actual strength values. For relatively moderate ratios of shear reinforcement, (beam # 31, 32, and 36), both the ACI and CHBDC over-estimate the beam strength while the BIR and (ACI, modified) introduce considerably closer values to the actual strength.

The ACI and CHBDC over-estimation is more significant for relatively high ratios of shear reinforcement, (beam # 15', 16, and 34), where the range of the percentage of error for the strength values calculated by ACI and CHBDC is (57.4% to 331.8%) and (70.3% to 369.9%) respectively. Even modifying the ACI formula for the concrete contribution, V_{cr}, (ACI, modified) has not imposed a considerable accuracy to the calculated strength values because of the small value of V_{cr} with respect to that of shear reinforcement, V_{sh}, especially for high values of shear reinforcement, ρ_{sh}.

132

The main reason for the deviation of the ACI and CHBDC results is the neglect of the possibility for a dowel failure of the longitudinal reinforcement which often governed the strength of these beams. Another reason is the assumptions based on which the shear reinforcement contribution, V_{sh}, is calculated. For example, the ACI guidelines (Equation 2-11) is based on assuming d/S stirrups crossing the crack, while the actual number of these stirrups equals $(X_i - D)/S$, as considered by the present analytical model (Equation 6-35). This number depends on the crack geometry as related to the crack starting point. It can be seen that the value of $(X_f - D)$ has been less than d for all the beams with stirrups that failed by the dowel failure of the CFRP bars (Tables 6-1 and 6-2). In addition, the tensile strain induced in the stirrups depends on the induced crack width so it may not reach the yield strain when the dowel failure of FRP bars takes place. In other words, the dowel failure of FRP bars, the geometry of the crack path, and the induced crack width governed the actual contribution of the shear reinforcement.

Consequently, for all the beams with stirrups presented in Fig. 6-6 (beam # 15', 16, 31, 32, 34, and 36), the proposed analytical model introduces the most accurate strength values, compared to the values calculated by all the investigated design guidelines, with a percentage of error that ranges between −9.5% to 10.4%. Meanwhile, the beam strength calculated by the Japanese design guidelines (BIR) can be considered the most accurate strength values, compared to the values calculated by the other investigated design guidelines, with a percentage of error that ranges between −16.9% to 57.6%. However, it should be noted that the BIR underestimates the magnitude of V_{cr} and neglects the dowel failure of reinforcement.

6.3.2 Part (II)

An experimental program was conducted by Park and Naaman (1999c), for testing concrete beams prestressed at different levels with CFRP and steel tendons. The configurations of the beams, which failed due to the dowel failure of CFRP tendons within shear span, are listed in Table 6-3 and shown in Fig. 6-7. The tensile strength of the 7.5 mm (5/16 in) CFRP tendons used in this program has been considered herein as 2250 MPa (327 ksi) which is the average value of the tensile strength of the same CFRP tendon samples tested by Park and Naaman (1999a). The ultimate shear displacement of the same tendons was also found to be 2.4 mm (0.095 in) under zero tensile force in the tendon. The bond strength of this type of tendons is considered 5.0 MPa (0.725 ksi) (Domenico et al. 1998).

In this verification phase, the flow chart illustrated in Fig. 6-5 has been used to calculate the beam strength based on two different crack paths. Crack path #2 presents the nearest crack to support, and Crack path #1 for a shear-flexure crack formed within shear span at the mid-distance between path #2 and the nearest loading point (Fig. 6-8). For each crack path, the analytical model calculates the stresses and strains in concrete and reinforcement, the beam capacity, $(P_{u,D})$ and the failure factor, F_{pl}, corresponding to the lower CFRP tendons (Table 6-4). The comparison between the model results at beam failure, the beam shear strength obtained by the ACI formulas (ACI-Committee 440H, 1996) as reported by Park and Naaman (1999c) and the corresponding results obtained experimentally is presented in Table 6-5.

It should be mentioned that for beams C3 and C4 where the upper tendon of each was of steel, the failure criterion of such tendons has been considered to be controlled by the induced principal stresses, $f_{pr,i}$, i.e. the tendon fails when $f_{pr,s}$ reaches the yield tensile strength, as follows:

$$f_{pr,i} = {}^{2}\sqrt{[(f_{p,i})^{2} + (v_{p,i})^{2}]} \qquad (6\text{-}41)$$

$$v_{p,i} = v_{py} \cdot W_{np,i} / W_{npy} \qquad (6\text{-}42)$$

where v_{py} = yield shear strength of steel tendons (=0.66 f_y), corresponding to W_{npy}; and W_{npy} = yield shear displacement of steel tendons (=5mm (0.2in) for the used ones) (Park and Naaman 1999a).

Herein, it is interesting to note that the mode of failure predicted analytically is the same as that observed experimentally (Table 6-5). Also, the failure location according to both approaches falls within the shear span. The average percentage of error in predicting the beam strength by the analytical model is −9.5%, while this percentage is − 31.4% for the strength values calculated by the ACI formulas.

Table 6-1: Failure Load and Crack Tip Coordinates obtained Analytically and Experimentally.

Beam # (1)	D_{fail} mm (in) (2)	$(P_f)_{mod}$ kN (kips) (2)	$(P_f)_{exp}$ kN (kips) (4)	$(Y_f)_{mod}$ mm (in) (5)	$(Y_f)_{exp}$ mm (in) (6)	$(X_f)_{mod}$ mm (in) (7)	$(X_f)_{exp}$ mm (in) (8)
2	1016 (40.0)	42.3 (9.5)	44.5 (10.0)	325.1 (12.8)	292 (11.5)	1447.8 (57.0)	1359 (53.5)
3	610 (24.0)	40.0 (9.0)	53.4 (12.0)	330.2 (13.0)	282 (11.1)	1328.4 (52.3)	1016 (40.0)
15'	1600 (63.0)	71.7 (16.0)	66.7 (15.0)	327.7 (12.9)	305 (12.0)	1694.2 (66.7)	1712 (67.0)
16	673 (26.5)	117.8 (26.5)	106.8 (24.0)	332.7 (13.1)	292 (11.5)	843.3 (33.2)	838 (33.0)
17	508 (20.0)	60.0 (13.5)	55.6 (12.5)	330.2 (13.0)	279 (11.0)	1145.5 (45.1)	991 (39.0)
24	483 (19.0)	53.4 (12.0)	53.4 (12.0)	340.4 (13.4)	305 (12.0)	1221.7 (48.1)	1194 (47.0)
25	838 (33.0)	62.3 (14.0)	48.9 (11.0)	335.3 (13.2)	267 (10.5)	1295.4 (51.0)	1156 (45.5)
26	419 (16.5)	60.0 (13.5)	40.3 (9.0)	332.7 (13.1)	305 (12.0)	1135.4 (44.7)	864 (34.0)
29	1524 (60.0)	84.5 (19.0)	88.9 (20.0)	330.2 (13.0)	318 (12.5)	Within (b)	Within (b)
30	1422 (56.0)	84.5 (19.0)	91.2 (20.5)	330.2 (13.0)	330 (13.0)	Within (b)	Within (b)
31	965 (38.0)	84.5 (19.0)	93.4 (21.0)	335.3 (13.2)	318 (12.5)	1143.0 (45.0)	1168 (46.0)
32	483 (19.0)	135.7 (30.5)	129.0 (29.0)	335.3 (13.2)	254 (10.0)	797.6 (31.4)	711 (28.0)
34	737 (29.0)	135.7 (30.5)	134.4 (30.0)	327.7 (12.9)	292 (11.5)	868.7 (34.2)	838 (33.0)
36	483 (19.0)	97.9 (22.0)	104.5 (23.5)	325.1 (12.8)	330 (13.0)	723.9 (28.5)	813 (32.0)

Table 6-2: Failure Type obtained Analytically and Experimentally.

Beam #	Analytical			Modeling	Results					Observed
	$f_{f,f}$ MPa (ksi)	$W_{n,f}$ mm (in)	$\varepsilon_{sh,f}$	$\varepsilon_{c,top,f}$	$\varepsilon_{p,f}$	$W_{np,f}$ mm (in)	$V_{c,f}$ KN (kip)	F_f	failure type	failure type
(1)	(2)	(3)	(4)	(5)	(6)	(7)	(8)	(9)	(10)	(11)
2	861.3 (125.0)	1.65 (0.065)	-	0.0006			12.5 (2.8)	1.00	BSTR	BSTR
3	585.7 (85.0)	1.85 (0.073)	-	0.0005			10.7 (2.4)	1.00	BSTR	BSTR
15'	1584.7 (230.0)	0.61 (0.024)	0.0084	0.0014	0.0106	0.43 (0.017)	0.49 (0.11)	1.00	BSTR / TY/ SY	BSTR
16	1378.0 (200.0)	1.04 (0.041)	0.0077	0.0010			5.8 (1.3)	1.00	BSTR / SY	BSTR
17	689.0 (100.0)	1.75 (0.069)	-	0.0008	0.0086	1.27 (0.050)	1.78 (0.40)	1.00	BSTR	BSTR
24	654.6 (95.0)	1.85 (0.073)	-	0.0007	0.0019	1.39 (0.055)	8.27 (1.20)	1.00	BSTR	BSTR
25	930.2 (135.0)	1.65 (0.065)	-	0.0009	0.0092	1.19 (0.047)	1.78 (0.40)	1.00	BSTR / TY	-
26	654.6 (95.0)	1.83 (0.072)	-	0.0007	0.0086	1.32 (0.052)	1.20 (0.27)	1.00	BSTR	-
29	1655.0 (240.0)	0.000	0.0000	0.0015			-	1.00	BTR	BTR
30	1655.0 (240.0)	0.000	0.0000	0.0015			-	1.00	BTR	BTR
31	1378.0 (200.0)	1.09 (0.043)	0.0041	0.0010			16.0 (3.6)	1.00	BSTR / SY	BSTR
32	1136.9 (165.0)	1.42 (0.056)	0.0044	0.0012	0.0097	1.09 (0.043)	2.49 (0.56)	1.00	BSTR / TY / SY	BSTR
34	1515.8 (220.0)	0.76 (0.030)	0.0080	0.0013	0.0108	0.56 (0.022)	5.33 (1.2)	1.00	BSTR / TY/ SY	BSTR
36	1033.5 (150.0)	1.55 (0.061)	0.0039	0.0008			10.3 (2.3)	1.00	BSTR / SY	BSTR

Note: BSTR: Bar Shear-Tension Rupture; BTR: Bar Tension Rupture; and SY: Stirrups Yield.

137

Table 6-3: *Configurations of the Tested Beams, Dimsensions are in mm (in),*
(Park and Naaman, 1999c).

Beam #	Setting Type	Setting Configurations			Pre-stressing Tendons		f_c'	Shear Reinforcement
		a	Lp	b	Upper Tendon	Lower Tendons	MPa (ksi)	(Steel Stirrups)
(1)	(2)	(3)	(4)	(5)	(6)	(7)	(2)	(8)
C1	I	279.4 (11.0)	546.1 (21.5)	-	1 – CFRP diam. 7.5 (5/16)	2 - CFRP diam. 7.5 (5/16)	44.4 (6.45)	-
C2	I	279.4 (11.0)	546.1 (21.5)	-	1 – CFRP diam. 7.5 (5/16)	2 - CFRP diam. 7.5 (5/16)	46.5 (6.75)	-
C3	I	279.4 (11.0)	546.1 (21.5)	-	1 – Steel diam. 12.5 (1/2)	2 - CFRP diam. 7.5 (5/16)	44.4 (6.45)	-
C4	I	279.4 (11.0)	546.1 (21.5)	-	1 – Steel diam. 12.5 (1/2)	2 - CFRP diam. 7.5 (5/16)	42.7 (6.20)	-
C7	I	279.4 (11.0)	546.1 (21.5)	-	1 – CFRP diam. 12.5 (1/2)	2 - CFRP diam. 7.5 (5/16)	35.9 (5.20)	2 – Leg # 2 @ 102.0 (4.0)

Beam # (1)	Crack Path # (2)	$P_{u,D}$ KN (kip) (3)	$(Y_f)_{mod}$ mm (in) (4)	$(X_f)_{mod}$ mm (in) (5)	$\varepsilon_{c,top,f}$ MPa (ksi) (6)	$f_{pl,f}$ MPa (ksi) (7)	$f_{pu,f}$ or $f_{pu,pr,f}$* MPa (ksi) (8)	$W_{n,pl,f}$ mm (in) (9)	$W_{n,pu,f}$ mm (in) (10)	$\varepsilon_{sh,f}$ (11)	F_{pl} (12)	failure type (13)
C1	1	157.9 (35.5)	223.5 (8.8)	487.7 (19.2)	0.0020	2191.0 (318.0)	1847.0 (268.0)	0.56 (0.022)	0.51 (0.020)	-	1.00	STTR
	2	177.9 (40.0)	221.0 (8.7)	424.2 (16.7)	0.0020	2067.0 (300.0)	1757.0 (255.0)	0.96 (0.038)	0.91 (0.036)	-	1.00	STTR
C2	1	160.1 (36.0)	226.1 (8.9)	490.2 (19.3)	0.0020	2191.0 (318.0)	1847.0 (268.0)	0.56 (0.022)	0.51 (0.020)	-	1.00	STTR
	2	177.9 (40.0)	228.6 (9.0)	431.8 (17.0)	0.0020	2053.0 (298.0)	1750.0 (254.0)	1.02 (0.040)	0.94 (0.037)	-	1.00	STTR
C3	1	213.5 (48.0)	205.7 (8.1)	477.5 (18.8)	0.0024	2232.4 (324.0)	1502.0 (218.0)	0.43 (0.017)	0.38 (0.015)	-	1.00	STTR
	2	253.5 (57.0)	198.1 (7.8)	403.9 (15.9)	0.0022	2142.8 (311.0)	1405.6 (204.0)	0.74 (0.029)	0.69 (0.027)	-	1.00	STTR
C4	1	213.5 (48.0)	205.7 (8.1)	477.5 (18.8)	0.0026	2232.4 (324.0)	1502.0 (218.0)	0.43 (0.017)	0.38 (0.015)	-	1.00	STTR
	2	253.5 (56.5)	198.1 (7.8)	403.9 (15.9)	0.0023	2142.8 (311.0)	1405.6 (204.0)	0.74 (0.029)	0.69 (0.027)	-	1.00	STTR
C7	1	197.9 (44.5)	203.2 (8.0)	490.2 (19.3)	0.0033	2184.1 (317.0)	1736.3 (252.0)	0.61 (0.024)	0.56 (0.022)	0.0023	0.75	STTR / SY
	2	222.4 (50.0)	208.3 (8.2)	376.0 (16.2)	0.0032	1998.1 (290.0)	1619.2 (235.0)	1.04 (0.041)	0.96 (0.038)	0.0020	0.70	STTR / SY

Note: STTR: Shear-Tension Tendon Rupture; and SY: Stirrups Yield.

* When upper tendons are of steel (e.g. beam C3 and C4).

Table 6-5: Results Obtained Analytically and Experimentally at Beam Failure.

Beam	Beam Strength					Failure Type		Failure Location	
Beam # (1)	$(P_f)_{exp}$ KN (kip) (2)	*by Analytical Modeling* KN (kip) (3)	*% error* (4)	*by ACI Formulas* (5)	*% error* (6)	*by Analytical Modeling* (7)	*Experimentally* (8)	*by Analytical Modeling* (9)	*Experimentally* (10)
C1	186.8 (41.7)	157.9 (35.5)	-14.9	114.0 (25.7)	-38.4	STTR	STTR	Within Lp	Within Lp
C2	186.8 (43.7)	160.1 (36.0)	-17.6	115.0 (25.9)	-40.7	STTR	STTR	Within Lp	Within Lp
C3	223.1 (49.8)	213.5 (48.0)	-3.6	138.0 (31.1)	-37.6	STTR	STTR	Within Lp	Within Lp
C4	228.5 (51.0)	213.5 (48.0)	-5.9	137.0 (30.9)	-39.4	STTR	STTR	Within Lp	Within Lp
C7	211.0 (47.1)	197.9 (44.5)	-5.5	208.0 (46.7)	-1.0	STTR / SY	STTR	Within Lp	Within Lp

Note: STTR: Shear-Tension Tendon Rupture and SY: Stirrups Yield.

(b) Deformations of Reinforcement at crack location.

(c) Final Crack Gap Configuration.

(a) Beam Longitudinal Elevation.
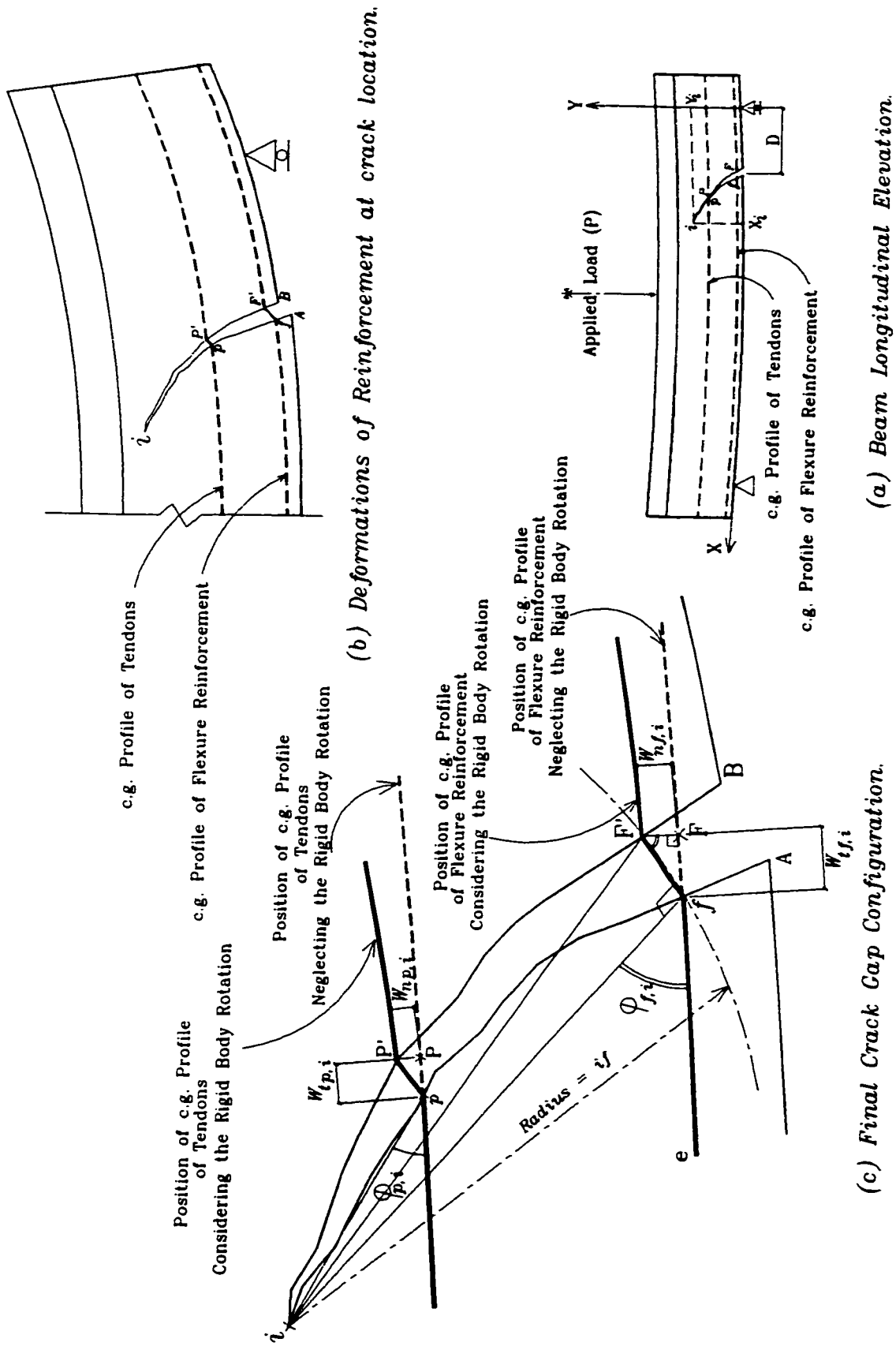
Fig. 6-1: Failure Mechanism of Reinforced and/or Prestressed Concrete Beams.

141

(c) Stress Distribution over Concrete.

(c) Strain Distribution over Beam X-Sec.

(b) Compressed Concrete above Neutral Axis.

(a) Free Body Diagram.
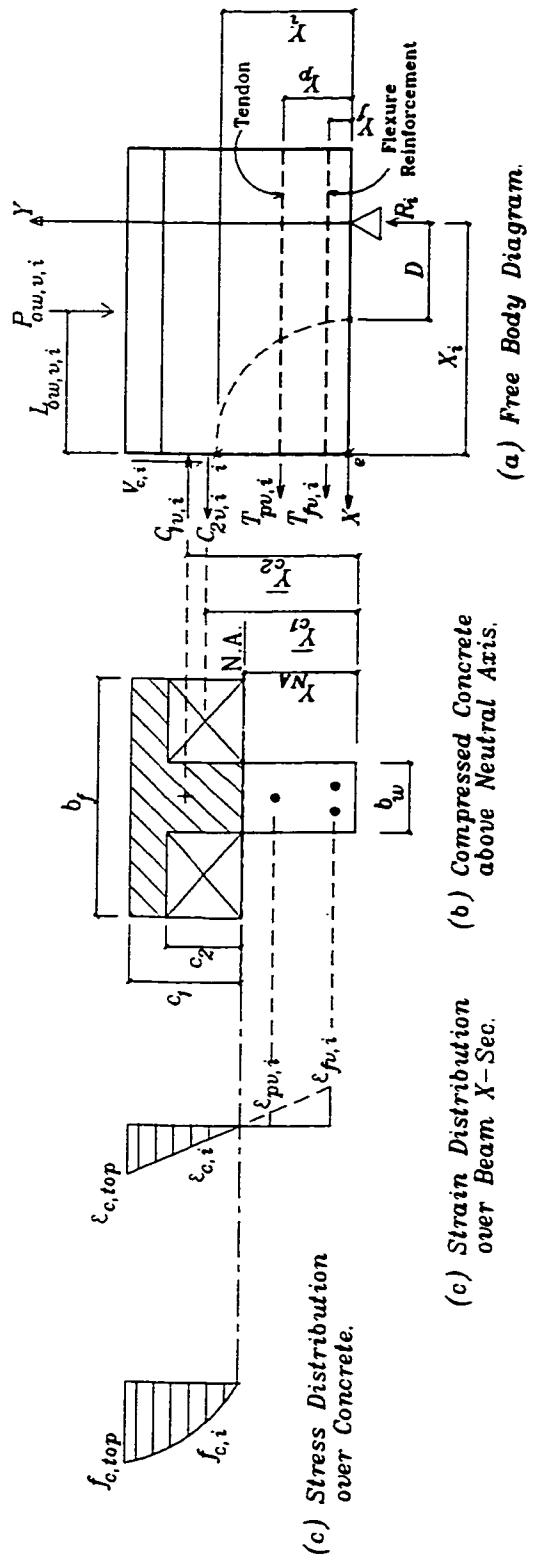
(a) Beam Equilibrium at Vertical X-section Passing Through Crack Tip.

(d) Stress Distribution above Crack Tip.

(c) Strain Distribution above Crack Tip.

(b) Compressed Concrete above Crack Tip.

(a) Free Body Diagram.
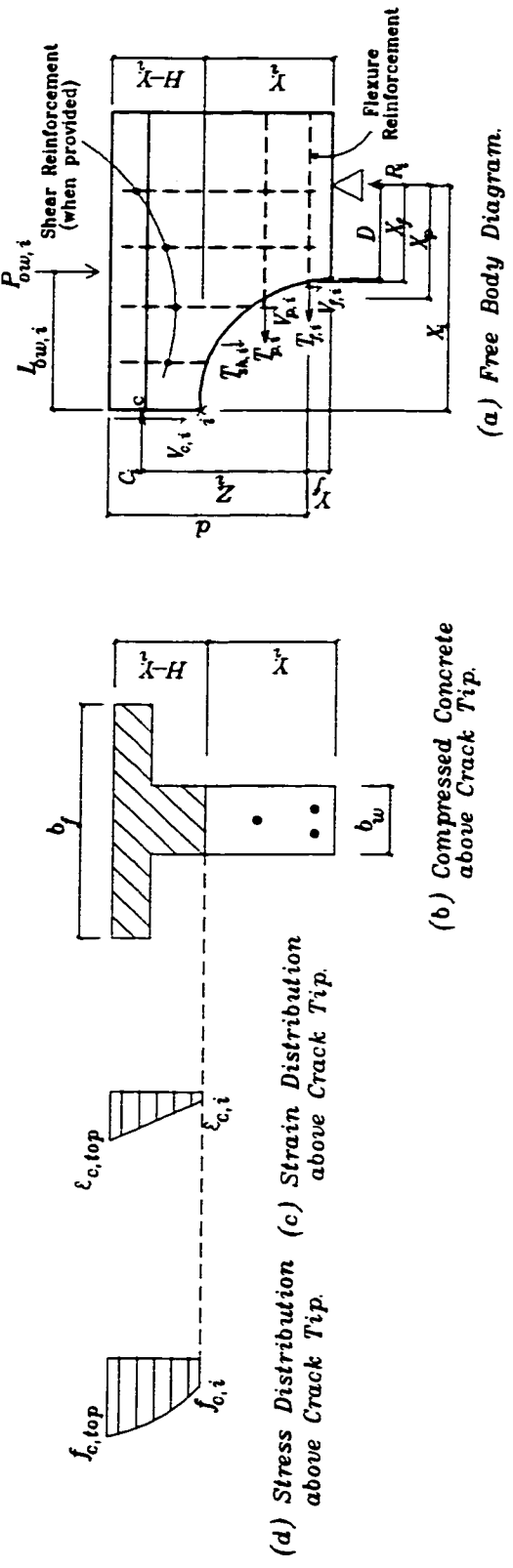
(b) Equilibrium of Beam Segment Passing through Crack Path.

Fig. 6-2: Beam Equilibrium and Concrete Compressive Strain/Stress Distribution at Crack Location.

142
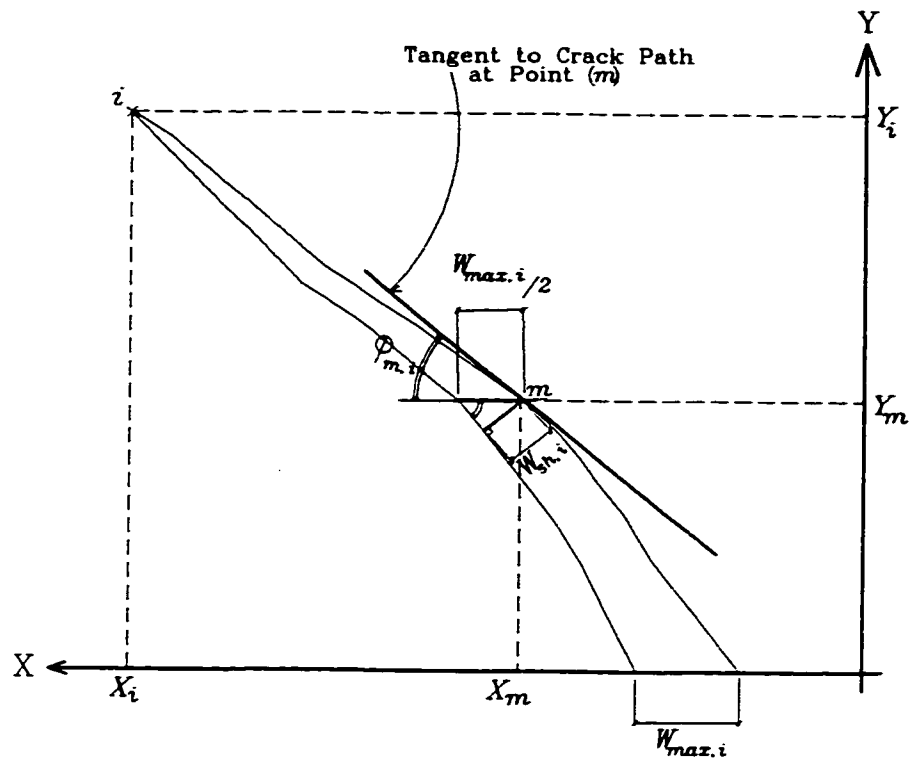
Fig. 6-3: Width of Shear Crack.

(b) Mohr's Circle at Crack Tip.

(a) Beam Segment under Study.

(c) Stresses induced at Crack Tip.
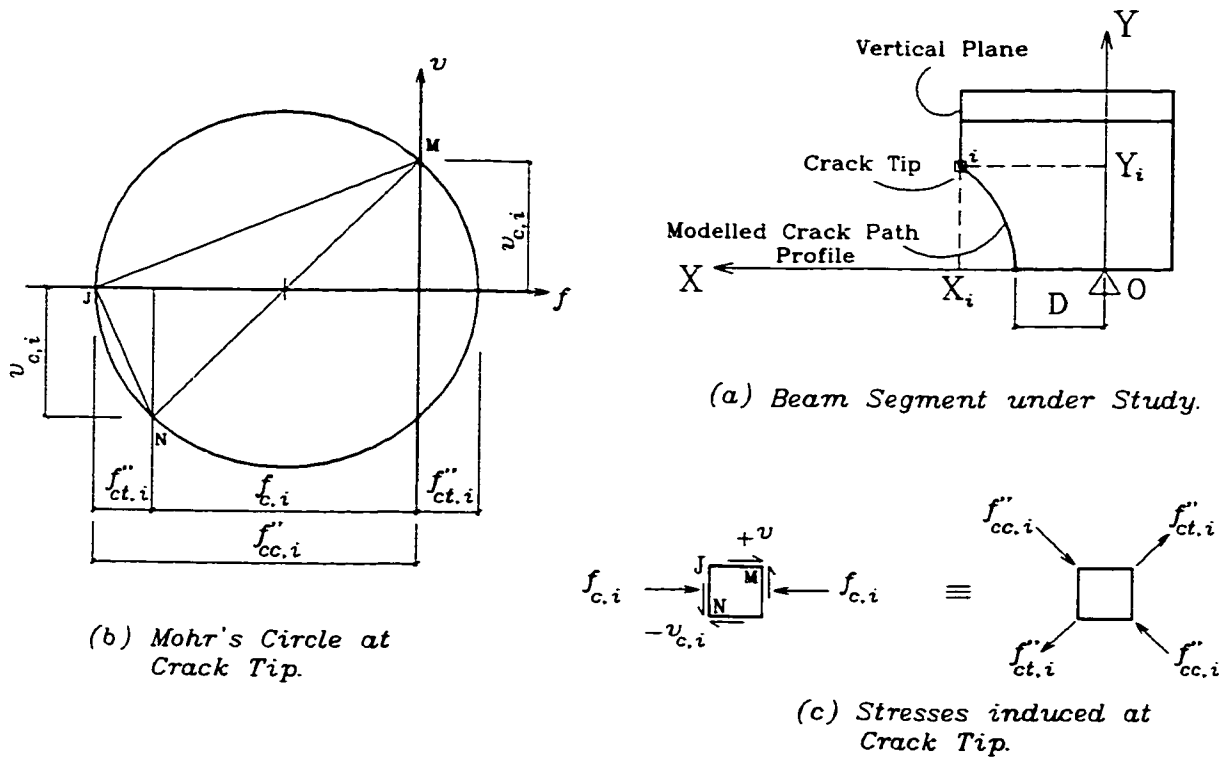
Fig. 6-4: Principal Stresses induced in Concrete at Crack Tip.

143

Start

Input D | Input $Y_i = \Delta Y$, e.g. $\Delta Y = H/10$

EQs. 4–5, 4–6 & 4–10. Calculate X_i

Assume Y_{NA} & $\varepsilon_{c.top.i}$

EQs. 6–11 to 6–21. Calculate $C_{v.i}, T_{fv.i}$ & $T_{pv.i}$

is EQ. 6–7 Satisfied ?

No | Yes

Calculate $P_{1.i}$ & C_i

EQs. 6–23 & 6–25 to 6–28. Calculate $T_{f.i}$ & $T_{p.i}$

EQs. 6–29 to 6–32. Calculate $V_{p.i}$ & $V_{f.i}$

EQs. 2–19 & 6–33 to 6–35. Calculate $W_{sh.i}$, $\varepsilon_{sh.i}$ & $T_{sh.i}$

EQ. 6–22. Calculate $P_{2.i}$

is $P_{2.i} = (1 \pm 0.005)\, P_{1.i}$?

No | Yes

EQ. 6–24. Calculate $V_{c.i}$

is EQ. 6–36 Satisfied ?

No | Yes

Check the Values of: $F_{f.i}$, $F_{p.i}$, $V_{c.i}$, $\varepsilon_{c.top.i}$ & $\varepsilon_{sh.i}$

Is there any Failure ?

No | Yes

Let $Y_{old} = Y_i$
Let $Y_i = Y_{old} + \Delta Y$

Crack Reaches a Failure Tip, i.e. Point (f).
$P_f = P_{u.D}$

Beam Strength = $(P_{u.D})_{min}$

Failure Mode, Failure Location
are Determined

End

Fig. 6-5: Flow chart of Beam Strength Calculations.
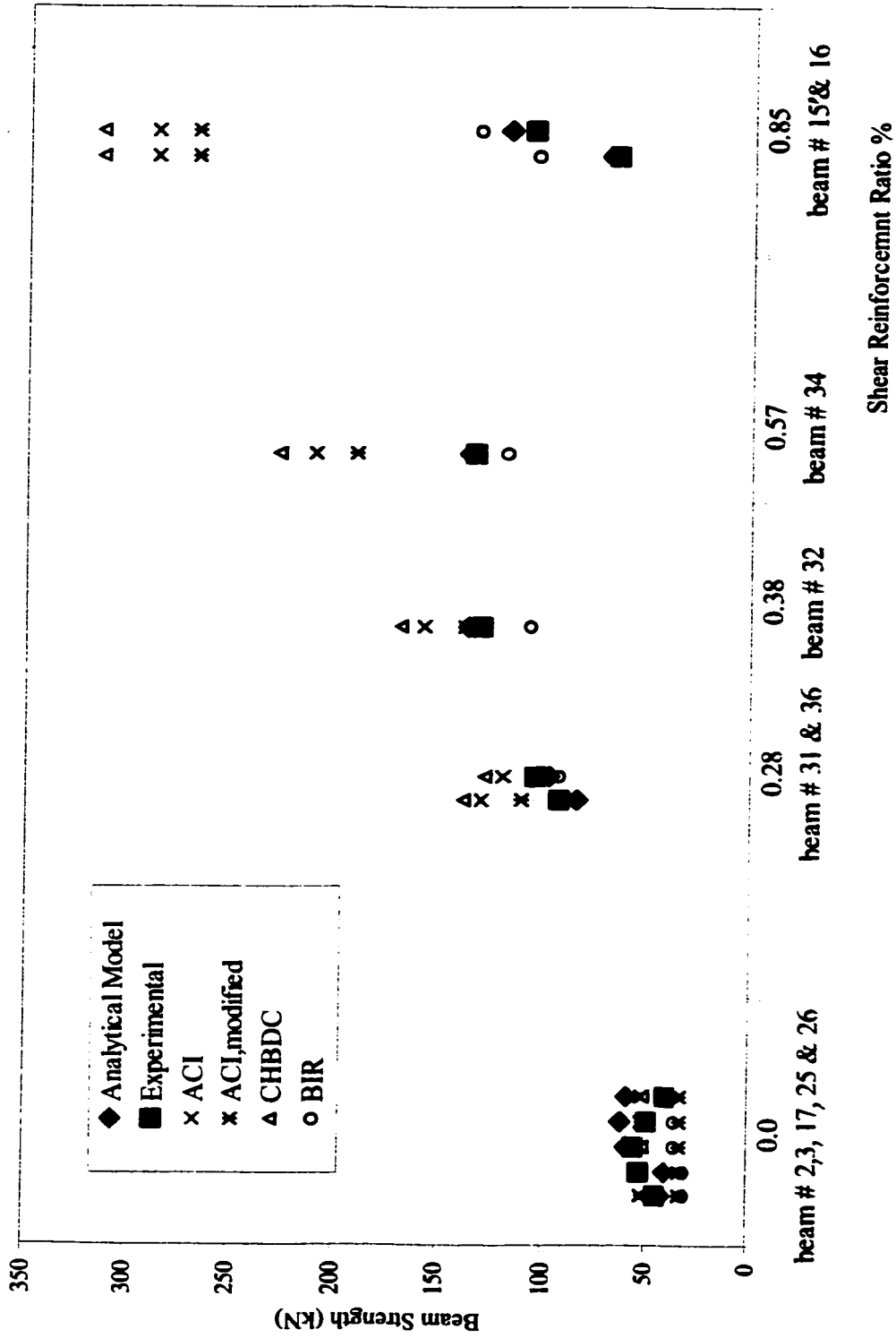
Fig. 6-6: Beam Strength vs. Shear Reinforcement Ratio.

Applied Load (P)
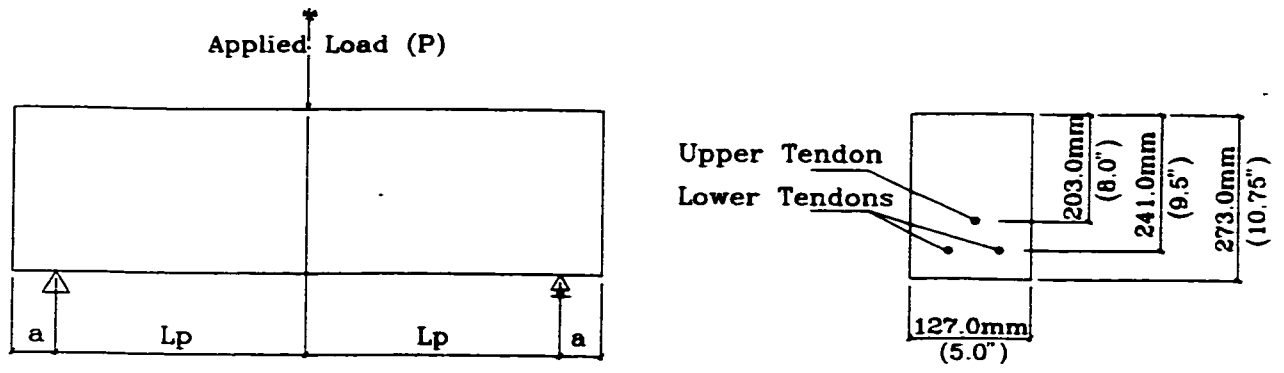
(a) Beam Set-up.	(b) Typical Cross Section.

Fig. 6-7: Tested Beams Configurations, (Park and Naaman, 1999c).
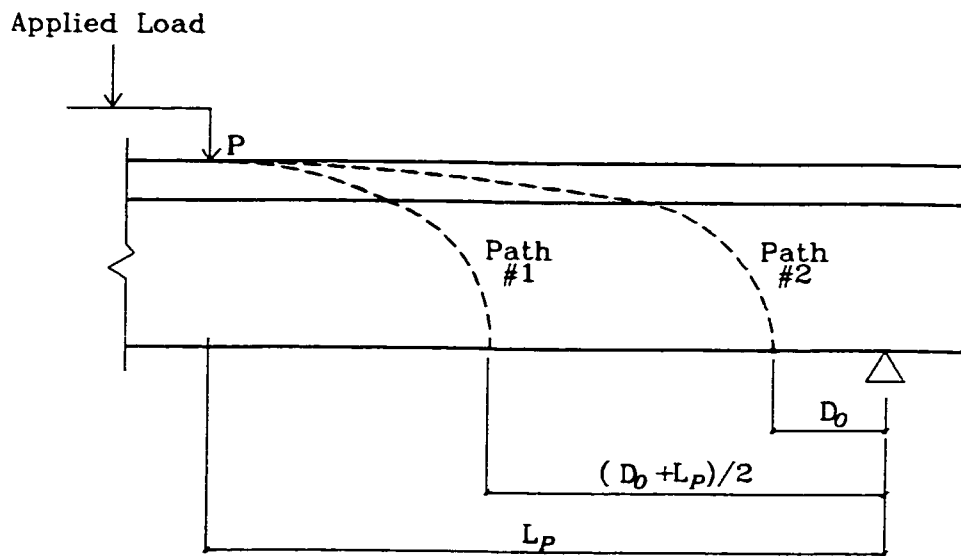
Fig. 6-8: Crack Paths Traced to Obtain the Beam Strength.

CHAPTER 7

STRENGTH OF CONCRETE BEAMS REINFORCED IN FLEXURE AND SHEAR WITH FRP BARS

7.1 General

The failure modes expressed in the analytical modelling developed in Chapter 6 have been extended to cover those when using FRP stirrups and/or FRP grids as shear reinforcement. The experimental results reported by Shehata et al. (1999) as well as by Erki and Bakht (1996) have been used to verify the results obtained from the analytical model.

7.2 Analytical Modelling Process

7.2.1 FRP Stirrups

The relationship between the diagonal crack width and the tensile strain induced in the stirrups as expressed in Equation 2-19 has been derived for concrete beams reinforced in shear with steel stirrups. Mizukawa et al. (1997) reported that the considerable difference between the experimental and analytical results obtained based on this relationship may be attributed to the difference between FRP and steel regarding both the mechanical properties as well as the bond characteristics where neither is introduced in that relationship (Section 2.14).

⟋ In this case, the tensile strain induced in the stirrups, $\varepsilon_{sh.i}$, cannot be determined based on the calculated value of the tensile stress in flexural reinforcement, $f_{f.i}$, and the total number of unknowns to be obtained from the three equiblirium equations (Equations 6-22, 6-23, and 6-24) becomes four ($f_{f.i}$, $V_{c.i}$, P_i, and $T_{sh.i}$). Consequently, the shear force developed by concrete, $V_{c.i}$, is assumed equal to V_{cr} obtained from Equation 2-10 where K' is calculated by Equation 2-13. Hence, the equilibrium equations can be solved for the values of $f_{f.i}$, P_i, and $T_{sh.i}$.

In order to account for the highly stressed/damaged fibres at the bend locations of the FRP stirrups, the reduction of the stirrup tensile strength presented in Equations 2-12 and 2-17 based on the ratio (r/d_b) is imposed to the analytical model as one of the beam failure limits unless enough experimental data about the failure limits of the used stirrups are available.

7.2.2 FRP Grids

In order to simplify the modelling of FRP grid, it is considered as a series of FRP bars in both longitudinal (horizontal) and transverse (vertical) directions. The longitudinal bars of the grid, located within the top quarter of beam height, are summed as top longitudinal reinforcement. However, these bars can be neglected due to the low shear/compressive strength of FRP bars. Besides, their contribution is actually negligible compared to the resistance of the surrounding concrete. The grid longitudinal bars, located within the middle zone of beam height, are summed as longitudinal reinforcement

located at the beam mid-height. This reinforcement can be modelled as FRP tendons as described in Chapter 6, taking into account that both T_{po} and T_{pl} are substituted as zeros. Finally, the grid longitudinal bars, located within the bottom quarter of beam height, are summed as additional flexural reinforcement. The vertical bars of the grid are modelled as FRP stirrups having the same spacing and cross sectional area of these bars except that the failure limit presented in Equations 2-12 and 2-17 is not applicable. These stirrups can be considered to have at least the same bond of deformed steel stirrups due to the considerable interlocking between each grid panel and the surrounding concrete.

The shear displacement induced in the summed longitudinal grid bars within the middle zone of beam height, $W_{n,sh-l-m,,i}$, can be calculated similar to that for the longitudinal reinforcement bars (Section 6.2) while the shear displacement induced in the vertical grid bars/stirrups, $W_{n,sh-v,,i}$, is obtained as shown in Fig. 7-1. Consider point (m) located at the mid-height of crack. Due to the relative rotation about crack tip (i), point (a) is displaced to (a ') along the crack side ie. Meanwhile, point (b) is displaced with the same distance along the same crack side to (b '). As can be seen in Fig. 7-1, the values of $W_{n,sh-l-m,,i}$ and $W_{n,sh-v,,i}$ can be calculated as follows:

$$W_{n,sh-l-m,i} = \frac{W_{max,i}}{2} \cot(\varphi_{m,i})$$

(7-1)

$$W_{n,sh-v,i} = W_{n,sh-l,i} \cos(\varphi_{m,i})$$

(7-2)

7.3 Beam Strength Calculations

Herein, the beam strength has been calculated based on three different crack paths. Crack path #1 presents a pure flexure crack, Crack path #3 presents the nearest crack to support, and Crack path #2 for a shear-flexure crack formed within shear span at the mid-distance between path #1 and path #3 (Fig. 7-2). The flow chart for beam strength calculations is shown in Fig. 7-3.

7.4 Verification Process

7.4.1 Part (I)

Shehata et al. (1999) published an experimental program for testing concrete beams reinforced in flexure with steel and CFRP bars. The material of the stirrups used as shear reinforcement (steel, CFRP, and GFRP), as well as the spacing between stirrups were among the main parameters of that study. The properties of both flexural and shear reinforcement are listed in Table 7-1. The configurations of the tested beams, failed in shear due to the rupture of FRP stirrups, are shown in Fig. 7-4 and listed in Table 7-2. It should be noted that for each beam which failed due to the rupture of stirrups, the reported measured average strain in stirrups at failure has been set as one of the failure limits of that beam (Tables 7-3 and 7-4). The comparison between the model results at beam failure and the corresponding results obtained experimentally is presented in Table 7-5.

Although that Shehata et al. (1999) did not report the load-displacement curve for the FRP bars used in their experimental program if they tested under direct shear loads, the shear displacement induced in the flexural bars, $W_{n,f,f}$, as well as in the stirrups, $W_{n,sh-v,f}$, which have been calculated by the analytical model for beams #CC-3 and # CG-3 at the failure corresponding to crack path #3 (Tables 7-3 and 7-4), is considered relatively high as it exceeds the maximum value for the CFRP bars used by Abdel-Sayed et al. (1998), as well as for those used by Park and Naaman (1999a; 1999b; 1999c). Therefore, these two beams might have failed due to the dowel failure of their reinforcement if a crack initiated at distance d from support.

The results listed in Table 7-5 shows that for all the tested beams, the analytical model predicted the same observed failure mode at the same observed failure location (e.g. within shear span). Also, the beam strength calculated by the modelling is considered very close to the actual strength as the percentage of the error in predicting the beam strength ranges from -8.2 % to 7.3 % for the all the tested beams.

Fig. 7-5 illustrates the ratio of (actual strength/calculated strength) for the tested beams based on the beam strength obtained experimentally and that calculated by the ACI, the CHBDC, and the BIR as reported by Shehata (1999), together with the same ratio obtained based on the beam strength calculated by the present model. It can be seen that the most accurate strength values have been introduced by the present analytical modelling. However, the strength values calculated by the ACI formulas can be

considered relatively accurate with respect to the strength values calculated by the CHBDC as well as by the BIR where both introduce very conservative strength.

7.4.2 Part (II)

Another experimental program was conducted by Erki and Bakht (1996) for testing concrete beams reinforced in flexure with steel bars and in shear with steel stirrups and CFRP grids. The first group of beams was reinforced in shear with U-shape steel stirrups of diameter 3.7 mm (0.15 in) and spacing 60 mm (2.36 in). In the second group, CFRP grids were used instead of the stirrups where three grid sheets were used on each beam face to provide the beam with the same axial rigidity of the stirrups. Two types of CFRP grids were used as shown in Fig. 7-6. The properties of both flexural and shear reinforcement are listed in Table 7-6. The configurations of the tested beams are shown in Fig. 7-7 and listed in Table 7-7. Similar to verification Part (I), the beam strength has been calculated based on three different crack paths (Fig. 7-2). The comparison between the model results at beam failure and the corresponding results obtained experimentally is presented in Tables 7-8 and 7-9. It can be seen that there is a good agreement between the results obtained by the analytical model and the observed behaviour of the beams tested in different experimental programs. It should be noted that when there are enough data to define the relationship between the shear displacement induced in the used FRP stirrups/grids under direct shear loads, the failure factor expressed in Equation 2-19 can be checked for the FRP stirrups/vertical bars of grid, F_{sh-v}, as well as for longitudinal bars of grid, F_{sh-l}, as mentioned in the flow chart for beam strength calculations illustrated in Fig. 7-3.

Table 7-1: Properties of Reinforcement, Verification Part (I).

Reinforcement Type (1)	Bar Area mm² (in²) (2)	Tensile Strength MPa (ksi) (3)	Modulus of Elasticity GPa (ksi) (4)
CFRP Flexural Bars	113.6 (0.176)	2200 (320)	137 (19900)
Steel Flexural Bars	140.0 (0.217)	1860 (270)	200 (29000)
CFRP Stirrups	38.48 (0.059)	1730 (250)	137 (19900)
GFRP Stirrups	113.0 (0.175)	640 (93)	41 (5950)

Table 7-2: Configurations of the Tested Beams, Verification Part (I).
Dims. are in mm (in).

Beam # (1)	Setting Type (2)	Setting Configurations			Shear Reinforcement		Flexural Reinforcement (8)	f_c' MPa (ksi) (8)
		a (3)	Lp (4)	b (5)	Type (6)	Spacing (7)		
SC-2	II	1000.0 (39.4)	1500.0 (59.0)	2000.0 (78.7)	CFRP Stirrups	@ 235.0 (9.3)	6 — Steel Bars diam. 15 (0.59)	54 (7.8)
SC-3	II	1000.0 (39.4)	1500.0 (59.0)	2000.0 (78.7)	CFRP Stirrups	@ 156.7 (6.2)	6 — Steel Bars diam. 15 (0.59)	54 (7.8)
SC-3	II	1000.0 (39.4)	1500.0 (59.0)	2000.0 (78.7)	CFRP Stirrups	@ 117.5 (4.6)	6 — Steel Bars diam. 15 (0.59)	51 (7.4)
SG-2	II	1000.0 (39.4)	1500.0 (59.0)	2000.0 (78.7)	GFRP Stirrups	@ 235.0 (9.3)	6 — Steel Bars diam. 15 (0.59)	54 (7.8)
CC-3	II	1000.0 (39.4)	1500.0 (59.0)	2000.0 (78.7)	CFRP Stirrups	@ 156.7 (6.2)	7 — CFRP Bars diam. 15 (0.59)	50 (7.3)
CG-3	II	1000.0 (39.4)	1500.0 (59.0)	2000.0 (78.7)	GFRP Stirrups	@ 156.7 (6.2)	7 — CFRP Bars diam. 15 (0.59)	50 (7.3)

Table 7-3: Beam Capacity Obtained Analytically for Beams with CFRP Stirrups for Different Crack paths.

Beam #	Crack Path #	$P_{u.D}$ kN (kip)	$(Y_f)_{mod}$ mm (in)	$(X_f)_{mod}$ mm (in)	$\varepsilon_{c.top.f}$	$f_{f.con.f}$ or $f_{f.pr.f}$* MPa (ksi)	$W_{n.f.f}$ mm (in)	$\varepsilon_{sh.f}$	$W_{n.sh-v.f}$ mm (in)	Failure type
(1)	(2)	(3)	(4)	(5)	(6)	(7)	(8)	(9)	(8)	(10)
SC-2	1	978.6 (220.0)	477.5 (18.8)	1500.0 (59.0)	0.0019	1860.3 (270.0)	-	-	-	FY
	2	533.8 (120.0)	500.4 (19.7)	1150.6 (45.3)	0.0009	826.8 (120.0)	0.58 (0.023)	0.0077	0.30 (0.012)	SR
	3	778.4 (175.0)	495.3 (19.5)	1320.8 (52.0)	0.0009	964.6 (140.0)	1.39 (0.055)	0.0077	0.86 (0.034)	SR
SC-3	1	978.6 (220.0)	477.5 (18.8)	1500.0 (59.0)	0.0019	1860.3 (270.0)	-	-	-	FY
	2	631.6 (142.0)	495.3 (19.5)	1320.8 (52.0)	0.0011	1033.5 (150.0)	0.74 (0.029)	0.0071	0.38 (0.015)	SR
	3	934.1 (210.0)	508.0 (20.0)	1176.0 (46.3)	0.0014	1136.9 (165.0)	1.67 (0.066)	0.0071	1.04 (0.041)	SR
SC-4	1	960.8 (216.0)	474.9 (18.7)	1500.0 (59.0)	0.0002	1860.3 (270.0)	-	-	-	FY
	2	689.4 (155.0)	482.6 (19.0)	1303.0 (51.3)	0.0012	1136.9 (165.0)	0.76 (0.030)	0.0055	0.41 (0.016)	SR
	3	1000.8 (225.0)	495.3 (19.5)	1137.9 (44.8)	0.0015	1205.8 (175.0)	1.73 (0.068)	0.0055	1.09 (0.043)	SR
CC-3	1	1023.0 (230.0)	487.7 (19.2)	1500.0 (59.0)	0.0028	2205.0 (320.0)	-	-	-	FF
	2	600.5 (135.0)	495.3 (19.5)	1320.8 (52.0)	0.0016	1240.2 (180.0)	1.75 (0.069)	0.0065	0.91 (0.036)	SR
	3	889.6 (200.0)	523.2 (20.6)	1224.3 (48.2)	0.0019	2205.0 (320.0)	6.35 (0.250)	0.0065	4.39 (0.157)	FF/SR

Note: FF: Flexural reinforcement Rupture; FY: Flexural reinforcement Yield; and SR: Stirrups Rupture.

* When flexural reinforcement bars are of steel.

Table 7-4: Beam Capacity Obtained Analytically for Beams with GFRP Stirrups for Different Crack paths.

Beam #	Crack Path #	$P_{u,D}$ KN (kip)	$(Y_f)_{mod}$ mm (in)	$(X_f)_{mod}$ mm (in)	$\varepsilon_{c,top,f}$	$f_{f,f}$ or $f_{f,pr,f}$ * MPa (ksi)	$W_{n,f,f}$ mm (in)	$\varepsilon_{sh,f}$	$W_{n,sh-v,f}$ mm (in)	Failure type
(1)	(2)	(3)	(4)	(5)	(6)	(7)	(8)	(9)	(8)	(10)
SG-2	1	978.6 (220.0)	477.5 (18.8)	1500.0 (59.0)	0.0019	1860.3 (270.0)	-	-	-	FY
	2	591.6 (133.0)	482.6 (19.0)	1303.0 (51.3)	0.0010	964.6 (140.0)	0.69 (0.027)	0.0091	0.36 (0.014)	SR
	3	822.9 (185.0)	487.7 (19.2)	1110.0 (43.7)	0.0015	1067.9 (155.0)	1.52 (0.060)	0.0091	0.97 (0.038)	SR
CG-3	1	1023.0 (230.0)	487.7 (19.2)	1500.0 (59.0)	0.0028	2205.0 (320.0)	-	-	-	FF
	2	653.9 (147.0)	492.8 (19.4)	1315.7 (51.8)	0.0014	1378.0 (200.0)	1.96 (0.077)	0.0085	0.99 (0.039)	SR
	3	934.1 (210.0)	520.7 (20.5)	1214.1 (47.8)	0.0020	2205.0 (320.0)	6.6 (0.260)	0.0078	3.96 (0.156)	FF

Note: FF: Flexural reinforcement Rupture; FY: Flexural reinforcement Yield; and SR: Stirrups Rupture.

* When flexural reinforcement bars are of steel.

155

Table 7-5: Results Obtained Analytically and Experimentally at Beam Failure, Verification Part (I).

Beam #	Beam Strength			Failure Type		Failure Location	
	Analytically kN (kip)	*Experimentally* kN (kip)	*% error*	*Analytically*	*Experimentally*	*Analytically*	*Experimentally*
(1)	(2)	(3)	(4)	(5)	(6)	(7)	(8)
SC-2	533.8 (120.0)	555.1 (124.8)	-3.8	SR	SR	Crack #2	Within Lp
SC-3	631.6 (142.0)	682.3 (153.4)	-7.4	SR	SR	Crack #2	Within Lp
SC-4	689.4 (155.0)	750.8 (168.8)	-8.2	SR	SR	Crack #2	Within Lp
CC-3	600.5 (135.0)	609.4 (137.0)	-1.4	SR	SR	Crack #2	Within Lp
SG-2	591.6 (133.0)	583.6 (131.2)	1.4	SR	SR	Crack #2	Within Lp
CG-3	653.9 (147.0)	608.9 (136.9)	7.3	SR	SR	Crack #2	Within Lp

Note: SR: Stirrup Rupture.

Table 7-6: Properties of Reinforcement, Verification Part (II).

Reinforcement Type	Tensile Strength MPa (ksi)	Modulus of Elasticity MPa (ksi)
(1)	(2)	(3)
Steel Bars	425.0 (62.0)	200000.0 (29000.0)
CFRP Grids	1200.0 (175.0)	71000.0 (10304.0)

156

Table 7-7: Configurations of the Tested Beams, Verification Part (II),
Dimensions are in mm (in).

| Beam # | Setting Type | Setting Configurations | | | Shear Reinforcement | Flexural Reinforcement | f'_c MPa (ksi) |
| | | a | Lp | b | | | |
(1)	(2)	(3)	(4)	(5)	(6)	(8)	(8)
N41 & N42	II	350.0 (13.8)	800.0 (31.5)	1800.0 (71.0)	6-CFRP Grids, Type I	Steel Bars 2-diam. 20 (0.78)+ 1-diam. 10 (0.39)	35 (5.1)
MN1 & MN2	II	350.0 (13.8)	800.0 (31.5)	1800.0 (71.0)	6-CFRP Grids, Type II	Steel Bars 2-diam. 20 (0.78)+ 1-diam. 10 (0.39)	35 (5.1)

Table 7-8: Beam Capacity Obtained Analytically for Beams with CFRP Grids
for Different Crack paths.

| Beam # | Crack Path # | $P_{u,D}$ kN (kip) | $(Y_f)_{mod}$ mm (in) | $(X_f)_{mod}$ mm (in) | $\varepsilon_{c,top,f}$ | $f_{f,pr,f}$ MPa (ksi) | $f_{sh-l-b,f}$ MPa (ksi) | $W_{nf,f}$ mm (in) | $\varepsilon_{sh-v,f}$ | $f_{sh-l-m,f}$ MPa (ksi) | $W_{n,sh-l-m,f}$ mm (in) | Failure type |
(1)	(2)	(3)	(4)	(5)	(6)	(7)	(8)	(9)	(10)	(11)	(12)	(13)
N41 & N42	1	289.1 (65.0)	368.3 (14.5)	800.0 (31.5)	0.0008	425.0 (61.7)	144.7 (21.0)	-	-	(7.0)	-	FY
	2	320.6 (72.0)	375.9 (14.8)	711.2 (28.0)	0.0008	400.0 (58.0)	137.8 (20.0)	0.10 (0.004)	0.017	(8.0)	0.03 (0.001)	GR
	3	431.5 (97.0)	381.0 (15.0)	645.2 (25.2)	0.0009	425.0 (61.7)	144.7 (21.0)	0.23 (0.009)	0.016	(7.0)	0.15 (0.006)	FY
MN1 & MN2	1	280.2 (63.0)	368.3 (14.5)	800.0 (31.5)	0.0008	425.0 (61.7)	144.7 (21.0)	-	-	(7.0)	-	FY
	2	315.8 (71.0)	381.0 (15.0)	718.8 (28.3)	0.0008	379.0 (55.0)	137.8 (19.0)	0.10 (0.004)	0.017	(8.0)	0.03 (0.001)	GR
	3	422.6 (95.0)	381.0 (15.0)	640.1 (25.2)	0.0009	425.0 (61.7)	144.7 (21.0)	0.23 (0.009)	0.015	(7.0)	0.15 (0.006)	FY

Note: FY: Flexural reinforcement Yield; and SR: Stirrups Rupture.

Table 7-9: Results Obtained Analytically and Experimentally at Beam Failure, Verification Part (II).

Beam # (1)	Beam Strength			Failure Type		Failure Location	
	Analytically kN (kip) (3)	*Experimentally* kN (kip) (3)	*% error* (4)	*Analytically* (5)	*Experimentally* (6)	*Analytically* (7)	*Experimentally* (8)
N41 & N42	289.1 (65.0)	310.0 (69.7)	-6.7	FY	FY	Crack # 1	Within Constant Moment Zone
MN1 & MN2	280.2 (63.0)	310.0 (69.7)	-9.6	FY	FY	Crack # 1	Within Constant Moment Zone

Note: FY: Flexural reinforcement Yield.
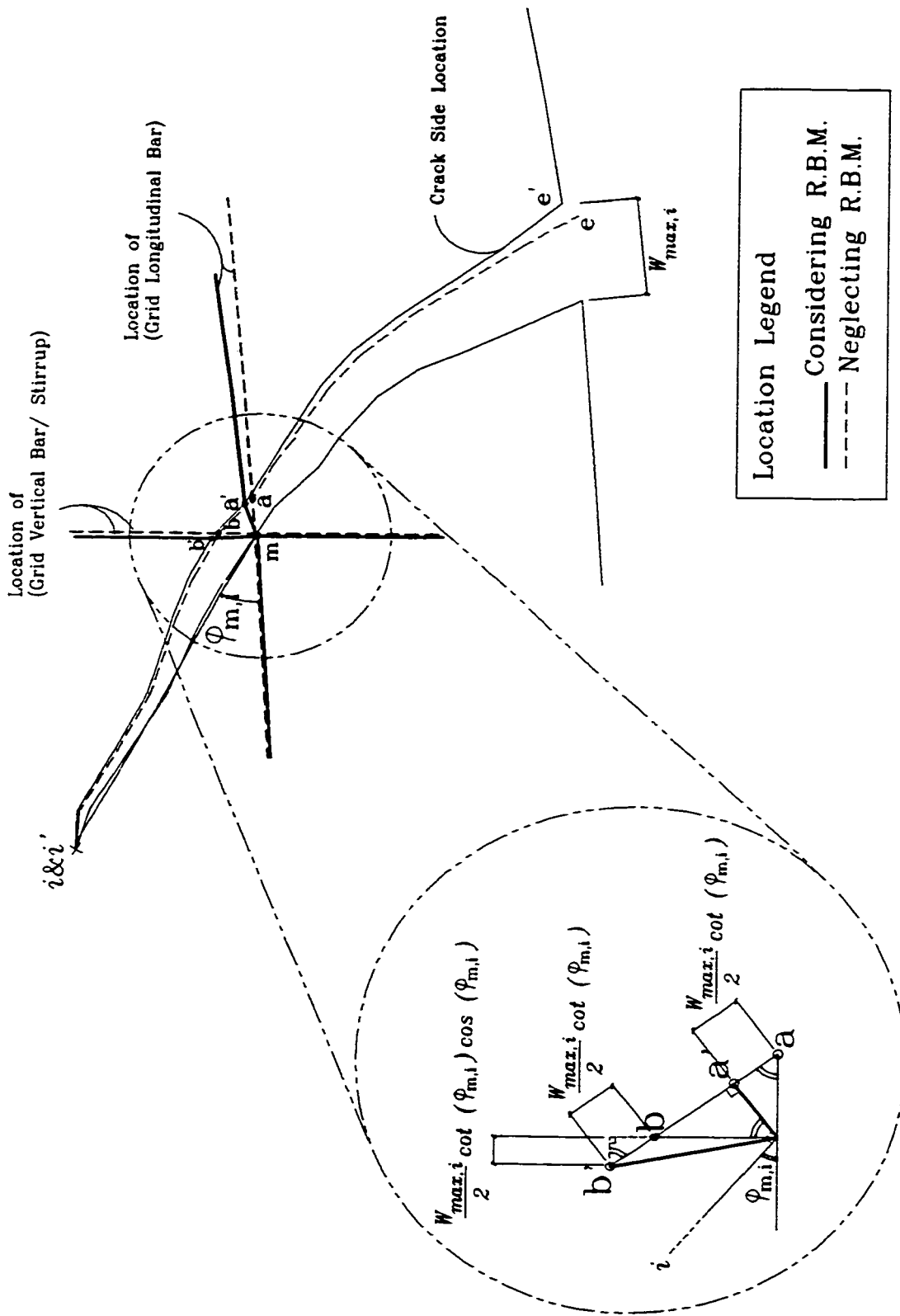
Fig. 7-1: Shear Displacement Induced in the Vertical Grid Bars/Stirrups.

159
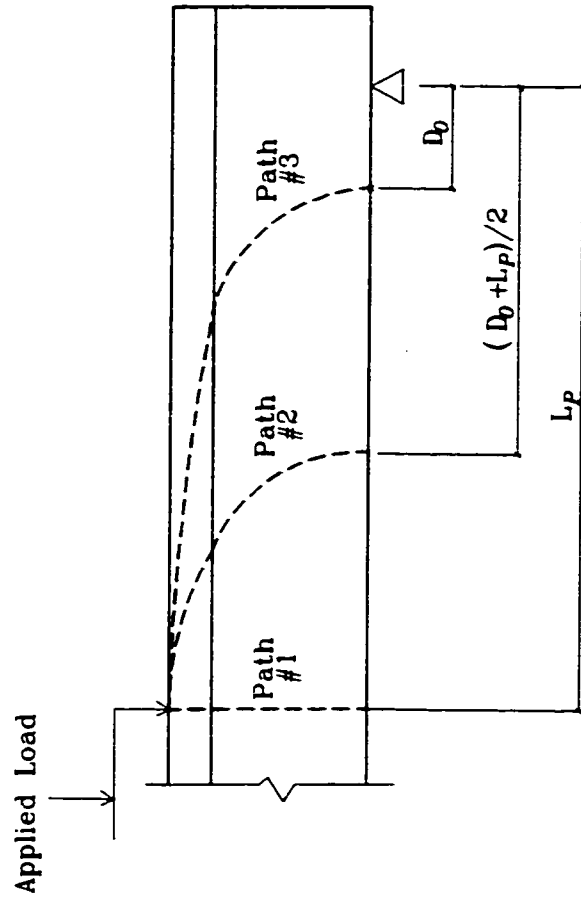
Fig. 7-2: Crack Paths Traced for Beam Strength Calculations.
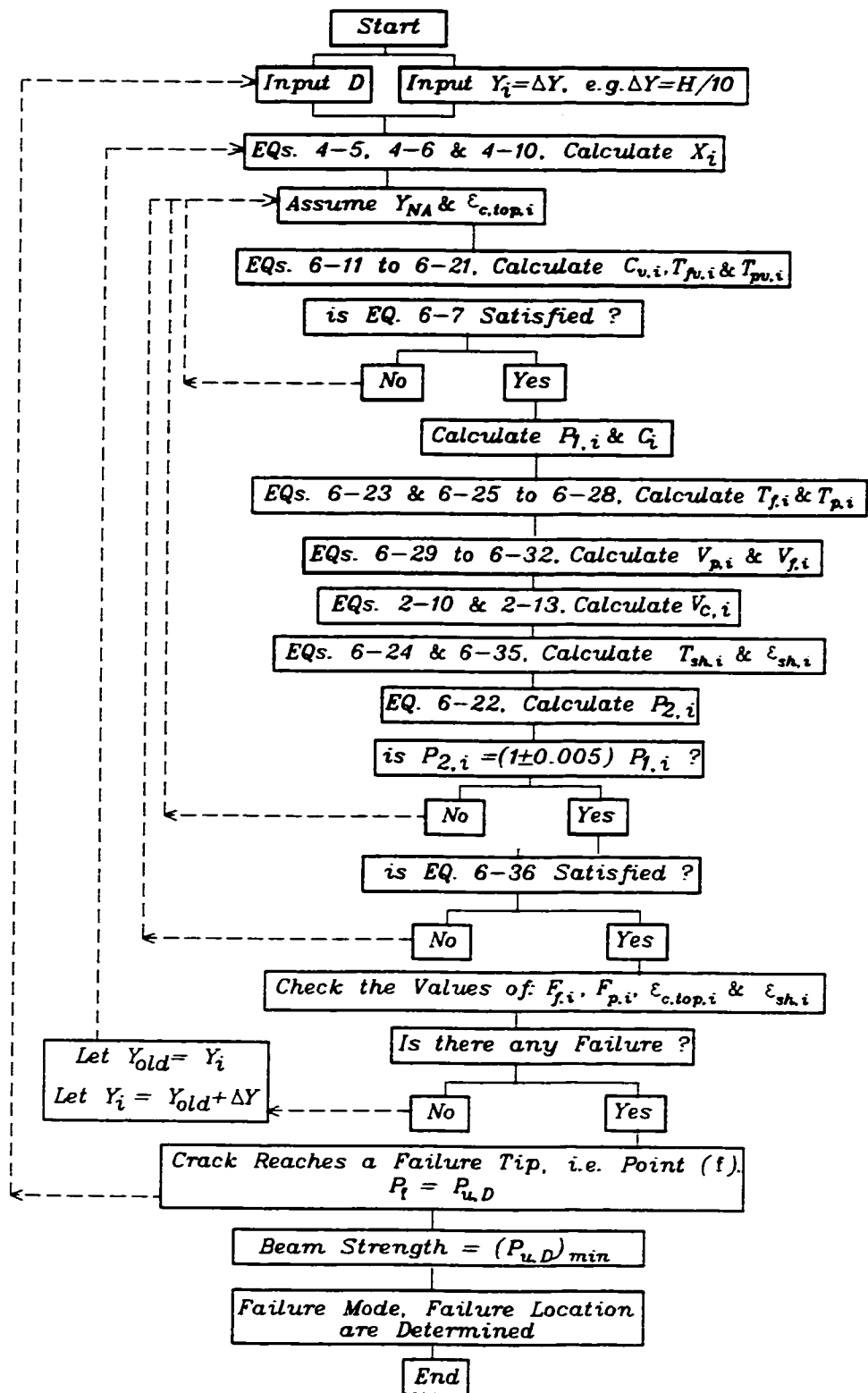
Fig. 7-3: Flow chart for the Calculations of Beam Strength.

161
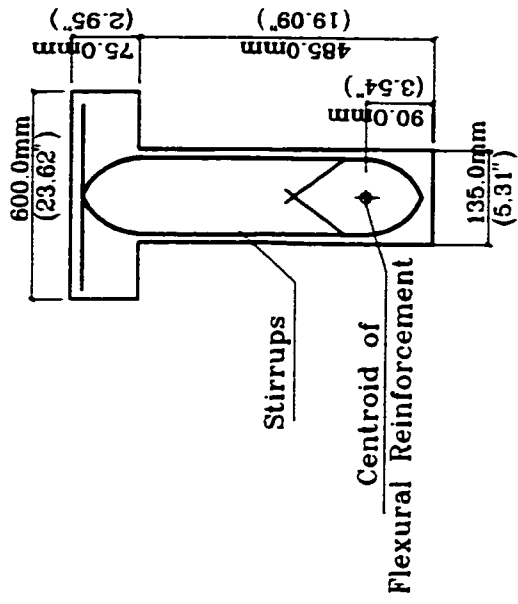
(b) Typical Cross Section.
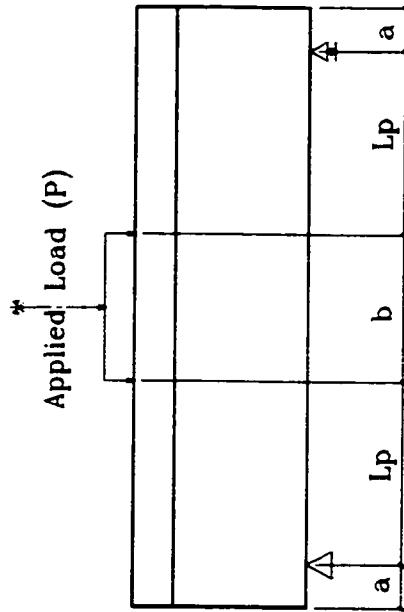
(b) Set-up Type (II).

Fig. 7-4: Configurations of the Tested Beams, (Shehata et al. 1999).

162
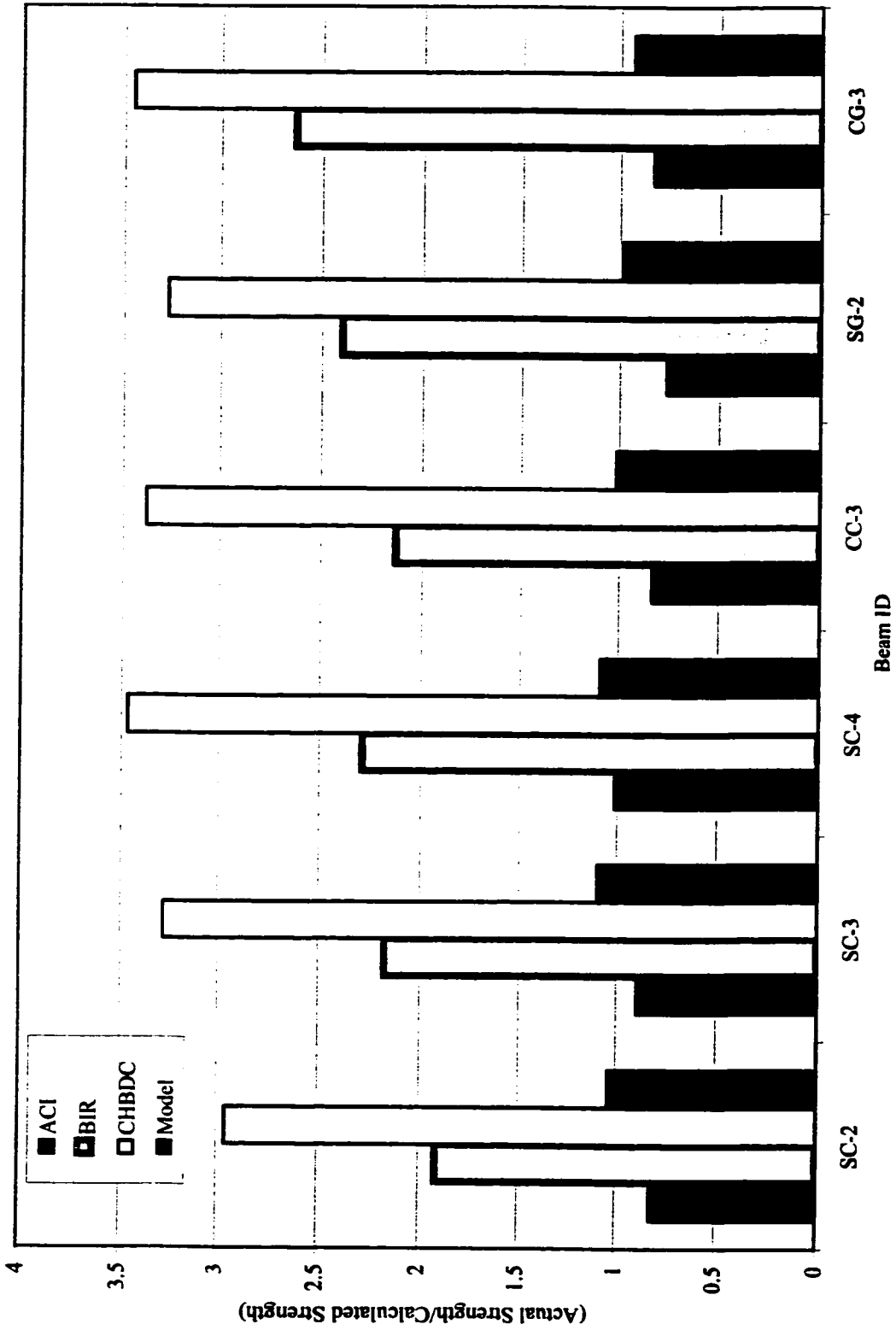
Fig. 7-5: Ratio of (Actual Strength/Calculated Strength) for the Tested Beams.
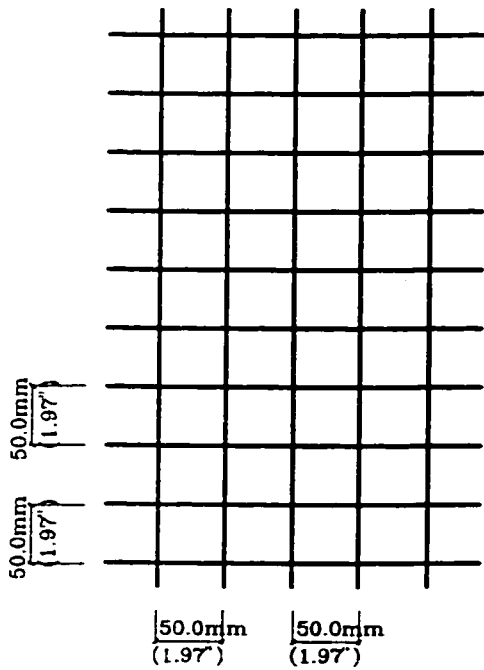
(a) Grid Type (I).
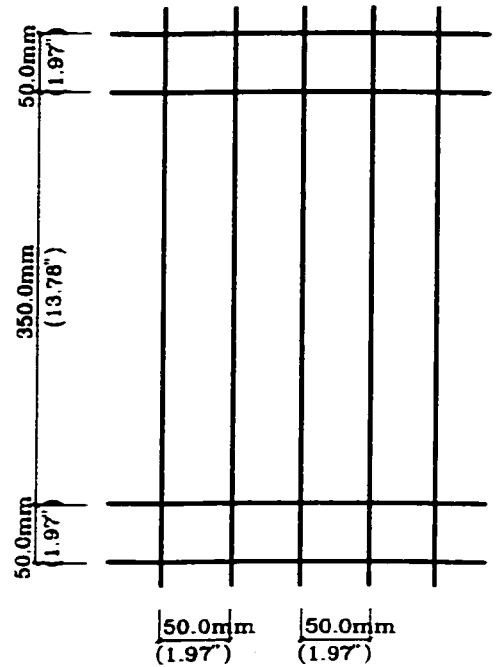
(b) Grid Type (II)

Fig. 7-6: Types of FRP Grids Used for Shear Reinforcement, (Erki and Bakht 1996).
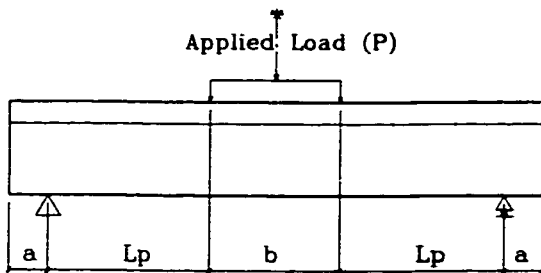
(b) Set-up Type (II).
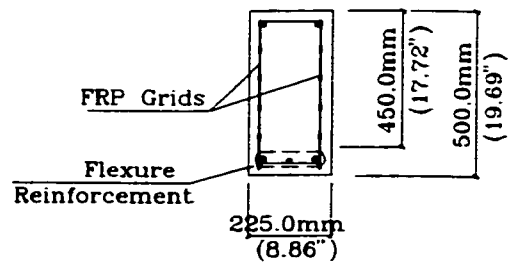
(b) Typical Cross Sec. I-I.

Fig. 7-7: Tested Beams Configurations, (Erki and Bakht 1996).

164

CHAPTER 8

SIGNIFICANCE OF AN ACCURATE MODELLING
OF CRACK PATH GEOMETRY

8.1 General

This chapter discuses the effect of the accuracy of the analytical modelling of crack geometry on the overall accuracy and reliability of the calculated beam strength as well as the beam conditions at failure crack location, (e.g. stresses/strains induced in concrete and reinforcement).

Herein, the proposed model for crack geometry described in Chapter 4, model (A), has been replaced by a line modelling of crack geometry, model (B). A comparison has been made for the analytical results obtained based on each model, (A) and (B), against the corresponding results obtained experimentally.

8.2 Line Modelling of Crack Geometry

The modelling of crack geometry can be simplified, as proposed by Jenq and Shah (1989), to be in the form of two lines, Fig. 8-1. The first line connects the crack starting point (st) vertically with the c.g. of the flexural reinforcement, point (f), while the second line connects point (f) with the nearest loading point (pt). This line presents the major segment of the crack path and its equation can be expressed as follows:

$$\frac{X_i - D}{Lp - D} = \frac{Y_i - Y_f}{H - Y_f}$$

(8-1)

8.3 Analytical Model vs. Experimental results

The comparison between the analytical results obtained at beam failure based on the models (A) and (B) and the corresponding results obtained experimentally is presented in Table. 8-1. In general, for the beams which experienced a dowel failure of FRP bars (e.g. beams # 2, 17, 34 and 36), the tensile stress induced in these bars at failure, $f_{f,f}$, was lower for model (B) than that for model (A) while the corresponding shear displacement, $W_{nf,f}$, was higher for model (B) than that for model (A).

Based on the relationship between crack width, $W_{tf,i}$, and the shear displacement of the bars crossing the crack, $W_{nf,i}$, expressed by Equation 6-1, $W_{nf,i}$ is directly proportional to $cot\varphi_{f,i}$ and $f_{f,i}$. At the same time, $\varphi_{f,i}$ is constant for any point (i) along the crack path profile in model (B), as well as being less than that in model (A). Consequently, the value of $f_{f,i}$ required to satisfy the failure condition of the FRP bars, i.e. $F_f = 1.00$, is less for model (B) than that for model (A). In order to demonstrate the degree of accuracy of each model, the error of the calculated beam strength, $(P_{fail})_{mod}$, with respect to the actual strength, $(P_{fail})_{exp}$, has been listed in Table 8-1.

It can be seen that the beam strength calculated based on model (A) is much more accurate than that calculated based on model (B), where the percentage of error in

predicting the beam strength based on model (A) ranges from -7.3 % to 8.0 % while this percentage ranges from -5.0 % to –30.0 %.

It can be noted that the difference in the modelling of crack geometry between model (A) and model (B) has no influence on the beams where failure is governed by pure flexure cracks, e.g. beams #29 and #30, since these cracks are modelled as vertical lines in both models.

Table 8-1: Results obtained Analytically and Experimentally.

| Beam # (1) | Based on (2) | Analytical Model Results | | | | | | Observed | %error |
		$f_{f.f}$ MPa (ksi) (3)	$W_{n.f}$ mm (in) (4)	$\varepsilon_{sh.f}$ (5)	$\varepsilon_{c.top.f}$ (6)	$\varepsilon_{p.f}$ (7)	$(P_{fail})_{mod}$ kN (kip) (9)	$(P_{fail})_{exp}$ kN (kip) (10)	(11)
2	Model (A)	861.3 (125.0)	1.65 (0.065)	-	0.0006	-	42.3 (9.5)	44.5 (10.0)	-5.0
	Model (B)	620.1 (90.0)	1.83 (0.072)	-	0.0007	-	31.1 (7.0)		-30.0
17	Model (A)	689.0 (100.0)	1.75 (0.069)	-	0.0008	0.0086	60.0 (13.5)	56.0 (12.5)	8.0
	Model (B)	516.8 (75.0)	1.88 (0.074)	-	0.0007	0.0082	42.3 (9.5)		-24.0
29	Model (A)	1655.0 (240.0)	0.000	0.0000	0.0015	-	85.0 (19.0)	89.6 (20.0)	-5.0
	Model (B)	1655.0 (240.0)	0.000	0.0000	0.0015	-	85.0 (19.0)		-5.0
30	Model (A)	1655.0 (240.0)	0.000	0.0000	0.0015	-	85.0 (19.0)	91.2 (20.5)	-7.3
	Model (B)	1655.0 (240.0)	0.000	0.0000	0.0015	-	85.0 (19.0)		-7.3
34	Model (A)	1515.8 (220.0)	0.76 (0.030)	0.0080	0.0013	0.0108	135.7 (30.5)	133.4 (30.0)	1.6
	Model (B)	1102.4 (160.0)	1.49 (0.059)	0.0065	0.0014	0.0096	108.9 (24.5)		-18.3
36	Model (A)	1033.5 (150.0)	1.55 (0.061)	0.0039	0.0008	-	98.0 (22.0)	104.6 (23.5)	-6.5
	Model (B)	861.3 (125.0)	1.70 (0.067)	0.0034	0.0007	-	82.3 (18.5)		-21.3
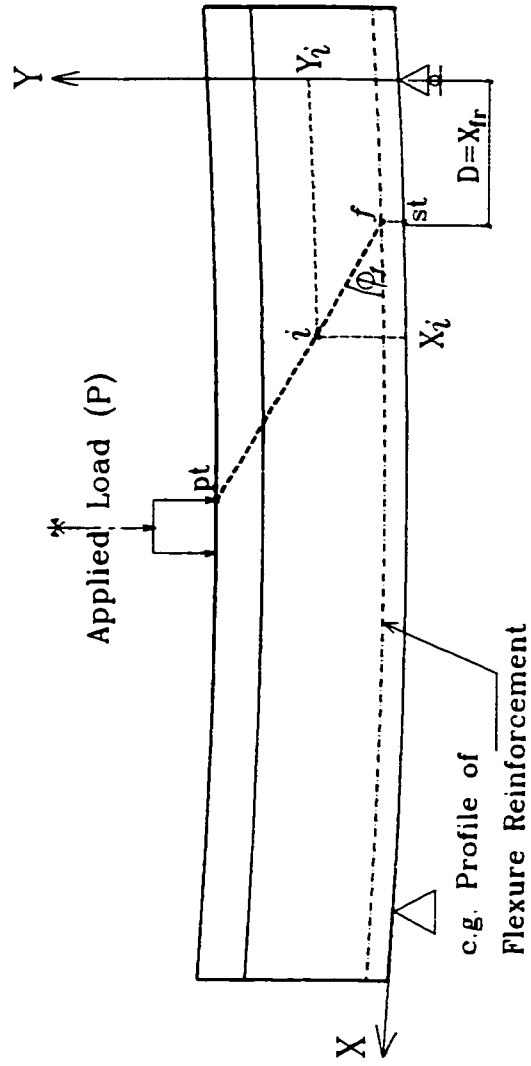
Fig. 8-1: Line Modelling of Crack Geometry.

CHAPTER 9

CONCLUSIONS

1- A comprehensive study for concrete beams reinforced and/or prestressed with FRP bars has been carried out. This study takes into account significant parameters that are usually neglected in the established methods of analysis and/or design of reinforced concrete beams. These parameters are as follows:

- the detailed geometry of the crack path profile,

- the induced crack width at the level of reinforcement,

- the dowel action of FRP bars, and

- the rigid body rotation of the beam portions on both sides of the crack.

2- An analytical model has been developed for the description of the crack path geometry. The results of the presented model are in good agreement with the corresponding results obtained experimentally for concrete beams reinforced with CFRP bars, as well as for beams reinforced with steel bars.

3- The crack width formulas for steel-reinforced concrete beams have been modified to account for the difference between steel and FRP bars regarding the mechanical properties and the bond characteristics. The results of the modified formulas are in good agreement with different analytical methods, as well as with experimental data.

4- The interaction between longitudinal reinforcement, shear reinforcement, crack formation, and the induced stresses and strains in both concrete and reinforcement has been expressed through a comprehensive analytical model.

5- The model calculates the contribution of shear reinforcement based on the induced crack width, the dowel action of reinforcement, the actual number of stirrups crossing the crack, and the beam equilibrium conditions.

6- The model can trace any possible failure mechanism of concrete and/or reinforcement (including the pre-mature failure of beam due to the dowel failure of their FRP reinforcement), and finally determining the beam strength, as well as the corresponding mode of failure.

7- The results of the presented analytical model are in good agreement with the corresponding results obtained from different experimental works for concrete beams reinforced and/or prestressed longitudinally with FRP and/or steel bars, and reinforced transversally with different types of shear reinforcement (steel stirrups, FRP stirrups, and FRP grids).

8- The current design guidelines for FRP-reinforced concrete structures over-estimate the beam strength significantly since they disregard the dowel failure of FRP reinforcement and the actual contribution of shear reinforcement.

APPENDIX I. REFERENCES

Abdel-Sayed, G., Salib, S., DeThomasis, J., and Grace, N. (1998). " Mechanical Properties and Structural Behavior of Glasform CFRP Bars", Report submitted to Glasform Inc., California.

ACI Committee 224 (1972), "Control of Cracking in Concrete Structures", Title No. 69-69, *Structural Journal, ACI,* pp. 717-734.

ACI (1995). "Building Code Requirements for Reinforced Concrete", (ACI 318-95 / ACI 318R-95), *American Concrete Institute,* Detroit, MI.

ACI Committee 440 (1996), "State-of-the-Art Report on Fiber Reinforced Plastic Reinforcement for Concrete Structures", American Concrete Institute, MI.

ACI Committee 440 (1999), "Provisional Design Recommendations for Concrete Reinforced with FRP Bars", American Concrete Institute, MI.

Bazent, Z.P., and Kim, J.K. (1984). "Size Effect in Shear Failure of Longitudinally Reinforced Beams", *ACI Journal,* Vol. 81, pp. 456-468.

Belarbi, K., Chandrashekhara, K., and Watkins, S.E. (1999). " Performance Evaluation of Fiber Reinforced Polymer Bar Featuring Ductility and Health Monitoring Capability ", *Fiber Reinforced Polymer for Reinforced Concrete Structures, 4th International Symposium, FRPRCS-4,* ML, USA, pp. 1-12.

"Canadian Bridge Design Code Provisions for Fiber-Reinforced Structures" (2000), *Journal of Composites for Construction, ASCE,* Vol. 4, No. 1, pp. 3-15.

Collins, M.P. (1978). "Towards a Rational Theory for RC Members in Shear", *Journal of the Structural Division, ASCE,* Vol. 104, pp. 649-666.

Collins, M.P., and Mitchell, D. (1980). "Shear and Torsion Design of Pre-stressed and Non Pre-stressed Concrete Beams", *PCI Journal*, Vol. 25, No. 5, pp. 32-100.

Collins, M.P., and Mitchell, D. (1991). "Pre-stressed Concrete Structures", *Prentice Hall*, Englewood Cliffs, New Jersey, 766 pp.

CSA Standard A23.3-84, "Design of Concrete Structures with Explanatory Notes", *Canadian Standard Association*, Toronto.

CSA Standard A23.3-94, "Design of Concrete Structures with Explanatory Notes", *Canadian Standard Association*, Toronto, 220 pp.

"Current and Future Applications of Advanced Composite Materials in Structural Engineering" (1994), *CSCE/ACMBS Network of Canada*, pp. 25-27.

"Design Guidelines of FRP Reinforced Concrete Building Structures" by the Building Institute of Research, BIR, the Japanese Ministry of Construction (1997), *Journal of Composites for Construction, ASCE*, Vol. 1, No. 3, pp. 90-115.

Domenico, N.G., Mahmoud, Z.I., and Rizkalla, S.H. (1998). " Bond Properties of Carbon Fiber Composite Pre-stressing Strands", *Structural Journal, ACI*, Vol. 95, No. 3, pp. 281-290.

Gaylord, E.H., Gaylord, C.N., and Stallmeyer, J.E. (1997). "Structural Engineering Handbook", *McGraw-Hill, Inc.*, New York, 4th ed., chapter 13.

Erki, M., and Bakht, B. (1996). "Non-Metallic Shear Reinforcement for Reinforced Concrete Beams", *1st Structural Speciality Conference, CSCE/SCGE*, Alberta, Canada, pp. 159-165.

Eurocode 2 (1991). "Design of Concrete Structures, Part 1: General Rules and Rules for Building", European Prestandard, ENV 1992-1: 1991E, *European Committee for Standardization*, Rue de Stassart 36, B-1050, Brussels, Belgium.

Ferguson, P.M., and Cowan, H.J. (1981), "Reinforced Concrete Fundamentals", *John Wiley & Sons, Inc.*, 4th ed., pp. 97-100.

Faza, S.S, and Gangarao, H.V.S. (1993). " Theoretical and Experimental Correlation of Behavior of Concrete Beams Reinforced with Fiber Reinforced Plastic Rebars", *Fiber-Reinforced-Plastic Reinforcement for Concrete Structures, International Symposium, ACI*, SP-138, pp. 559-612.

Gergely, P., and Lutz, L.A. (1968). " Maximum Crack Width in Reinforced Concrete Flexure Members", Causes, Mechanisms, and Control of Cracking in Concrete, *Structural Journal, ACI*, SP-20, pp. 87-117.

Ghali, A., and Favre, R. (1994). "Concrete Structures: Stresses and Deformations", E&FN Spon, London, 2nd ed., pp. 417-422.

Goodspeed, C., and Yost, J., (1994). "Concrete Beams and Slabs Reinforced with FRP grids", *Fiber Reinforced Plastics for Highway Structures Workshop*, Washington, D.C., USA.

Gustafsson, P.J., and Hillerborg, A. (1988). "Sensitivity in Shear Strength of Longitudinally Reinforced Concrete Beams to Fracture Energy of Concrete", *ACI Journal*, Vol. 85, pp. 286-294.

Hassan, H.M. (1991). " Displacement at Shear Crack in Beams with Shear Reinforcement under Static and Fatigue Loading", *Japan Society of Civil Engineers, JSCE*, No. 433/V-15, Japan, pp. 215-222.

Jenq, Y.-S., and Shah, S.P. (1989). "Shear Resistance of Reinforced Concrete Beams-A Fracture Mechanics Approach" in Fracture Mechanics: Application to Concrete, edited by Li, V.C., and Bazent, Z.P., SP-118, *ACI Journal*, pp. 237-258.

Leet, K. (1991). "Reinforced Concrete Design", *McGraw-Hill, Inc.*, 2nd ed., pp. 160-163.

Lin, T.Y., and Burns, N.H. (1981). "Design of Pre-stressed Concrete Structures", *John Wiley & Sons, Inc.*, New York, 3rd ed.

Lutz, L.A. (1974). " Crack Control Factor for Bundled Bars and for Bars of Different Sizes ", *Structural Journal, ACI*, pp. 9-10.

MacGregor, J.G. (1988). "Reinforced Concrete Mechanics and Design", *Prentice Hall*, Englewood Cliffs, New Jersey, 799 pp.

Mizukawa, Y., Sato, Y., Ueda, T., and Kakuta, Y. (1997). "A Study on Shear Fatigue Behavior of Concrete Beams with FRP Rods", *Non-Metallic (FRP) Reinforcement for Concrete Structures, 3rd International Symposium*, Vol. 2, Japan, pp. 309-316.

Mufti, A., Erki, M.,-A, and Jaeger, L., Editors (1991). " Advanced Composite Materials with Applications to Bridges", *Canadian Society of Civil Engineers, CSCE.*

Park, S.Y., and Naaman, A.E. (1999a). " Dowel Behavior of Tensioned Fiber Reinforced Polymer (FRP) Tendons", *Structural Journal, ACI*, Vol. 96, No. 5, pp. 799-806.

Park, S.Y., and Naaman, A.E. (1999b). "Mathematical Model for FRP Dowels Subject to Tension and Shear Forces", *Fiber Reinforced Polymers for Reinforced Concrete Structures, 4th International Symposium, FRPRCS-4*, Baltimore, USA, pp. 55-63.

Park, S.Y., and Naaman, A.E. (1999c). " Shear Behavior of Concrete Beams Prestressed with FRP Tendons", *PCI Journal*, Vol. 44, No.1, pp. 74-85.

"Recommendation for Design and Construction of Concrete Structures using Continuous Fiber Reinforcing Materials" (1997), Research Committee on Continuous Fiber Reinforcing Materials, *Japan Society of Civil Engineers*, *JSCE*, Japan, pp. 18-25.

Salib, S., Abdel-Sayed, G., and Grace, N. (1999a). "Towards a Comprehensive Theory for the Strength of Concrete Beams Reinforced by FRP", *The Second Middle East Symposium on Structural Composites for Infrastructure Applications*, Hurghada, Egypt, pp. 186-198.

Salib, S., Abdel-Sayed, G., and Grace, N. (1999b). " Crack Formation in FRP Reinforced Concrete Beams ", *Fiber Reinforced Polymers for Reinforced Concrete Structures, 4th International Symposium*, **FRPRCS-4**, ML, USA, pp. 219-232.

Shehata, E., Morphy, R., and Rizkalla, S. (1999). "Fiber Reinforced Polymer Reinforcement for Concrete Structures", *Fiber Reinforced Polymers for Reinforced Concrete Structures, 4th International Symposium*, **FRPRCS-4**, ML, USA, pp. 157-167.

Shehata, E., (1999), "FRP for Shear Reinforcement in Concrete Structures", Ph.D. dissertation submitted to the department of Civil Engineering at the University of Manitoba, Winnipeg, Manitoba, Canada, pp. 237-239.

"Standard for Structural Calculation of Reinforced Concrete Structures", (1988), Architectural Institute of Japan, *AIJ*, Tokyo, Japan.

Surendra, P.S., Stuart, E.S., and Chengsheng O. (1995), "Fracture Mechanics of Concrete", *John Wiley & Sons Inc.*, 1st ed., pp. 111- 113.

Tomaszewicz, A.J., and Markeset, G. (1997). "Shear Transfer in Concrete Reinforced with FRP Bars", *Non-Metallic (FRP) Reinforcement for Concrete Structures, 3rd International Symposium*, Vol. 2, Japan, pp. 325-332.

Toutanji, H.A., and Saafi, M. (1999), " Deflection and crack width prediction of Concrete Beams Reinforced with Fiber Reinforced Polymers", *Fiber Reinforced Polymers for Reinforced Concrete Structures, 4th International Symposium, FRPRCS-4*, Baltimore, USA, pp. 1023-1034.

Vecchio, F.J., and Collins, M.P. (1986). "The Modified Compression Field Theory for Reinforced Concrete Elements Subjected to Shear", *Structural Journal, ACI*, Vol. 83, No. 2, pp. 219-231.

Vecchio, F.J. (2000). "Analysis of Shear-Critical Reinforced Concrete Beams", *Structural Journal, ACI*, Vol. 97, No. 1, pp. 102-110.

APPENDIX II. NOTATION

A_l = tension area per longitudinal bar;

A_b = cross sectional area of one longitudinal bar;

A = longitudinal reinforcement cross sectional area;

A_{sh} = cross sectional area of shear reinforcement within the distance S;

a = length of the over-hung beam portion;

b = distance between the two concentrated loads, i.e. constant moment zone;

b_w = width of beam web;

C = compressive force induced in concrete above crack tip;

C_D, C_o, C_{Lp} = dimensionless coefficients used to locate the starting point of the new elliptical path of crack geometry modeling;

c = depth of compression zone;

D = distance between crack starting point and nearest support;

d = beam depth;

d_b = diameter of the reinforcing bar;

d_c = concrete cover of outer most bar measured from the center of that bar;

$d_{c.eq}$ = equivalent concrete cover;

E = modulus of elasticity of longitudinal reinforcement;

F = bar failure factor;

f = tensile stress induced in longitudinal reinforcement;

f' = tensile strength of longitudinal reinforcement;

f_l = the stress induced in tendons corresponding to either initial cracking moment or the decompression condition;

f_2 = the tensile stress induced in tendons at the specified loading level;

f_c = concrete compressive stress;

f_c' = concrete compressive strength;

f_c'' = concrete principle compressive stress;

f_{con} = tensile stress in longitudinal reinforcement segment crossing the crack;

$f_{c,t}'$ = concrete tensile strength,

f_{pr} = principle stress induced in tendons;

f_t'' = concrete principle tensile stress;

f_y = yield stress of steel reinforcement;

H = beam height;

h_f = beam flange thickness;

I_b = bond strength index of longitudinal bars;

j = distance between the centres of tension and compression ($\approx 7d/8$);

K = shear strength constant for steel-reinforced concrete beams;

K' = modified shear strength constant ($=K*E_{sh}/E_s$);

k_1 = coefficient based on bond quality between concrete and bars.(1.6 for plain bars and 0.8 for high bond bars);

k_2 = coefficient based on strain distribution over the member cross section. (0.5 for members subject to bending and 1.0 for members subject to axial tension);

k_p = coefficient depends on ρ_f [$=0.82\,(100\rho_f)^{0.23}$];

k_p' = equivalent coefficient depends on ρ_f [$=0.82\,(E_f\,100\rho_f\,/\,E_s)^{0.23}$];

k_u = coefficient depends on d [$=0.72$ for d $\geq$ 40cm];

L_{ow} = moment arm of P_{ow} about crack tip;

Lp = shear span;

M = Bending moment at the beam section under consideration;

M_n = flexural strength;

N = number of longitudinal bars;

P = total applied load on beam;

P_{ow} = own weight of the beam segment between crack and nearest support;

$P_{ow,beam}$ = total own weight of the beam;

$P_{u,D}$ = beam strength corresponding to a certain crack;

Q = shear force induced in longitudinal reinforcement;

Q_c = shear force induced in concrete;

q = shear stress induced in longitudinal reinforcement.;

q' = shear strength of longitudinal reinforcement;

R = total reaction at the nearest support to the developed crack;

R_{ow} = reaction at the same support due to beam own weight only;

r = bend raduis of the stirrup bar;

S = spacing between two successive stirrups;

S_c = average spacing between two successive cracks;

S_d = average slip of the stirrups crossing the crack,

S_{rm} = average spacing between cracks;

T = tensile force induced in shear or longitudinal reinforcement;

T_{pl} = total loss in prestressing force;

T_{po} = initial prestressing force;

u_u = bond strength between longitudinal reinforcement and concrete;

V = Shear force at the beam section under consideration;

V_n = the shear strength, consists of two components; the concrete contribution, V_c, and the shear reinforcement contribution, V_{sh};

V_{n1} = shear strength corresponds to stirrups rupture;

V_{n2} = shear strength corresponds to concrete compressive failure

W_{max} = maximum crack width measured at the extreme bottom level of beam;

W_n = crack gap component normal to longitudinal reinforcement;

W_{nu} = ultimate shear displacement of longitudinal reinforcement;

$W_{n,ys}$ = yield shear displacement of longitudinal steel reinforcement;

W_t = crack gap component along longitudinal reinforcement;

X and Y = coordinates of crack tip;

X_f and Y_f = coordinates of the intersection between centroid of flexural reinforcement and the modeled crack path profile;

X_p and Y_p = coordinates of the intersection between centroid of pre-stressing tendons and the modeled crack path profile;

Z = effective beam depth;

β = ratio of distances to the neutral axis from the extreme beam bottom level and from the c.g. of longitudinal bars;

ε = tensile strain induced in shear or longitudinal reinforcement;

ε_c = compressive strain induced in concrete;

ε_c' = concrete compressive strain corresponding to f_c';

$\varepsilon_{c,top}$ = compressive strain induced in concrete at top of beam level;

ε_{cu} = ultimate concrete compressive strain;

ε_s = tensile strain of the longitudinal steel bars;

ζ = dimensionless coefficient between 0.0 and 1.0 representing the degree of participation of concrete in the tensioned zone;

θ = the angle between the tangent to crack profile at crack tip and Y-axis;

ρ = reinforcement ratio;

$\rho_{f,b}$ = the balanced flexural reinforcement ratio;

ρ_{ft} = FRP bars ratio based on the effective tension area of concrete surrounding the bars and having the same centroid.

ρ_r = steel bars ratio based on the effective tension area of concrete surrounding the bars;

ρ_{sh}' = equivalent shear reinforcement ratio $[=\rho_{sh}(E_{sh}/E_s)]$.

σ = tensile stress induced in tendon based on its full cross sectional area;

φ = angle between X-axis and the line connecting crack tip with the intersection of crack profile and the centroid of longitudinal reinforcement;

Subscripts

eq = value corresponding to the equivalent beam reinforced with steel bars that has the same diameter of the original FRP bars;

exp = value obtained from experimental work;

f = value when crack reaches a failure tip (f);

fr = value corresponds to the intersection between the centroid of flexural reinforcement and the crack path profile;

fl = value corresponds to the intersection between the bottom level of beam flange and the crack path profile;

f = value corresponding to flexural reinforcement;

fail = value corresponds to beam failure;

i = value when crack reaches an arbitrary crack tip (i);

mod = value calculated by the present analytical modeling;

p = value corresponding to pre-stressing tendons;

pl = value corresponding to lower tendons;

pt = value corresponds to the nearest loading point, located at the top of beam flange, to the developed crack;

pu = value corresponding to upper tendons;

s = value corresponding to steel reinforcement;

sh = value corresponding to shear reinforcement;

sh-l-b = value corresponding to the longitudinal bars of FRP grid located within the bottom zone of beam; and

sh-l-m = value corresponding to the longitudinal bars of FRP grid located within the middle zone of beam;

VITA AUCTORIS

Sameh Michel Rafla Salib

1969   Born in Cairo, Egypt.

1991   Graduated with B.Sc. degree (Very Good with Honour) from the Civil Engineering Dept., Cairo University, Cairo, Egypt.

1996   Obtained his M.Sc. degree from the Civil Engineering Dept., Cairo University, Egypt.

1997   Enrolled in the Faculty of Graduate Studies and Research, University of Windsor, Windsor, Ontario, Canada, in a program leading to the degree of Doctor of Philosophy in Civil Engineering. Also, joined the Department of Civil and Environmental Engineering as a Teaching and Research Assistant.